Transport in quantum materials: lessons from (almost) exactly solvable models

by

Tessa Sky Cookmeyer

A dissertation submitted in partial satisfaction of the

requirements for the degree of

Doctor of Philosophy

in

Physics

in the

Graduate Division

of the

University of California, Berkeley

Committee in charge:

Professor Joel E. Moore, Chair
Professor Ehud Altman
Professor Jeffrey Long

Spring 2023

Transport in quantum materials: lessons from (almost) exactly solvable models

Abstract

Transport in quantum materials: lessons from (almost) exactly solvable models

by

Tessa Sky Cookmeyer

Doctor of Philosophy in Physics

University of California, Berkeley

Professor Joel E. Moore, Chair

In this dissertation, I develop new approaches, and apply and extend known techniques towards theoretical understanding of transport experiments in two quantum materials: α-$RuCl_3$ and $CeCoIn_5$. The first material, α-$RuCl_3$, is a candidate Kitaev material as it may realize the Kiteav model, a rare example of an exactly solvable two-dimensional (2D) quantum spin system. The Kitaev model exhibits a spin liquid ground state, where the spins do not align even at zero temperature, with anyonic elementary excitations, a kind of excitation unique to 2D. Being able to generate and manipulate these anyons may form some of the key components of topological quantum computers. The second material, $CeCoIn_5$, has a similar phase diagram to the high-temperature superconductors, implying that insights gained from understanding this material may lead to breakthroughs in other high-temperature superconductors.

After the introduction, in the second chapter of this thesis, I discuss the Kitaev model, its exact solution, and time-dependent mean-field theory (TDMFT). Although TDMFT was developed by other authors, I rederive and extend it to be able to compute any experimentally relevant quantity. With this approach, TDMFT agrees with exact results, and its main advantage is that it can be applied for more general models than the Kitaev model, unlike the exact solution. We demonstrate the value of the technique via computation of the expected results of an inelastic neutron experiment on a hypothetical Kitaev material.

In the third chapter, I start by briefly discussing the key experiments performed on α-$RuCl_3$ and focus on two experiments in particular that measure the longitudinal and Hall conductivity. Recent experiments have observed what appear to be quantum oscillations in the low-temperature longitudinal thermal conductivity. I will set up an application of our newly formulated TDMFT approach to theoretically predict the longitudinal thermal transport for the Kitaev model in a magnetic field, since not many methods can compute the necessary quantities for a 2D system and it is not known what the effect of the field will be. Furthermore, in the absence of an in-plane magnetic field, α-$RuCl_3$ becomes an

antiferromagnet at around seven Kelvin. In this phase, I am able to compute the thermal Hall effect via spin-wave theory (SWT), a well-established theory that works for systems with magnetic ordering, and compare the results directly with experiments on α-$RuCl_3$.

Starting part two of the thesis, in chapter four, I discuss a series of experiments on $CeCoIn_5$. I interpret these experiments as observing an exotic quantum critical point (QCP) separating two Fermi liquids with different sized Fermi surfaces. I discuss a theoretical model exhibiting such a phase transition and compute the electrical Hall resistivity expected near this QCP. In doing so, I explain one of the most surprising features of the experiment—a large peak in the Hall resistivity as a function of temperature. The computation, however, cannot perfectly capture all the features of the experiment, including the T-linear longitudinal resistivity that is a hallmark of the high-temperature superconductors in the normal state.

In the fifth chapter, I introduce a new model for the above QCP that is exactly solvable in the same way as the Sachdev-Ye-Kitaev (SYK) model, a model that exhibits T-linear resistivity. Within my model, I compute the longitudinal and Hall resistivities and find T-linear resistivity in the critical fan above the QCP, which compares favorably with experiments on high-temperature superconductors, particularly $CeCoIn_5$.

In the final chapter, I discuss other potential uses for TDMFT and these SYK inspired models, and the large open questions that remain about these two materials.

To the friends I have loved here

Contents

Acknowledgments

I want to first of all thank Joel Moore for his consistent guidance on research throughout the years and his thoughtful approach to physics, academia, and life. I am additionally indebted to Ehud Altman for guiding me through multiple fun and engaging projects and offering seemingly infinite depth of knowledge. I would also like to thank James Analytis for always being excited to share his recent experimental results with me and whose friendly presence has made the department and the physics community more welcoming. I further thank my experimental and theory colleagues Vikram Nagarajan, Olive Eilbott, Nikola Maksimovic, Shannon Haley, Johannes Motruk, Erik Aldape, Aavishkar Patel, Shubhayu Chatterjee, Tomohiro Soejima, and Elizabeth Dresselhaus for the myriad conversations we have had over the years.

Grad school is long and challenging, and I want to thank my mom for her love and care for me throughout these years and all others. I would also like to thank my dear partner and best friend Emily Ruppel for her support, attention, patience, and love. My friends, Grace, Tiffany, Cory, Chloe, Aruna, Anna, Olive, Nell, Jackie, Vikram, and many others, I cannot express how much strength I draw from the time we spend together.

And, of course, thank you Vikram for showing me real-life samples of α-$RuCl_3$, and letting me know that it is sticky.

Chapter 1

Introduction

"In the land of quantum, words mean nothing. There is only math[.]" – CGP Grey

1.1 What are quantum materials

In principle, it is simple enough to describe a solid. Simply write down the Hamiltonian describing 10^{23} atomic nuclei and their associated electrons interacting through electromagnetism, and solve for the ground state. This starting point, although correct, is utterly useless. Instead we simplify: take the nuclei as roughly fixed, and consider the electrons on top of that periodic background potential.

Here is where many solid state physics courses begin, and in simple metals and insulators, much of their properties can be characterized by (essentially) non-interacting electrons. With 10^{23} particles occupying a solid, it would be surprising if we could understand all the possible phenomenon with this paradigm. Indeed, solids can exhibit fundamentally different physics from the universe at large such as realizing new kinds of excitations that are neither boson nor fermion, a separation of the spin and electron degrees of freedom of the electron, and topological order, and these emergent properties often require a fully quantum mechanical approach, as we will see below.

Like many broad categories, a "quantum material" is not rigorously defined but is perhaps meant to capture such "novel" physics. One definition of a "quantum material" requires a solid to exhibit properties we cannot understand through contemporary condensed matter techniques [136]. However, this definition makes the category of quantum materials time dependent: as we study a quantum material and develop the necessary analytic and numerical techniques to understand it, such insights will render it no longer a quantum material. In particular, even though the physics of fractional quantum Hall states at $\nu = p/(2p+1)$ are well-understood through analysis of a Laughlin wave function, since they exhibit anyons, excitations with fractional statistics, they should likely be classified as quantum materials.

As the name suggests, an alternative definition is any material whose observed properties

cannot be understood without quantum mechanics [23]. A (partial) list of quantum materials would then be (fractional) quantum Hall systems, superconductors, spin liquids, Weyl semimetals, Dirac materials, (fractional) Chern insulators, and quantum magnets. Even though the latter definition will include materials we already firmly understand, it has the advantage of being clearly stated, even to non-experts.

Regardless of the definition, materials where large open questions exist provide some of the most intriguing directions for current and future research as a condensed matter theorist. We will now describe two such categories of materials that will be relevant to the work contained in this dissertation.

1.2 Spin liquid

To arrive at a spin liquid, we should first describe a "spin solid." The familiar example is iron or other ferromagnets that exhibit a magnetic moment in the absence of a magnetic field. One way to capture this physics is the nearest-neighbor Heisenberg model[1]

$$H = J \sum_{\langle ij \rangle} \boldsymbol{S}_i \cdot \boldsymbol{S}_j \tag{1.1}$$

where we have spins localized on a lattice of sites where nearest-neighbor pairs, $\langle ij \rangle$, interact.

Although the question of why iron is magnetic is more complex [184], we can see how this kind of interaction arises in a simplified model of a material. The Hubbard model describes a single band of spinful electrons on a lattice interacting with each other only on the same site

$$H = t \sum_{\langle ij \rangle} \sum_{\sigma=\uparrow,\downarrow} c^\dagger_{i\sigma} c_{i\sigma} + U \sum_i c^\dagger_{i\uparrow} c_{i\uparrow} c^\dagger_{i\downarrow} c_{i\downarrow}. \tag{1.2}$$

The interaction is meant to approximate the coulomb interaction, which, due to screening, becomes short ranged. Depending on the lattice and the dimension, the Hubbard model is difficult to solve for general t/U and number of electrons. However, when t/U is small and the band is half-filled, there will be one electron per site. Effectively, then, we have a spin degree of freedom per site, which interact with each other when t is non-zero. The approximate Hamiltonian is given by the Hubbard model with $J = t^2/U$ [118] where the spins are spin-1/2 moments.

Although this approach generates an antiferromagnetic interaction, it is worth considering what happens for J or either sign. If $J < 0$, the interaction is ferromagnetic the ground state will have all the spins aligned, which we can consider a spin solid. Even when $J > 0$, the ground state can still be ordered if the lattice is bipartite. Due to the Mermin-Wagner theorem, there will only be a spontaneously chosen direction in three dimensions, but, in lower dimensions, the spins can still be "aligned", in the sense that $\langle \boldsymbol{S}_i \cdot \boldsymbol{S}_j \rangle$ can be large even

[1] Unless explicitly stated, $\hbar = k_B = c = |e| = 1$.

at large distances (e.g. [86, 226, 70, 54, 205, 156, 53, 69]). This quantity has the advantage of being probed by neutron scattering experiments [103].

However, if the lattice is not bipartite, the ground state is less clear. Particularly, what is the ground state of the antiferromagnetic Hubbard model on the triangular lattice? This question is what led Anderson to propose the first spin liquid state [3]. Instead of an "aligned" state, he considered a state that was a superposition of all possible singlet coverings of the lattice. With the advent of the density-matrix renormalization group method [204], it was instead confirmed that the ground state is ordered but, by adding other physically motivated terms, a spin liquid can appear [86, 226, 70, 54, 205, 156, 53, 69, 36]. Other frustrated lattices, such as the Kagome lattice [125, 52, 60, 206, 71, 55, 61], are also likely to exhibit spin liquid states.

Unfortunately, there is no uniform definition of what a "spin liquid" is. Based on the above discussion, as long as $\langle \boldsymbol{S}_i \cdot \boldsymbol{S}_j \rangle$ is short-ranged, the state could be considered a spin liquid, but there are other possible orderings that might not be bona fide spin liquids. For instance, spins can pair up to form singlets and the pattern of singlets could be ordered [59].

The definition put forth in Ref. [168] is long-ranged entanglement. Entanglement is an expected feature of a quantum state, but the distinction that the authors of Ref. [168] make is that, in a spin liquid, the entanglement is essential for the properties of the phase and therefore a spin-liquid state cannot be "continuously deformed" into an unentangled state. Although this definition may, in principle, be suitable for all spin liquids, we lack a fully general rigorous definition of long-range entanglement and the above deformation picture, and it is further not clear how to apply this definition to experiments. Nevertheless, one of the consequences of long-range entanglement is fractionalization, where the good quasiparticles are non-bosonic excitations. The idea is simply that spin flips carry integer spin, and if the entanglement is local or can be made local, any excitation will then only carry integer spin. However, if there exist excitations carrying fractional spin, it necessarily means that the excitations have long-ranged effects. Although good quasiparticles may not exist for every spin liquid, when they do, they have the potential to be observed experimentally and detected numerically, and therefore can serve as a sufficient signature of a spin liquid.

In 2+1 dimensions, for the same reasons that knot theory is only interesting in three spatial dimensions, the fractionalized excitations can be neither bosons nor fermions but instead anyons [94]. In this case, a wave function containing multiple anyons does not need to just pick up a factor ± 1 from exchange of the two anyons, but it instead can pick up a complex phase or, if there are other degenerate states, can become a superposition of other states in the manifold. Both the Toric code [93] and the Kitaev model [94] (discussed more below) are important paradigmatic spin liquid models as they are exactly solvable and exhibit anyons; numerical evidence for the bosonic analog of a fractional quantum Hall state, having different anyonic excitations, has also been found [189, 36, 206].

The list of spin liquids is long [168], but which have been found in real materials? Unforutnately, there are no materials that are confidently known to exhibit a specific kind of spin liquid, and it remains an ever-more-important task to find and characterize a concrete example material. Candidate materials exist through multiple routes: Herbertsmithite real-

izes a Kagome lattice, known to harbor many varieties of spin liquid, and has broad features in its inelastic neutron scattering spectrum; the rare-earth pyrochlores, like $Yb_2Ti_2O_7$, are expected to be well-modeled by a Hamiltonian known to harbor a spin-liquid in a range of parameters; triangular-lattice organic compounds, like κ-$(ET)_2Cu_2(CN)_3$ and $EtMe_3Sb[Pd(dmit)_2]_2$, potentially realize an extended Hubbard model on the triangular lattice and are in insulating phases without clear magnetic order; and, as we will talk more below, there is a range of Kitaev materials that may be close to realizing the Kitaev spin liquid [168]. Furthermore, advances in cold atoms have allowed for the possibility of generating spin-liquid states or probing spin-liquid physics in two-dimensional trapped atom systems [174, 162]. In part, the excitement of α-$RuCl_3$ is due to it potentially being the first confirmed spin liquid: it seems likely to exhibit the Kitaev spin liquid phase, which has a clear experimental signature that has been observed in some experiments [87, 218, 20]. Unfortunately, as we discuss below, the experimental signature is not as clear cut, and it remains an open question whether α-$RuCl_3$ has a spin liquid phase at all.

We will discuss a specific example, the Kitaev spin liquid in detail in Chapter 2 and the experimental case of α-$RuCl_3$, as well as other Kitaev materials, in Chapter 3. However, we have only scratched the surface of spin-liquid research in general, and, for more background, we recommend Ref. [168] as a thorough review article.

1.3 Heavy fermion compounds and strange metals

In the presence of large interactions the resulting degrees of freedom behave quite differently than the noninteracting system. As discussed above, the Hubbard model, at small t/U and half-filling, has localized electrons. In contrast, in the absence of interactions, the half-filled band should produce metallic behavior with delocalized electrons and a well-defined Fermi surface.

In many systems, though, the interactions produce surprisingly little effect, as elucidated by Fermi liquid theory (FLT) [171, 2]. The basic idea of FLT is that the quantum numbers of the excitations at the Fermi surface do not change in the presence of interactions, and they remain quasiparticles albeit with a finite lifetime. However, the lifetime, due to decay to other particles near the Fermi surface, becomes longer and longer as the momentum gets closer and closer to the fermi momentum. The main effect of the interactions, then, is that the various parameters, most importantly the effective mass of the excitation, can be renormalized. For thermodynamic quantities, FLT predicts the following scaling with temperature [194, 2]

$$\begin{aligned} C_V &= \gamma T \\ \rho &= \rho_0 + AT^2 \end{aligned} \tag{1.3}$$

where $\gamma \sim \sqrt{A} \sim m_*$, the effective mass.

In many materials, the mass is only slightly renormalized (i.e. $m_*/m_e \sim 1$), but in the heavy-fermion compounds m_*/m_e can be almost 1000. As we will discuss in Chapter 4, the

large effective mass can be understood through Kondo lattice physics as hybridization of a localized and conduction band. One consequence of a large effective mass is the reduction of the kinetic energy of the excitations, which creates the opportunity for interactions to play a more important role and uncover new states of matter [194]. Phenomenologically, using the Hubbard model example, this is understood as reducing t thereby reducing t/U.

In many of these compounds, antiferromagnetism can be induced or suppressed leading to a quantum critical point where there are large departures from the FLT scaling. Indeed, the resistivity appears to scale as $\rho = \rho_0 + A'T$, having a strong *linear*-in-temperature component [194].

This scaling is the most abundant example of non-Fermi liquid physics. Termed "strange metal" behavior, it is seen across numerous heavy-fermion compounds [194], magic-angle twisted bilayer graphene [22], and high-temperature superconductors [109]. Due to its ubiquity, it is hoped that there some kind of universal mechanism that can explain the origin of strange metal physics [109, 194, 42, 57, 201]. Furthermore, the connection to high-temperature superconductors, understanding the mechanism behind strange metal physics may lead to the engineering of higher temperature superconductors.

It is important, however, that this scaling occurs at *low* temperature; in an ordinary Fermi liquid, at temperatures much larger than the bandwidth, the resistivity is T-linear [27] and this regime is considered a "bad metal." The dividing line between "bad" and "strange" metals is given heuristically by the Mott-Ioffe-Regel criterion, where the mean-free path is shorter than the lattice spacing [27] and coherent quasiparticles are unable to be formed [57].

One further unifying features is that many materials seem to exhibit a "Planckian bound" on the scattering rate [57, 194, 109]. In these analyses, the timescale $\tau_{\mathrm{Pl}} = \hbar/(k_B T)$ is thought to be a lower bound on the scattering rate for the system, and, in carrying out a Drude analysis of strongly correlated materials, it is found that the relevant scattering rate is of the same order as τ_{Pl} [194, 109]. At temperatures $T \gtrsim T_{\mathrm{D}}$, the Debye temperature, scattering off of phonons is expected to produce this Planckian transport, but at low temperatures, a quantum critical explanation is expected [57]. Not all criticality, however, will produce Planckian transport and T-linear resistance extending from low temperature to temperatures comparable to the Debye scale is seen in materials requiring a crossover from one mechanism to another [57]. It is also argued that systems without quasiparticles will exhibit relaxation on the Planckian timescale [27].

Even with years of concentrated effort, there is no accepted model that produces strange metal behavior. One well-explored route, as mentioned above, is the role of a quantum critical point (QCP) where a metal with a fermi surface are interacting with a gapless boson. Depending on the nature of the critical point, the resulting transport properties can be different than those expected from a Fermi liquid [27, 13, 175, 145]. This line of theoretical work aligns with experimental evidence that there is a QCP beneath superconducting dome of some of the cuprates [13].

One of the key issues is that needing analytic tractability limits the models that we can consider and fully understand. With the advent of larger-scale numerics, transport can be

predicted in a wider range of models with quantum critical points. Remarkably, the Hubbard model on the square lattice, being studied with quantum Monte Carlo methods, yields a strange metal at certain dopings with T-linear resistivity over several decades [72], though the results are limited to temperature of order the hopping strength. Recent advances further allow for a sign-problem-free formulation of quantum Monte Carlo simulations of nematic-ising or spin-density wave transitions [13] All these cases show T-linear resistivity but are subject to the usual challenge in QMC of analytic continuation. A Kondo-Ising model amenable to *classical* Monte Carlo, without the need to carry out analytic continuation, provides further examples of the role of critical fluctuations in producing T-linear resistivity [216].

One phenomenological idea is that of a marginal Fermi liquid, where the self-energy is proposed to have the following form [201]

$$\Sigma(\omega, \boldsymbol{k}) \sim g^2 \nu_0^2 \left[\omega \ln \left(\frac{x}{\Lambda} \right) - ix \frac{\pi}{2} \right] \tag{1.4}$$

where $x \sim \max(|\omega|, T)$, ν_0 is the density of states at the Fermi surface, and Λ is a cutoff scale. Although proposed without a microscopic picture of its origin, this form of the self-energy captures much of the phenomenology of high-temperature superconductivity [201]. However, a simple model with "hot" electron pockets shows that the electrons can still behave as a Fermi liquid and produce strange-metal physics [127].

As we will discuss in more detail in Chapter 5, a major recent advance has been the Sachdev-Ye-Kitaev (SYK) model [27, 161]. Originally describing an all-to-all random coupling, several lattice models were introduced often containing strange metal phases [143, 144, 28, 1]. Furthermore, the original model is dual to a black hole in two-dimensional anti-de Sitter space [158, 157] indicating perhaps a tantalizing connection between black holes and strange metals. The analytic tractability occurs in these models due to the presence of a large number of flavors (or bands) and the random couplings. Although the randomness is not clearly of a physical origin, perhaps in materials with many relevant bands, the couplings between them are *effectively* random. Regardless, the SYK approach gives a new analytic method for understanding strongly-interacting compounds that can even clarify the physics of the previously-mentioned models [27].

Given the wide range of theories of strange metallicity, it may be the case that there are several mechanisms needed to understand all the various compounds. Experiments continue to provide new information about strange metals, like the recent B-linear resistivity scaling in certain strange metal compounds [58, 112, 166], allowing some models to be ruled out. The ultimate test in any theory would be to predict new strange metal compounds due to an understanding of the necessary ingredients.

1.4 This dissertation

In the remainder of this dissertation, our eyes are oriented towards two quantum materials: α-$RuCl_3$ and $CeCoIn_5$. The first is an example of a Kitaev material, which is hoped to

exhibit a particular Kitaev spin liquid phase. In Chapter 2, we will discuss the Kitaev model, its exact solution and its spin liquid ground state, and a technique that I extended to compute any desired quantity approximately beyond the exactly solvable point. We will use that technique to compute the signal expected in inelastic neutron scattering experiments to emphasize its accuracy and utility.

With the set up, we will explore the situation for α-$RuCl_3$ in Chapter 3. As we will see, the best-fit models that come out of various *ab initio* or experimental fits do not predict a transition to a spin liquid phase that is reportedly seen in the material. We will set up an additional calculation for the longitudinal thermal conductivity in the presence of a magnetic field, which we will carry out in future work. Although there are promising experimental signatures for α-$RuCl_3$, there remain significant challenges towards reconciling our theoretical understanding with the experiments.

The second material, $CeCoIn_5$, is a heavy-fermion compound which exhibits a strange metal phase, and recent experiments have indicated that it might be close to an unusual quantum critical point. We will consider the experimental situation and provide a semiclassical calculation of transport to support this interpretation in Chapter 4. Our model will be able to capture a surprising amount of the experiments, but it is not exactly solvable and does not predict a strange metal phase.

We will then consider an exactly solvable model for the quantum critical point in Chapter 5. In addition to capturing much of the phenomenology of this material, we will capture the strange metallicity in the critical fan. This model may be adaptable to other strange metal systems like the cuprates.

Finally, in Chapter 6, we will discuss the outlook for Kitaev materials and understanding strange metals. Throughout this work, we will review the theoretical techniques in sufficient detail that they may be applied to other systems.

Chapter 2

The Kitaev model: exact and approximate approaches

In the introduction we discussed a potential spin liquid state that variationally has a low ground state energy for the Heisenberg antiferromagnet on the triangular lattice [3]. As numerical work demonstrates, it is not the ground state. Are there models where we can exactly demonstrate that their ground state is a spin liquid? The answer is yes and we will discuss one such example that has become critical in spin-liquid research: the Kitaev model.

The exact solution will demonstrate the presence of non-bosonic low-energy excitations, implying the necessary long-ranged entanglement for a spin liquid [168]. As an experimental signature, we will compute inelastic neutron scattering whose broad features are implied by the fractionalization of the spins.

2.1 The model, Majoranas, and exact approach

This section largely draws on Kitaev's original work [94], which is itself quite accessible, and a few other works [12, 130]. The model starts with spin-1/2's located at each of the sites of a honeycomb lattice. Each site has three nearest neighbors, and they are connected by bonds that we label x, y, and z as shown in Fig. 2.1. The Kitaev model Hamiltonian is then given by

$$H_K = K \sum_{\langle ij \rangle_\alpha} S_i^\alpha S_j^\alpha. \tag{2.1}$$

The notation $\langle ij \rangle_\alpha$ indicates a sum over nearest neighbor pairs and α specifies which of the three bonds connects the pair.

Although the model appears contrived, it is unique because it has an extensive number of conserved quantities, the plaquette operators W_P. These operators are defined around a plaquette (i.e. a hexagon) and are given by

$$W_P = 2^6 S_1^x S_2^y S_3^z S_4^x S_5^y S_6^z \tag{2.2}$$

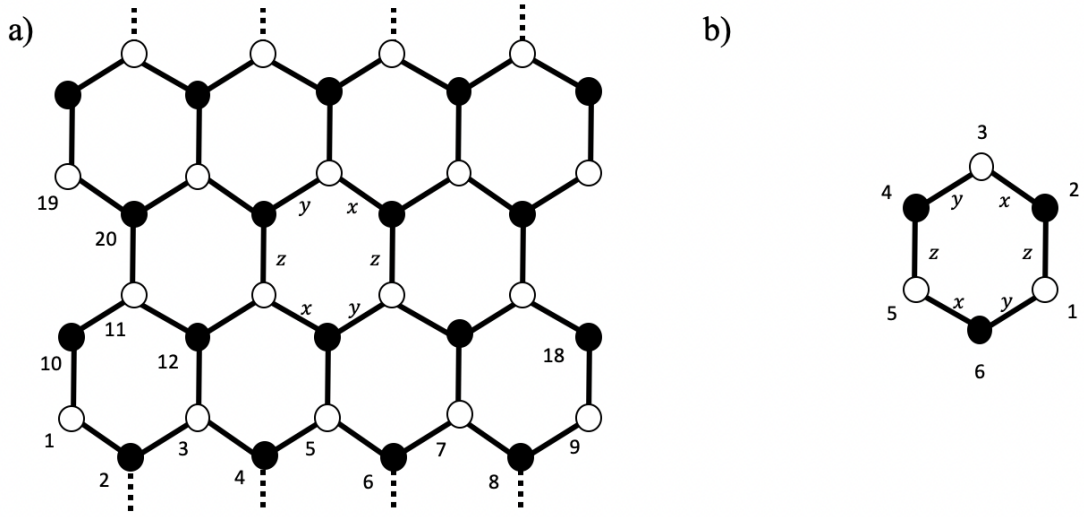

Figure 2.1: a) The honeycomb lattice with bond labeling around one hexagon and with the lattice sites labeled in accordance with the Jordan-Wigner transformation. Note the A sublattice is represented in black circles and the B sublattice in white. b) The plaquette operator labeling.

as shown in Fig. 2.1b. Beyond making the model integrable, this feature suggests that it may be exactly solvable. We will solve the model in two ways: the familiar Jordan-Wigner transformation and a different Majorana rewriting.

Jordan-Wigner transformation

The idea of the Jordan-Wigner (JW) transformation is to replace our spin degrees of freedom with fermionic ones. For this transformation, we pick a labeling of sites through the system such that adding or subtracting one gives a site connected by an x or y bond (except at the boundaries) as shown in Fig. 2.1. The JW transformation is then given by

$$\begin{aligned} 2S_i^z &= 2f_i^\dagger f_i - 1; \qquad & \mathcal{S}_i &= \prod_{j<i}(-2S_j^z); \\ 2S_i^x &= \mathcal{S}_i(f_i + f_i^\dagger); \qquad & 2S_i^y &= i\mathcal{S}_i(f_i - f_i^\dagger). \end{aligned} \tag{2.3}$$

where f_i are the usual fermion creation and annihilation operators.

The $\mathcal{S}_i$ are called the JW strings, and, in many one-dimensional models, they no longer appear in the Hamiltonian. With periodic boundary conditions in 1D, the string that stretches across the entire system does appear in the Hamiltonian and splits the excitation spectrum into physical and unphysical states, but no such complication arises when there are open boundaries. In this case, we think about the various sites connected by x and y bonds as

constituting a "row" and these rows are connected by the z bonds. As a slightly technical point, we must use open boundary conditions on the left and right side of the model as otherwise the JW strings corresponding to stretching across entire rows will appear in H_K. Ordinarily, in one-dimensional models, this feature is acceptable as the JW string containing all sites commutes with the Hamiltonian. In this case however, the string corresponding to just a single row, for instance, does not commute with the Hamiltonian and therefore cannot be simultaneously diagonalized. The restriction to open boundary conditions only is often ignored in the literature, but rigorously it must be used if we use the JW transformation.

Instead of writing the degrees of freedom in terms of complex fermions f_i, we consider Majorana fermions. We define two Majoranas per site

$$c_i = \begin{cases} f_i + f_i^\dagger & \text{if } i \in A \\ -i(f_i - f_i^\dagger) & \text{if } i \in B \end{cases} \qquad \bar{c}_i = \begin{cases} f_i + f_i^\dagger & \text{if } i \in B \\ -i(f_i - f_i^\dagger) & \text{if } i \in A \end{cases} \tag{2.4}$$

where A and B denote the two sublattices of the honeycomb lattice. Note that $c_i^\dagger = c_i$, $\{c_i, c_j\} = 2\delta_{ij}$, and $\{c_i, \bar{c}_j\} = 0$ (and similarly for $\bar{c}_i$).

With these restrictions, after carrying out the transformation, we find

$$H_K = i\frac{K}{4}\sum_i c_i c_{i+x} + c_i c_{i+y} + c_i c_{i+z}(i\bar{c}_i\bar{c}_{i+z}) \tag{2.5}$$

where $i + \alpha$ refers to the site where we have moved from i along and α bond. The magic of this model is that the products $\bar{c}_i\bar{c}_{i+z}$ commute with the Hamiltonian, which we can interpret as directly linked to the conserved plaquetter operators as they can rewritten as $W_P = (i\bar{c}_1\bar{c}_2)(i\bar{c}_5\bar{c}_4)$. From here, we can simultaneously diagonalize H_K and all of the $\bar{c}_i\bar{c}_{i+z}$ and confirm, either numerically or through a theorem due to Lieb, that the ground state occurs when all the $i\bar{c}_i\bar{c}_{i+z} = 1$ [94]. It is worth noting that *every* eigenstate has some distribution of the values of these conserved quantities. To just find the ground state, then, we restrict to the sector where the $i\bar{c}_i\bar{c}_{i+z} = 1$ are uniform, and we are left with a Hamiltonian quadratic in Majorana operators

$$H_{K,c} = i\frac{K}{4}\sum_{i\in A}\sum_\alpha c_i c_{i+\alpha} = \frac{1}{4}\sum_{ij} c_i h_{ij} c_j \tag{2.6}$$

We can diagonalize this Hamiltonian in the usual way. We introduce a scaling to the Majorana's, $c_i = \tilde{c}_i\sqrt{2}$, which allows them to be transformed into a complex fermion basis by a unitary operator. That is, $\tilde{c}_i = U_{0,ij}\bar{a}_j$ where $\bar{a}^T = (a_1, a_2, ..., a_N, a_1^\dagger, ..., a_N^\dagger)$. We then have

$$\frac{1}{2}\tilde{c}^\dagger h\tilde{c} = \frac{1}{2}\bar{a}^\dagger U_0^\dagger h U_0\bar{a} = \frac{1}{2}\bar{a}^\dagger\Lambda\bar{a} = \sum_{i=1}^N E_i\left(a_i^\dagger a_i - \frac{1}{2}\right) \tag{2.7}$$

where $\Lambda = \text{diag}\{E_1, E_2, ..., E_N, -E_1, ..., -E_N\}$ is a diagonal matrix with the set as its entries. Recall that for Majorana's, the energy spectrum can be chosen to be all positive (or all negative).

Because of the translation invariance in the ground state sector, the diagonalization just amounts to performing a Fourier transform. The dispersion relation is given by [94]

$$E_{\boldsymbol{k}} = |K| \left| e^{i\boldsymbol{k}\cdot\boldsymbol{n}_+} + e^{i\boldsymbol{k}\cdot\boldsymbol{n}_-} + 1 \right| \tag{2.8}$$

where $\boldsymbol{n}_\pm = \left(\pm\frac{1}{2}, \frac{\sqrt{3}}{2}\right)$, which are the basis vectors of the underlying triangular Bravais lattice of the honeycomb lattice.

Nature of the excitations

Since the excitations are written in terms of complex fermions, we have fractionalization and therefore a spin liquid (using the definition in the introduction). In fact, there are two different excitations: the $a_{\boldsymbol{k}}$ that diagonalize the quadratic c_i Hamiltonian, and the excitations of the conserved quantities $i\bar{c}_i\bar{c}_j$.

The former are gapless, as can be seen by plugging in $\boldsymbol{k} = (\pm 2\pi/3, 0)$ into $E_{\boldsymbol{k}}$ above. The latter are gapped: by flipping $i\bar{c}_i\bar{c}_j = -1$ for one of the conserved quantities, the resulting Hamiltonian is still quadratic in the c_i. The difference in the lowest energy of that Hamiltonian and the ground state energy is the flux gap, $\Delta_F \approx 0.065|K|$. Physically, the energy cost is associated with creating two "fluxes" by flipping the values of two of the plaquette operators W_P.

Notice that, due to the Jordan-Wigner transformation, the $a_{\boldsymbol{k}}$ carry superpositions of strings of spin operators. That is, they are non-local when written in the spin degrees of freedom. Furthermore, notice that if we want to flip a single plaquette, we must flip all the $i\bar{c}_k\bar{c}_l$ to the left of $i\bar{c}_i\bar{c}_j$. Therefore, a single flux carries with it a "string" as well.

As a consequence of these "strings," the excitations exhibit anyonic statistic [94]. Strictly speaking, we need to gap out the $a_{\boldsymbol{k}}$ through an applied magnetic field to define the statistics, but, once that is done, we can consider braiding a flux and a $a_{\boldsymbol{k}}$ excitation. In general, when we consider excitations of different types, there is no effect one the wave-function of wrapping one around the other. Instead, in this case, the wave function picks up a -1 indicating that these excitations are anyons [94].

Dynamic spin-spin correlator

Beyond calculating the static properties of the ground state, we can even evaluate time-dependent correlators exactly. Our prototypical example is the dynamic spin-spin correlator, which is defined for a system with N sites to be:

$$S^{\alpha\beta}(q,\omega) = \frac{1}{N}\sum_{i,j} e^{-i\boldsymbol{q}\cdot(\boldsymbol{x}_i - \boldsymbol{x}_j)} \int dt e^{i\omega t} \langle S_i^\alpha(t) S_j^\beta \rangle \tag{2.9}$$

By symmetry, we only need to consider $\alpha = z$ and $\beta = \{z, x\}$. Since the Hamiltonian is quadratic in Majorana's and S^x is written as the product of an odd number of Majorana's,

it is identically true that $\langle S_i^z(t)S_j^x\rangle = 0$. Therefore, we only need to consider

$$4\langle S_i^z(t)S_j^z\rangle = i(-1)^{i+j}e^{iE_0t}\langle c_i\bar{c}_i e^{-iH_Kt}c_j\bar{c}_j\rangle \tag{2.10}$$

where we have chosen a convention so that i is even on A sites and odd on B sites.

Since $\bar{c}_i$ appears in only one term in H_K, we can see

$$[H_K,\bar{c}_i] = i(K/2)c_ic_{i+(-1)^iz}(i\bar{c}_i\bar{c}_{i+(-1)^iz})\bar{c}_i, \tag{2.11}$$

from which it follows

$$4\langle S_i^z(t)S_j^z\rangle = -i(-1)^{i+j}e^{iE_0t}\langle c_i e^{-i(H_K - i\frac{K}{2}c_ic_{i+(-1)^iz}(i\bar{c}_i\bar{c}_{i+(-1)^iz}))t}c_j\bar{c}_i\bar{c}_j\rangle. \tag{2.12}$$

Now, the key observation is that $\bar{c}_i$ ($\bar{c}_j$) flips the value of the conserved quantity $i\bar{c}_i\bar{c}_{i+(-1)^iz}$ ($i\bar{c}_j\bar{c}_{j+(-1)^jz}$), respectively. All other terms commute with the conserved quantities, so their flips must cancel in order to return to the same sector. Therefore, the only non-zero terms are when $i=j$ and when $j = i+(-1)^iz$. Picking i to be on the A sublattice, we find

$$\begin{aligned} 4\langle S_i^z(t)S_i^z\rangle &= -ie^{iE_0t}\langle c_i e^{-i(H_{K,c}-i\frac{K}{2}c_ic_{i+z})t}c_i\rangle \\ 4\langle S_i^z(t)S_j^z\rangle &= e^{iE_0t}\langle c_i e^{-i(H_{K,c}-i\frac{K}{2}c_ic_{i+z})t}c_j\rangle. \end{aligned} \tag{2.13}$$

These expression can be generalized to any eigenstate. Because the c_j Majorana are evolving in time through a perturbed Hamiltonian, these expressions are reminiscent of the x-ray edge problem [12]. I will discuss how to numerically evaluate them below, but it is worth noting that there is an exact approach [97].

Alternative transformation

The JW transformation's main drawback is the presence of the non-local strings, which makes applying this approach impossible to most Hamiltonians. There is an alternative local transformation where we instead have a local constraint. It is

$$2S_i^\alpha = ib_i^0b_i^\alpha \tag{2.14}$$

where $\alpha\in\{x,y,z\}$ and b_i^μ (with $\mu\in\{0,x,y,z\}$) are four Majorana operators. This transformation is equivalent to the Abrikosov fermion approach [169], which has the constraint of one fermion per site. In this case, the constraint is written as $b_i^0b_i^xb_i^yb_i^z = D_i = 1$.

In this language, the Hamiltonian becomes

$$H_K = -\frac{K}{4}\sum_{\langle ij\rangle_\alpha} ib_i^0b_j^0(ib_i^\alpha b_j^\alpha) \tag{2.15}$$

and now the $ib_i^\alpha b_j^\alpha = u_{\langle ij\rangle_\alpha}$ commute with the Hamiltonian. To fix the sign ambiguity, $u_{\langle ij\rangle_\alpha}$ specifies that i is on the B sublattice and j is on the A sublattice. If we set all of them to

$u_{\langle ij\rangle_\alpha} = -1$, we recover the same quadratic Hamiltonian as before. The plaquette operators can again be rewritten, and are given by $W_P = u_{\langle 12\rangle_z} u_{\langle 32\rangle_x} u_{\langle 34\rangle_y} u_{\langle 54\rangle_z} u_{\langle 56\rangle_x} u_{\langle 15\rangle_y}$.

The main complication from the constraint can be handled by noting that D_i commutes with the physical spin operators $\boldsymbol{S}_i$ and therefore the Hamiltonian. If $|\Psi\rangle$ is an eigenstate of H_K, then so is $D_i|\Psi\rangle$. With

$$P = \prod_i \frac{1 + D_i}{2} \tag{2.16}$$

the state $P|\Psi\rangle$ is then an eigenstate satisfying the constraint. Although this representation of the state appears unwieldy, its main effect is to enforce a parity requirement on excited states [34, 146, 199].

2.2 An approximate method: time-dependent mean-field theory

As we will discuss in the next chapter, in realistic materials, we do not just have the Kitaev term in the Hamiltonian.[1] In particular, we will have a Hamiltonian with the following spin interactions:

$$H = -\sum_{\langle ij\rangle_\alpha} \left[K S_i^\alpha S_j^\alpha + \Gamma \sum_{\beta\neq\bar{\beta}\neq\alpha} S_i^\beta S_j^{\bar{\beta}} + J \boldsymbol{S}_i \cdot \boldsymbol{S}_j \right] + \sum_i \boldsymbol{h} \cdot \boldsymbol{S}_i. \tag{2.17}$$

The sum is over all nearest-neighbor bonds and each bond has an index $\alpha = x, y, z$ according to its type.

One challenge in studying the Kitaev model is that adding such generic perturbations will break either of the exact solutions described above. One natural way to extend the analysis is to treat the conserved quantities, the $i\bar{c}_i\bar{c}_{i+z}$ or the $ib_i^\alpha b_j^\alpha$ as mean-fields. In applying mean-field theory, it was noted that the ground state energy and static correlators reproduce the exact result [169, 133, 111, 43, 14, 81, 26, 222, 135, 173, 151, 44, 49, 124], but the authors of Ref. [98] argue that mean-field theory fails to capture the exact result.

Although the latter critique may be true, depending on your definition of mean-field theory, a natural self-consistent application of the idea of mean-field theory, time-depnendent mean-field theory (TDMFT), *does* recover the exact result. TDMFT as applied to electrons has been around, under the name time-dependent Hartree-Fock approximation (TDHFA), since Dirac [40, 102, 17], and, more recently, has been used to study lattice Hamiltonians relevant to solids [195, 193, 66]. The general analysis is natural and straightforward [34], and is predicated on the observation that the mean-field approximation requires reference to a state (or density matrix) that is being acted on.

Let us first review the case where the Hamiltonian is number-conserving. For N particles with creation operators $f_i^\dagger$, one computes the self-consistent decoupling of the Hamiltonian

[1] This section is adapted from [34]

and diagonalizes the system into $H(\Theta) = H_0 = \vec{f}^\dagger M_0(\Theta)\vec{f} = \sum_n \epsilon_n \gamma_n^\dagger \gamma_n$ via $\vec{f} = U\vec{\gamma}$ where Θ denotes some mean-field parameters like the density $\langle f_i^\dagger f_i \rangle$, and $\epsilon_n \leq \epsilon_{n+1}$. The ground state wave-function is given by

$$|\Psi(t=0)\rangle = \gamma_1^\dagger \gamma_2^\dagger \cdots \gamma_N^\dagger |0\rangle \tag{2.18}$$

with $|0\rangle$ being the vacuum.

One can then imagine evolving this state under some time-dependent Hamiltonian, $H(\Theta(t)) = \sum_{n,m} f_m^\dagger M_{m,n}(\Theta) f_n$ which depends on the time-dependent values of $\Theta(t)$, and time-evolution over a short time is given by $e^{-iH(\Theta(t))\Delta t}$. Evolution then follows by commuting the infinitesimal time evolution past each of the $\gamma_i^\dagger$

$$\begin{aligned} |\Psi(t+\Delta t)\rangle &= e^{-iH(t)\Delta t}\gamma_1^\dagger(-t)\cdots\gamma_N^\dagger(-t)|0\rangle \\ &= \gamma_1^\dagger(-t-\Delta t)\cdots\gamma_N^\dagger(-t-\Delta t)|0\rangle \end{aligned} \tag{2.19}$$

where $\gamma_i^\dagger(-t-\Delta t) = e^{-iH(t)\Delta t}\gamma_i^\dagger(-t)e^{iH(t)\Delta t} = f_j^\dagger U_{ji}(t+\Delta t)$.

We can compute that $U(t+\Delta t) = e^{-iM(\Theta)\Delta t}U(t)$ and therefore the columns of $U(t)$ satisfy a Schrodinger equation evolving under the single-particle Hamiltonian $M_{n,m}(\Theta)$. It is then straightforward to compute any expectation needed for $\Theta(t)$ by converting to the basis of $\gamma_i^\dagger(-t)$. In practice, $\gamma_i^\dagger(-t)$ is used to compute $\Theta(t)$, which is used to evolve $\gamma_i^\dagger(-t)$ to $\gamma_i^\dagger(-t-\Delta t)$, though methods with higher order error in Δt exist [193, 102].

In order to study the Kitaev model, this method has recently been extended to Majoranas [130, 126, 190]. In that case, number is not a conserved quantity, and the authors of Ref. [130] argue by analogy that the same method would work. Here we rigorously derive *why* this analogy holds and provide an explicit expression for the wave function at time t.

In the Majorana case, we have some Hamiltonian

$$H(M^{(t;\theta_{ij})}) = \frac{1}{4}\sum_{ij} c_i M_{ij}^{(t;\theta_{ij})} c_j \tag{2.20}$$

where M_{ij} is a function of time and MFT parameters θ_{ij} and $c_i^2 = 1$ is a typical Majorana operator. Here $\theta_{ij} = i\langle c_i c_j \rangle$ and is implicitly a function of time. We imagine that any constant term (which can depend on t or θ_{ij}) has been written separately from the Hamiltonian, and that we have $M^T = -M$. The factor of $1/4$ is chosen such that

$$[H(M), H(N)] = H([M,N]) \tag{2.21}$$

as can easily be checked [94]. As above, we introduce rescaled Majoranas $c_i \to \tilde{c}_i\sqrt{2}$ so that $\tilde{c}_i^2 = \frac{1}{2}$ and $\{\tilde{c}_i, \tilde{c}_j\} = \delta_{ij}$. It is still true that $\tilde{c}_i^\dagger = \tilde{c}_i$, and we choose this rescaling because it makes M diagonalizable by a unitary matrix into a complex fermion basis.

At time $t = 0$, we diagonalize $H_0 = \frac{1}{2}\bar{a}^\dagger \Lambda_0 \bar{a}$ where $\tilde{c}_i = U_{0,ij}\bar{a}_j$ for $\bar{a}^T = (a_1, a_2, ..., a_N, a_1^\dagger, ..., a_N^\dagger)$ and $\Lambda_0 = \mathrm{diag}\{E_1, E_2, ..., E_N, -E_1, ..., -E_N\}$ as before. The

ground state is now given by the unique state $|v\rangle$ such that $a_i|v\rangle = 0$. Arguing by analogy, we should expect that the time-evolved state will always be the vacuum of operators $\bar{a}^{(t)} = U(t)^\dagger \vec{\tilde{c}}$ where instantaneously, we evolve the columns of the matrix $U(t)$ via a Schrodinger equation. Noting that infinitesimal time evolution is governed by the quadratic Hamiltonian $H(M^{(t;\theta_{ij})})$, it is clear that

$$\begin{aligned} \bar{a}^{(t+\Delta t)} &= e^{-iH(M^{(t;\theta_{ij})})\Delta t}\bar{a}^{(t)}e^{iH(M^{(t;\theta_{ij})})\Delta t} \\ &= U(t)^\dagger e^{i\Delta t M^{(t;\theta_{ij})}}\vec{\tilde{c}} \end{aligned} \tag{2.22}$$

will annihilate $|v_{t+\Delta t}\rangle = e^{-iH(M^{(t;\theta_{ij})})\Delta t}|v_t\rangle$ where $|v_t\rangle$ is the vacuum for $\bar{a}^{(t)}$. It follows that $U(t+\Delta t) = e^{-i\Delta t M^{(t;\theta_{ij})}}U(t)$ implying, once again, that $U(t)$ satisfies a Schrodinger equation under the single-particle matrix $M^{(t;\theta_{ij})}$ confirming our expectation.

However, this calculation does not fix the phase, and it will be necessary in our case. Using standard results for the expression of the relationship between the vacuum states for two different fermionic bases, and the result of Ref. [97] for the evaluation of $\langle e^{-iH(M^{(t;\theta_{ij})})\Delta t}\rangle$, we find

$$e^{-iH(\mathcal{M}_t)}|v\rangle = \sqrt{\det X}\, e^{\frac{1}{2}(\vec{a}^\dagger)^T F \vec{a}^\dagger}|v\rangle. \tag{2.23}$$

The matrix $e^{-iH(\mathcal{M}_t)} = \prod_n e^{-iH(M^{(t_n,\theta_{ij})})\Delta t}$ is the approximate time evolution operator, and we use the notation $e^{-i\mathcal{M}_t} = \prod_n e^{-iM^{(t_n,\theta_{ij})}\Delta t}$. The matrices $F = -X^{-1}Y$, X, and Y are determined by the change of basis formula between the operators $\bar{a}^{(t)}$ and $\bar{a}$, namely

$$\bar{a}^{(t)} = U^\dagger(t)\vec{\tilde{c}} = U_0^\dagger e^{i\mathcal{M}_t}U_0\bar{a} = \begin{pmatrix} X & Y \\ Y^* & X^* \end{pmatrix}\bar{a}. \tag{2.24}$$

As in Ref. [97], we evaluate $\sqrt{\det X} = \sqrt{|\det X|}e^{-i\phi(t)/2}$ and the sign ambiguity due to $\phi(t) = \arg[\det(X)]$ is avoided by requiring that $\phi(t)/2$ is a continuous function.

Now, evolving $|v\rangle$ proceeds as in the number-conserving case. At any time step, we compute θ_{ij} by rewriting $c_i c_j$ in the $a^{(t)}$ basis and using Eq. (2.23). The θ_{ij} specify the approximate infinitesmial time evolution operator $\mathcal{U}(t+\Delta t, t) = e^{-iH(M^{(t,\theta_{ij})})\Delta t}$, which is then used to find the $a^{(t+\Delta t)}$ basis and contribution to the phase $\phi(t+\Delta t)$. This procedure can straightforwardly be extended to other states beyond $|v\rangle$, an example of which we will see below.

An alternative perspective on the above results comes from considering more carefully the approximate time-evolution operator.

$$\begin{aligned} \mathcal{U}(t,0) = e^{-iH(\mathcal{M}_t)} &= \prod_n e^{-iH(M^{(t_n,\theta_{ij})})\Delta t} \\ &= \exp\left[H\left(\log\left(\prod_n e^{-i\Delta t M^{(t_n;\theta_{ij})}}\right)\right)\right] \\ &= \exp\left[H\left(\log\left(e^{-i\mathcal{M}_t}\right)\right)\right] \end{aligned} \tag{2.25}$$

where the second step follows by the Baker-Campbell-Hausdorff theorem since the $H(M)$ distributes over addition, multiplication, and commutation, and $[M, N]$ is still an antisymmetric matrix with no trace [199]. This calculation justifies our use of the notation $e^{-i\mathcal{M}_t}$ from earlier. It is only, therefore, necessary to be able to compute the θ_{ij} and, instead of evolving the wavefunction, one can just consider updating the time-evolution operator.

We can generalize this procedure to evaluate ground-state time-dependent correlators of the form

$$\langle \mathcal{O}(t)\mathcal{O}\rangle = e^{iE_{\rm MF}t}\langle \mathcal{O}U(t,0)\mathcal{O}\rangle \approx e^{iE_{\rm MF}t}\langle \mathcal{O}\mathcal{U}(t,0)\mathcal{O}\rangle. \tag{2.26}$$

where we have introduced $E_{\rm MF}$ as the mean-field ground state energy. Now, we simply compute θ_{ij} for the state $\mathcal{O}|v\rangle$ and we need a way to evaluate the expression $\langle \mathcal{O}e^{-iH(\mathcal{M}_t)}\mathcal{O}\rangle$ for an arbitrary matrix $\mathcal{M}_t$. If $\mathcal{O}$ is a product over the Majorana operators, we can evaluate these correlators with the following modified versions of Wick contractions. That is, [34, 199, 97]

$$\langle \tilde{c}_1 e^{-iH(\mathcal{M}_t)}\tilde{c}_2\rangle = \sqrt{\det X}(U\tilde{U}^\dagger - UF\tilde{U}^T)_{12} \tag{2.27}$$

$$\begin{aligned}\langle \tilde{c}_1\tilde{c}_2 e^{-iH(\mathcal{M}_t)}\tilde{c}_3\tilde{c}_4\rangle = \sqrt{\det X}\,\Big[&(UU^\dagger - UFU^T)_{12}(\tilde{U}\tilde{U}^\dagger - \tilde{U}F\tilde{U}^T)_{34}\\ &-(U\tilde{U}^\dagger - UF\tilde{U}^T)_{13}(U\tilde{U}^\dagger - UF\tilde{U}^T)_{24}\\ &+(U\tilde{U}^\dagger - UF\tilde{U}^T)_{14}(U\tilde{U}^\dagger - UF\tilde{U}^T)_{23}\Big]\end{aligned} \tag{2.28}$$

where U is the first N columns of U_0, $\tilde{U} = e^{i\mathcal{M}_t}U$, and X and F are defined from Eq. (2.24). These expressions can be straightforwardly derived from the time evolution of the vacuum, Eq. (2.23). They generalize to arbitrary correlators in the obvious way [34, 199].

Application: dynamic spin correlators in the perturbed Kitaev model

To make this process concrete, let us consider the Hamiltonian given above in Eq. (2.17). The presence of the J and Γ term makes the JW transformation unwieldy; consequently, we will use the alternative transformation $2S_i^\alpha = ib_i^0 b_i^\alpha$ [94]. We get

$$\begin{aligned}H = \frac{1}{4}\sum_{\langle ij\rangle_\alpha}\Big[&Kib_i^0b_j^0(ib_i^\alpha b_j^\alpha) + J\sum_\beta ib_i^0b_j^0(ib_i^\beta b_j^\beta)\\ &+\Gamma\sum_{\beta\neq\bar{\beta}\neq\alpha} ib_i^0b_j^0(ib_i^{\bar{\beta}}b_j^\beta)\Big] + \frac{1}{2}\sum_i\sum_\alpha h_\alpha ib_i^0b_i^\alpha.\end{aligned} \tag{2.29}$$

We mean-field decouple all the four Majorana terms in every possible channel.

$$H = H'_{\rm MF} = \underbrace{H_{b0} + H_b + H_h}_{H'_b} + \underbrace{H_C + H'_C}_{H''_C} = \frac{1}{8}\sum_{a,b}\psi_a M_{ab}\psi_b + H''_C \tag{2.30}$$

$$H_{b0} = \frac{1}{4}\sum_{\langle ij\rangle_\alpha}\left[(K+J)\langle ib_i^\alpha b_j^\alpha\rangle + J\sum_{\beta\neq\alpha}\langle ib_i^\beta b_j^\beta\rangle + \Gamma\sum_{\bar\beta\neq\beta\neq\alpha}\langle ib_i^{\bar\beta}b_j^\beta\rangle\right] ib_i^0 b_j^0 = \frac{1}{8}\sum_{i,j} M_{ij}^{b0} b_i^0 b_j^0$$

$$H_b = \frac{1}{4}\sum_{\langle ij\rangle_\gamma}\langle ib_i^0 b_j^0\rangle\left[\Gamma\sum_{\bar\beta\neq\beta\neq\gamma} ib_i^{\bar\beta}b_j^\beta + \sum_\alpha (K\delta_{\alpha,\gamma}+J)\, ib_i^\alpha b_j^\alpha\right] = \frac{1}{8}\sum_{i,j} M_{ij}^{b\alpha} b_i^\alpha b_j^\alpha$$

$$H_C = -\langle H_{b0}\rangle = -\frac{1}{4}\sum_{\langle ij\rangle_\alpha}\left[(K+J)\langle ib_i^\alpha b_j^\alpha\rangle + J\sum_{\beta\neq\alpha}\langle ib_i^\beta b_j^\beta\rangle + \Gamma\sum_{\bar\beta\neq\beta\neq\alpha}\langle ib_i^{\bar\beta}b_j^\beta\rangle\right]\langle ib_i^0 b_j^0\rangle \tag{2.31}$$

$$H_h = \frac{1}{4}\sum_{\langle ij\rangle_\alpha}\left[\sum_\beta (J+K\delta_{\alpha,\beta})\left(ib_i^0 b_j^\beta\langle ib_j^0 b_i^\beta\rangle + ib_j^0 b_i^\beta\langle ib_i^0 b_j^\beta\rangle - ib_i^0 b_i^\beta\langle ib_j^0 b_j^\beta\rangle - ib_j^0 b_j^\beta\langle ib_i^0 b_i^\beta\rangle\right)\right.$$

$$\left. + \sum_{\beta\neq\bar\beta\neq\alpha}\Gamma\left(ib_i^0 b_j^\beta\langle ib_j^0 b_i^{\bar\beta}\rangle + ib_j^0 b_i^{\bar\beta}\langle ib_i^0 b_j^\beta\rangle - ib_i^0 b_i^{\bar\beta}\langle ib_j^0 b_j^\beta\rangle - ib_j^0 b_j^\beta\langle ib_i^0 b_i^{\bar\beta}\rangle\right)\right] + \frac{1}{2}\sum_i\sum_\alpha h_\alpha ib_i^0 b_i^\alpha \tag{2.32}$$

$$H_C' = \frac{1}{4}\sum_{\langle ij\rangle_\alpha}\left[\sum_\beta (J+K\delta_{\alpha,\beta})\left(\langle ib_i^0 b_i^\beta\rangle\langle ib_j^0 b_j^\beta\rangle - \langle ib_i^0 b_j^\beta\rangle\langle ib_j^0 b_i^\beta\rangle\right)\right.$$
$$\left. + \sum_{\beta\neq\bar\beta\neq\alpha}\Gamma\left(\langle ib_i^0 b_i^\beta\rangle\langle ib_j^0 b_j^{\bar\beta}\rangle - \langle ib_i^0 b_j^\beta\rangle\langle ib_j^0 b_i^{\bar\beta}\rangle\right)\right] \tag{2.33}$$

Since all the Majorana's are being intermixed, we introduced $\psi^T = (b_1^0, ..., b_{2N}^0, b_1^x, ..., b_{2N}^x, b_1^y, ..., b_{2N}^y, b_1^z, ..., b_{2N}^z)$. For ease of notation, we will let $(b_i^0, b_i^1, b_i^2, b_i^3) = (b_i^0, b_i^x, b_i^y, b_i^z)$ so that $\psi_{i_\alpha} = b_i^\alpha$ where $i_\alpha = i + 2N\alpha$.

All the expectation values $\langle ib_i^a b_j^b\rangle$ for $a, b \in \{0,1,2,3\}$ are the θ_{ij} from the previous section.[2] We find a self-consistent ground state $a_j|v\rangle = 0$ starting with initial guess of correlators corresponding to the exact solution of the unperturbed model where $\psi = U_0\bar a$ diagonalizes the Hamiltonian. Letting $E_{\rm MF}$ be the ground state energy from mean-field theory, we have

$$S_{ij}^{\alpha\beta}(t) = \langle S_i^\alpha(t) S_j^\beta\rangle = -\frac{1}{4}e^{iE_{\rm MF}t}\langle b_i^0 b_i^\alpha U(t,0) b_j^0 b_j^\beta\rangle. \tag{2.34}$$

We now evolve the state $|\Psi\rangle = c_j b_j^\beta|v\rangle$ in time, and we will need to compute the correlators like $\theta_{jk}^{ab}(t) = i\langle b_i^\alpha b_i^0 b_j^a(t) b_k^b(t) b_i^0 b_i^\alpha\rangle$. We can evaluate these expressions using standard

[2] We use Roman letters to indicate belonging to the set $\{0,1,2,3\}$ and Greek letters to indicate belonging to the set $\{1,2,3\}$.

techniques (i.e. Wick's theorem). We then need to evaluate the expression

$$\begin{aligned} S_{ij}^{\alpha\beta}(t) &= -\frac{1}{4}e^{iE_{\mathrm{MF}}t - i\phi_{C'}(t)}\langle b_i^0 b_i^\alpha e^{-iH_b'(\mathcal{M}_t)} b_j^0 b_j^\beta\rangle \\ e^{-iH_b'(\mathcal{M}_t)} &= \prod_n e^{-i\Delta t H_b'(t_n)}; \qquad \phi_{C'}(t) = \int_0^t ds H_C''(s). \end{aligned} \tag{2.35}$$

where $H_b'(t_n)$ is evaluated using the correlators $\theta_{ij}^{ab}(t_n)$.

Using Eq. (2.28), we have

$$\begin{aligned} S_{ij}^{\alpha\beta}(t) = -\frac{1}{4}\sqrt{\det X}e^{iE_{\mathrm{MF}}t - i\phi_{C'}(t)} \\ \times \Big[(UU^\dagger - UFU^T)_{ii_\alpha}(\tilde{U}\tilde{U}^\dagger - \tilde{U}F\tilde{U}^T)_{jj_\beta} \\ - (U\tilde{U}^\dagger - UF\tilde{U}^T)_{ij}(U\tilde{U}^\dagger - UF\tilde{U}^T)_{i_\alpha j_\beta} \\ + (U\tilde{U}^\dagger - UF\tilde{U}^T)_{ij_\beta}(U\tilde{U}^\dagger - UF\tilde{U}^T)_{i_\alpha j}\Big], \end{aligned} \tag{2.36}$$

where the various matrices are defined above.

There is one additional subtlety, however. In a magnetic field, $\langle S_i^\alpha\rangle$ can develop an expectation. Then, $S^{\alpha\beta}(\boldsymbol{q},\omega) = \tilde{S}^{\alpha\beta}(\boldsymbol{q},\omega) + \delta(\omega)\delta(\boldsymbol{q})\langle S_i^\alpha\rangle\langle S_j^\beta\rangle$. We therefore only really want to calculate

$$\tilde{S}_{ij}^{\alpha\beta}(t) = S_{ij}^{\alpha\beta}(t) - \langle S_i^\alpha(t)\rangle\langle S_j^\beta\rangle. \tag{2.37}$$

If we focus on the first term of Eq. (2.36), we see that it can alternatively be written

$$T_1 = -\frac{1}{4}\langle U^\dagger(0,t)\psi_i\psi_{i_\alpha}\mathcal{U}(t,0)\rangle\frac{\langle\mathcal{U}(t,0)\psi_j\psi_{j_\beta}\rangle}{\langle\mathcal{U}(t,0)\rangle}. \tag{2.38}$$

Remember, though, that $\mathcal{U}(t,0) = e^{-iH_{bc}'(\mathcal{M}_t) - i\phi'(t)} \approx U(t,0)$ is just an approximation for the true time-evolution operator. Using the fact that the ground state should be an eigenstate of $U(t,0)$, we undo the approximation and find $T_1 = \langle S_i^\alpha(t)\rangle\langle S_j^\beta\rangle$. Therefore, $\tilde{S}_{ij}^{\alpha\beta}(t)$ simply involves the last two terms of Eq. (2.36).

If we do not cancel the term exactly, then when computing $\tilde{S}^{\alpha\beta} = (\boldsymbol{q} = 0, \omega)$ in a magnetic field, the small approximation on every site gets amplified by the number of sites. A percent-level error then translates to a large discrepancy.

Recovering the exact solution

At the exactly solvable point $J = \Gamma = \boldsymbol{h} = 0$, it is clear that the three directional flavors of b's decouple and $H_b = \sum_\alpha H_b^\alpha$ can always be diagonalized by the transformation $ib_i^\alpha b_j^\alpha = 1 - 2\chi_{\langle ij\rangle_\alpha}^\dagger\chi_{\langle ij\rangle_\alpha}$; put another way, H_b^α are all diagonal in the bond-fermion basis [12]. We choose the gauge where $\chi_{\langle ij\rangle_\alpha}^\dagger\chi_{\langle ij\rangle_\alpha} = 0$ describing the ground state, meaning that the expectations needed for H_{b0} can be readily evaluated: $\langle v|ib_k^\beta b_l^\beta|v\rangle(t) = 1$, if k and l are connected via a

β bond. When computing the time-evolution operator acting on the state $|\Psi\rangle = b_j^0 b_j^\alpha |v\rangle$, all the expectations remain the same, i.e. $\langle\Psi|ib_k^\beta b_l^\beta|\Psi\rangle = 1$, except that $\langle\Psi|ib_i^\alpha b_j^\alpha|\Psi\rangle\rangle(t) = -\langle v|ib_i^\alpha b_j^\alpha|v\rangle$. Therefore, H_{b0} is the same as the exact Hamiltonian, H_K where one $u_{\langle ij\rangle}^\alpha$ has changed sign.

Due to the absence of a magnetic field, we can break apart the b^0 and b^α parts of Eq. (2.35) giving

$$S_{ij}^{\epsilon\beta}(t) = \frac{1}{4} e^{iE_{\mathrm{MF}}t - i\phi_{C'}(t)} \langle b_i^0 e^{-iH_{b0}(\mathcal{M}_t^{b0})} b_j^0\rangle \langle b_i^\epsilon e^{-iH_b(M_t^b)} b_j^\beta\rangle \tag{2.39}$$

where $e^{-iH_b(\mathcal{M}_t^b)}$ and $e^{-iH_{b0}(\mathcal{M}_t^{b0})}$ have the analogous definition to $e^{-iH_b'(\mathcal{M}_t)}$.

Because $H_b^\alpha(t_n)$ is diagonal in the bond-fermion basis, it is clear the bond-fermions cannot move. Breaking the ground state into a product of the ground states of each of the b^α's we therefore compute

$$\begin{aligned}\langle v_b|b_i^\epsilon e^{-iH_b(M_t^b)} b_j^\alpha|v_b\rangle &= \delta_{\alpha\epsilon}\langle v_{b^\alpha} b_i^\alpha e^{-iH_b^\alpha(\mathcal{M}_t^{b^\alpha})} b_j^\alpha|v_{b^\alpha}\rangle \\ &\times \langle v_{b^\beta}|e^{-iH_b^\beta(\mathcal{M}_t^{b^\beta})}|v_{b^\beta}\rangle\langle v_{b^\gamma}|e^{-iH_b^\gamma(\mathcal{M}_t^{b^\gamma})}|v_{b^\gamma}\rangle \\ &= -i\delta_{\alpha\epsilon} e^{i\phi_{C'}(t)}\langle v_{b^\alpha}|ib_i^\alpha b_j^\alpha|v_{b^\alpha}\rangle.\end{aligned} \tag{2.40}$$

The phase exactly cancels that accumulated from the H_C term because $|\Psi(t)\rangle$ is still an eigenstate of the bond-fermion operators so $ib_i^\alpha b_j^\alpha = \langle ib_i^\alpha b_j^\alpha\rangle$. In the ground state, $\langle b_i^\alpha b_j^\alpha\rangle = 0$ unless i, j are connected by an α bond.

Putting everything together, and noting that E_{MF} is exactly the ground state energy for the Kitaev model, we find that we recover the exact result [12, 97]:

$$\begin{aligned}H_{b0}(t_n) = H_F &= -\frac{1}{2}Kic_ic_j + \frac{1}{4}\sum_{\langle kl\rangle_\alpha} Kic_kc_l \\ S_{ij}^{\alpha\alpha} &= -\frac{i}{4}e^{iE_0t}\langle c_i e^{-iH_Ft} c_j\rangle \\ S_{ii}^{\alpha\alpha} &= \frac{1}{4}e^{iE_0t}\langle c_i e^{-iH_Ft} c_i\rangle.\end{aligned} \tag{2.41}$$

In our approach, the flip of the value of $ib_i^\alpha b_j^\alpha$ in the Hamiltonian for the time-evolution operator, as seen in the exact case [12], occurs because we recompute the mean-field parameters for the state on which the Hamiltonian is acting.

Recovering the flux gap

One further critique of mean-field theory as applied to the Kitaev model is that it fails to reproduce the flux gap as the energy of one bond fermion excitation, as read off of the mean-field Hamiltonian, is four times larger than the flux gap [98]. However, if we consider what changes when we add in excitations, the flux gap is reproduced within the framework of TDMFT. To stay in the physical subspace, we should actually add two excitations [146,

199], but we will consider only single excitations since the argument is simpler and straightforwardly generalized. First, let us consider adding one itinerant Majorana excitation. The Fourier transform nearly diagonalizes H_c, so we know the excitations have the rough form $\gamma_{\boldsymbol{k}}^\dagger = \frac{1}{\sqrt{2N}} \sum_i c_i e^{i\boldsymbol{k}\cdot\boldsymbol{x}_i}$ where $\boldsymbol{x}_i$ is the location of site i. If want to compute $H\gamma_{\boldsymbol{k}}^\dagger|v\rangle$, we need to mean-field decouple H with respect to the state $\gamma_{\boldsymbol{k}}^\dagger|v\rangle$. In the thermodynamic limit, the mean-field parameters will be the same and therefore this state is an approximate eigenstate of H.

If we attempt the same calculation with the state $\chi_{\langle ij\rangle_\alpha}^\dagger|v\rangle$, the mean-field parameters will not stay the same in the thermodynamic limit because $\langle ib_i^\alpha b_j^\alpha\rangle = 1$. When $J = \Gamma = 0$, the state is still an eigenstate of H_b but is no longer an eigenstate of H_c. Therefore, this excitation is not an energy eigenstate.

If we wanted to describe the state with one bond fermion inserted, we would need to search for a different self-consistent mean-field deocupling with $\langle ib_i^\alpha b_j^\alpha\rangle = 1$ and, on all other bonds $\langle kl\rangle_\beta$, $\langle ib_k^\beta b_l^\beta\rangle = -1$. Without any perturbations, this will clearly reproduce the flux gap energy, and, in the presence of perturbations, we can use the self-consistent solution as an initial guess to find how the flux gap changes.

Comparing with augmented mean-field theory

It is worth comparing TDMFT to the augmented mean-field theory approach of Ref. [98]. In order to recover the correct expressions for $S_{ij}^{\alpha\beta}(t)$ the "flip" in the value of $u_{\langle ij\rangle_\alpha}$ occurs due to the anticommutation relations between b_i^α and a newly introduce $\mathbb{Z}_2$ link variable. A series of approximations is needed in order to perform the computation, and the presence of perturbations leads to modifications in how the computation is carried out. In TDMFT, the only approximation is mean-field theory applied self-consistently.

Despite agreeing for the exact case, we will see that these two different approaches predict quite different physics in the presence of perturbations. Furthermore, their approach relies on time evolution being generated by the mean-field Hamiltonian. Combining TDMFT and their approach will lead to disagreement in the exact case.

Finally, Ref. [98] proposes computing $\langle b_i^\alpha H b_i^\alpha\rangle - \langle H\rangle$ in the ground state to find the flux gap, Δ_F. However, it is worth noting that this calculation, when performed using the exact solution, yields $4\Delta_F$, just as you would get in a mean-field calculation without modifications or TDMFT, and not Δ_F as they claim to find with augmented mean-field theory.

The necessity and validity of TDMFT

Although TDMFT clearly is an important starting point for the Kitaev case, the computation of the mean-field parameters at each time step and the exponentiation of $\mathcal{M}_t$ greatly increases the cost of computing dynamical quantities. For other systems, this may make TDMFT impracticable. When, then, is it necessary to apply TDMFT instead of evolving in time under the ground-state mean-field decoupled Hamiltonian?

It depends on why MFT is expected to be valid. There are at least two distinct scenarios: a large coordination number or the mean-fields being approximately conserved quantities. In the former limit, TDMFT is likely unnecessary because only a small number of mean-field parameters will change, which will be suppressed by the large coordination number of unchanged parameters.

To see where the other limit arises, we are, at the highest level, breaking apart interaction terms in the Hamiltonian into non-interacting ones. In general, we break apart four e.g. Majorana terms as

$$\begin{aligned} c_1c_2c_3c_4 - \hat{\delta} = &\langle c_1c_2\rangle c_3c_4 + \langle c_3c_4\rangle c_1c_2 - \langle c_1c_2\rangle\langle c_3c_4\rangle \\ &+ \langle c_1c_4\rangle c_2c_3 + \langle c_2c_3\rangle c_1c_4 - \langle c_1c_4\rangle\langle c_2c_3\rangle \\ &- \langle c_1c_3\rangle c_2c_4 - \langle c_2c_4\rangle c_1c_3 + \langle c_1c_3\rangle\langle c_2c_4\rangle \end{aligned} \tag{2.42}$$

and we ignore $\hat{\delta}$. Notice that $\langle\hat{\delta}\rangle = 0$ for the resulting self-consistent mean-field ground state (since it is quadratic in Majorana's), and MFT would be rigorously valid if $|\langle\hat{\delta}^2\rangle| \ll |\langle c_1c_2c_3c_4\rangle|^2$. In the simplest case where one decoupling channel dominates, we can show

$$\langle\hat{\delta}^2\rangle = (\langle[ic_1c_2]^2\rangle - \langle ic_1c_2\rangle^2)(\langle[ic_3c_4]^2\rangle - \langle ic_3c_4\rangle^2) \tag{2.43}$$

implying that the variance of either ic_1c_2 or ic_3c_4 is small compared to its mean value, and the other's mean-field value is not too close to zero (to ensure $\langle c_1c_2c_3c_4\rangle \neq 0$). Without loss of generality, say that $ic_1c_2 \approx \langle ic_1c_2\rangle$, but this simultaneously implies that ic_1c_2 is an approximately conserved quantity in the ground state of the (full) Hamiltonian since a constant commutes with the Hamiltonian. The reverse direction is also true–namely, if ic_1c_2 commutes with the Hamiltonian, $\langle\hat{\delta}^2\rangle = 0$ and MFT is rigorously valid.

The same argument can be made for the low-energy excited states as well, if MFT is valid for those states. Now when computing a dynamic correlator $\langle\mathcal{O}(t)\mathcal{O}\rangle$, TDMFT will be necessary if and only if $\mathcal{O}$ connects excited states with different values of the constants of motion.

As an explicit example, in the Kiteav model, TDMFT would not be necessary if we compute $\langle c_i(t)c_j\rangle$, but it is necessary for $\langle S_i(t)S_j\rangle$ because the fluxes, the conserved quantities, are changed.

The above calculation additionally points to when TDFMT is rigorously valid. As we have seen above, TDMFT is able to reproduce key features of the exact solution, and we expect that a careful application of it will reproduce any feature since $\langle\hat{\delta}^2\rangle = 0$. In the presence of perturbations, it is not the case that $\langle\hat{\delta}^2\rangle = 0$, but it is possible that for some perturbations it will be small. Additionally, TDMFT has been compared against density-matrix renormalization group methods, which can produce exact results, on small systems and qualitative and semi-quantitative agreement is found [34].

Finally, we are making the mean-field approximation because we cannot solve the model exactly–whether or not this approximation is a good starting point depends on the model. However, TDMFT is a consistent mean-field approach, where we always mean-field decouple the Hamiltonian with respect to the state it is acting on. Any time that mean-field theory is not applied this way implies that the approach is potentially inconsistent.

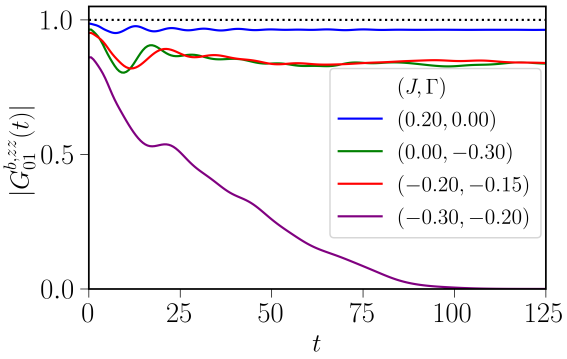

Figure 2.2: We plot $|G_{01}^{b,zz}|$, where sites 0 and 1 are connected by a z bond, for a variety of parameters. For small parameters, the asymptotic value as $t \to \infty$ is not substantially different than the starting value. Only when both J and Γ are large do we see the value drop, which we can interpret as the fluxes becoming mobile [98]. The dashed line indicates the exact ($J = \Gamma = 0$) result, and the system sizes are the same as in Fig. 2.3.

2.3 Inelastic neutron scattering: exact and approximate results

As I discuss in the introduction, to determine whether a spin liquid is present, it is helpful to study the nature of the excitations of the ground state, which requires a probe of dynamic correlators. Our focus will be the dynamic spin-spin correlator $\langle \boldsymbol{S}_i^\alpha(t) \boldsymbol{S}_j^\beta \rangle$ and its Fourier transform $S^{\alpha\beta}(\boldsymbol{q}, \omega)$ as we have already introduced above.

The necessary experimental technique to probe this quantity is inelastic neutron scattering, which, as its name suggests, involves scattering a beam of neutrons off of a material and measuring the resulting neutron's momentum and energy. We can compute the INS signal with [103]

$$I(\boldsymbol{q}, \omega) \sim f(q)^2 \sum_{\alpha,\beta} \left(\delta_{\alpha\beta} - \frac{q_\alpha q_\beta}{q^2} \right) S^{\alpha\beta}(\boldsymbol{q}, \omega). \tag{2.44}$$

where $f(q)$ is the magnetic form factor specified by the atoms around which the spin is localized.

The neutrons probe integer spin excitations. If the system is ordered, the excitations are magnons, and $S^{\alpha\beta}(\boldsymbol{q}, \omega)$ will have sharp features in energy and momentum corresponding to the magnon bands [83]. If the system is a spin liquid, though, the excitations carry non-integer spin and there will be broad features in momentum and energy corresponding to bound states [168].

We will now compute some of the inelastic neutron scattering results for our model Hamiltonian Eq. (2.17).

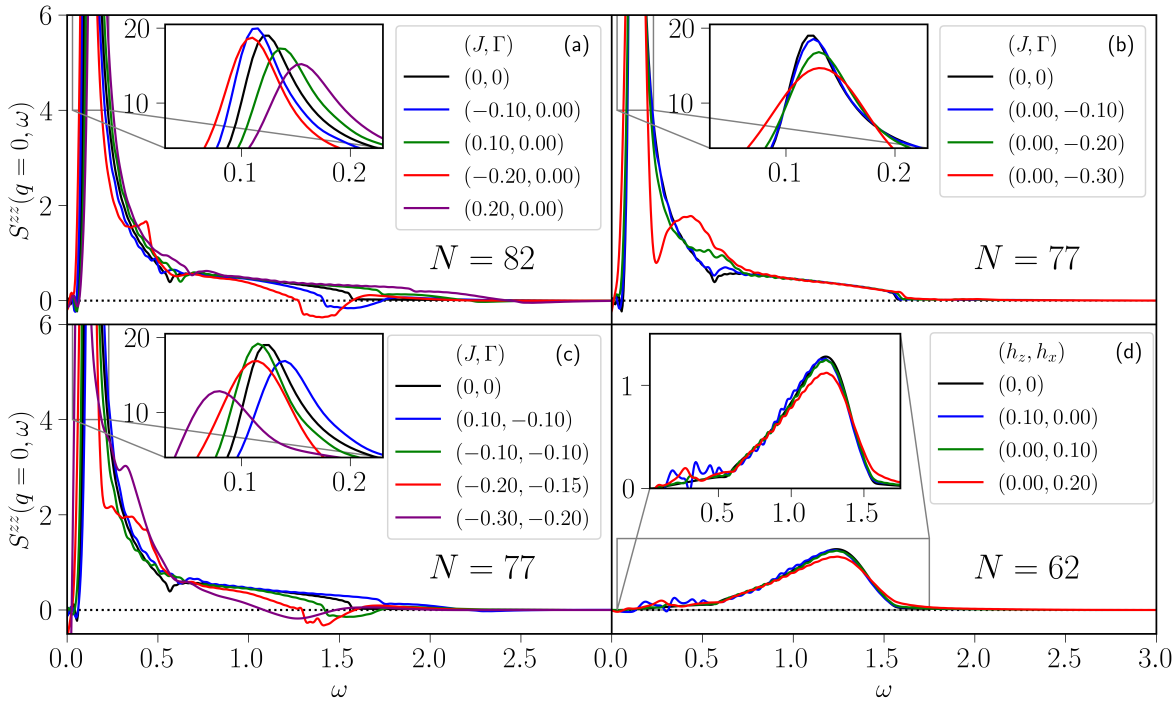

Figure 2.3: (Color online) We plot $S(q,\omega)$ for a variety of parameters for an $N \times N$ unit cell system. The exact result (black line) is the result from a $N = 100$ system and the other parameters have N as specified in each of the panels. In (a), we consider the effect of $J \neq 0$ and $\Gamma = 0$ and see that the primary effect is shifting the features from the exact case to higher or lower energy. In (b), we plot the same but for $J = 0$ and $\Gamma \neq 0$. Beyond some minor adjustments to the peak, the main effect seems to be to smooth out the kink in the exact result. For (c), we see the combination of both $J \neq 0$ and $\Gamma \neq 0$ and, for small parameters, the two effects seem roughly additive. For larger parameters, as the flux becomes mobile, there are more substantial changes. In (d), $J = \Gamma = 0$ but we consider the effect of a magnetic field in the z direction and x direction. Due to a smaller time-step, we are not able to consider as large of systems, and so we multiply $S(\boldsymbol{q},t)$ by a Gaussian of width $\sigma = 60$, equivalent to convolving $S(\boldsymbol{q},\omega)$ with a Gaussian of width $1/\sigma$. The main effect of the magnetic field that we see is a smoothing of the high-energy features, and some oscillatory features at low-ω. We pick Δt small enough to ensure convergence.

Numerical Results

First, we must evaluate $S(q,\omega)$. In the exact case, we have expressions Eq. (2.13), which can be evaluated exactly [97] or numerically using Eq. (2.27). For TDMFT, we must evaluate all expressions numerically.

One limiting factor in the numerics is finite size determined by how long it takes for the Majorana's to travel across the entire system. In the ground state for $\boldsymbol{h} = 0$, the b^0 fermions experience an effective coupling of $\tilde{K} = (K+J)\langle ib_i^z b_j^z\rangle + 2J\langle ib_i^x b_j^x\rangle + 2\Gamma\langle ib_i^x b_j^y\rangle$ giving a speed of $3\tilde{K}/4$ [126]. A system with $N \times N$ unit cells will then experience finite size effects at roughly $t = 4N/(3\tilde{K})$. The only other knob we turn, for a given set of parameters is Δt, and we ensure that decreasing Δt or increasing N has minimal effect on the resulting $S(q,\omega)$ plots. We additionally avoid N that are multiples of 3 to avoid the gapless points in the Majorana spectrum at the K points [94] as they introduce additional complications to the numerics. For additional discussion of convergence, see [34]. The finite size effects makes it most difficult to probe small ω, which are also least accessible for inelastic neutron scattering experiments.

We are primarily interested in computing the results for parameters that we expect to be in the Kitaev phase. For varying J and Γ, we use the phase diagrams produced via exact diagonalization on 24 sites in Ref. [154], however we additionally include points at larger $|J|$ when $\Gamma = 0$ and vice-versa to highlight the effects that each perturbation has individually. We focus on the ferromagnetic Kitaev model ($K = 1$) as it has larger parameter space when $J, \Gamma \neq 0$, but the qualitative results hold true for $K = -1$.

One of the main differences between our results and those of Ref. [98] is the flux remains fixed much longer. There are two ways that we can probe this: either by the time evolution of the mean-field parameter $i\langle b_j^\alpha b_i^\alpha(t) b_j^\alpha(t) b_j^\alpha\rangle$ or by the b^α component of Eq. (2.39), $G_{ij}^{b,\alpha\beta}(t) = \langle b_i^\alpha e^{-iH_b^\alpha(\mathcal{M}_t^b)} b_j^\beta\rangle$. We will use the former as a more direct comparison with Ref. [98].

We plot $G_b^{zz}(t)$ in Fig. 2.2 and see that even for fairly large perturbations, the flux remains fixed. Only when both J and Γ are substantial does the flux begin to move, consistent with the finding of Ref. [183]. [3] Though quite different from the result of Ref. [98], if we modify their approach to be symmetric between the b^0 and b^α, we find the flux remains fixed as well.

We now plot $S(q = 0, \omega)$ in Fig. 2.3 for a variety of parameters. In total, we see that the perturbations have only a small effect on the exact result. The Heisenberg term, J, primarily moves the features to higher or lower ω, depending on the sign, but the overall qualitative features are the same. For Γ, there is more power near the kink in the exact result and less power at the peak. When combined, we get some of both features, but, overall, the results are less dramatically different than those found in Ref. [98].

For the magnetic field, we consider the antiferromagnetic model $K = -1$ as the ferromagnetic model changes phase with $h = 0.042$ [133] when the magnetic field is aligned with one of the three spin-axes. We additionally find it useful to use a higher order time-evolution

[3] It is possible very large J or Γ individually would be enough to make the fluxes mobile, by this definition, but we have checked for $J = 0.4$ and $\Gamma = -0.3$ have not seen this effect

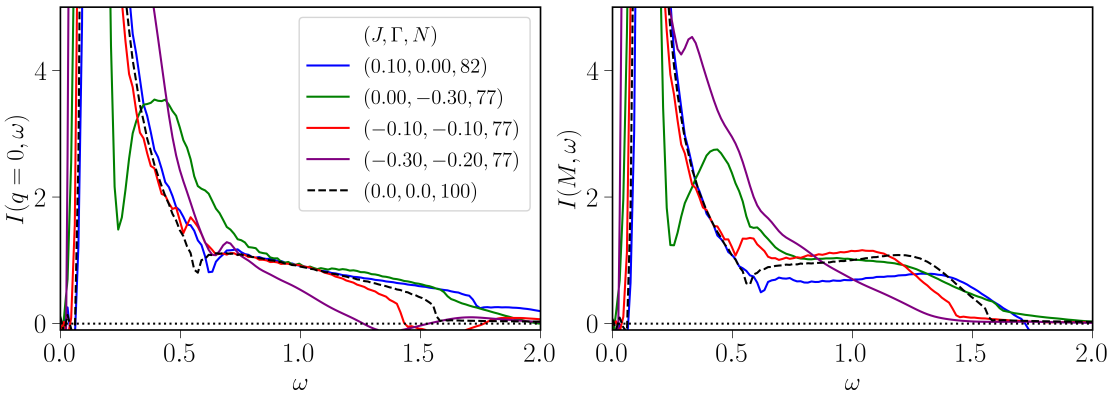

Figure 2.4: (Color online) We plot the INS intensity (in arbitrary units) at the (a) Γ and (b) M point. The legend specifies the size of the system, N used for each parameter set, and when N is not divisible by two, we use the point slightly off of the M point which satisfies the boundary conditions. For smaller perturbations, the features of the exact result are not substantially modified.

scheme [193] as the time-step necessary for convergence needs to be smaller. In the presence of a magnetic field, we can no longer separate the b^0 and b^α Majorana's, and therefore cannot compute G_b.

Due to the smaller time-step, it is difficult to get to as large of system sizes and a well-converged $S(\boldsymbol{q}, \omega)$, so we multiply $S(\boldsymbol{q}, t)$ by a Gaussian of width $\sigma = 60$. In Fig. 2.3(d), we plot some results for a magnetic field in the z or x direction. We still find only small effects, such as a smoothing out of high-energy features and oscillatory features at low-ω.

In order to compute the INS results, we will have an eye towards experiments on α-$RuCl_3$, discussed more in the next chapter. We follow Ref. [103] in averaging over q_z (assuming that $S^{\alpha\beta}(\boldsymbol{q}, \omega)$ is independent of q_z) as is done in the experiment. The exact form of the form factor is not too important; for concreteness, we will use $f(q) = e^{-q^2 c}$ with $c = (0.25 \times 4\pi)^{-2}$ Å^2, relevant to α-$RuCl_3$ [41, 34].[4]

The large peak in the exact case is not greatly modified by the perturbations, but the smaller higher energy features are. Our results appear quite far from available INS data on α-$RuCl_3$ [10, 9] perhaps providing some evidence against the interpretation of its field-induced phase as a Kitaev spin liquid; in particular, though the signal at the Γ point may be well-captured by the Kitaev model, the field-induced phase appears to have little signal at the M point [9], which is inconsistent with our results unless the inclusion of an in-plane magnetic field leads to substantial changes.

[4] As we will discuss in the next chapter, since we are envisioning the Jackeli-Khaliulin mechanism [78] for producing a Kitaev material, the x-, y-, and z-axes for the spins have out-of-plane components, and we account for that when computing $I(\boldsymbol{q}, \omega)$.

2.4 Discussion

In total we have seen numerous approaches for theoretically analyzing the Kitaev spin liquid phase. There are two exact approaches that work in the absence of perturbations, from which we can understand the nature and character of the spin liquid phase. TDMFT serves as a third technique that reproduces the exact results and can be applied in the presence of arbitrary perturbations. The main interpretation for experiments is succinctly stated: even in the presence of perturbations, the INS signal should closely match the Kitaev model if the material is in the Kitaev phase.

As exemplified in Fig. 2.3, though the features of the exact result do change in the presence of perturbation, the signal looks surprisingly similar. This finding is consistent with the idea that the Kitaev phase is stable to small perturbations [64], though it appears inconsistent with the conclusion that the flux gap is fine-tuned [183, 196]. As mentioned above, the flux gap is expected to persist when $\boldsymbol{h} = 0$ and either $J = 0$ or $\Gamma = 0$ [183], and when $J \neq 0$ and $\Gamma \neq 0$, the fluxes acquire a hopping that scales like $J^2\Gamma^2/K^3$. When J and Γ are small, the corresponding time scale is much longer than what we can achieve numerically, and we further see that the low-ω features of the $S(\boldsymbol{q}, \omega)$ are not well-enough converged to make definitive statements about the gap persisting or not (or whether the scaling at low-ω matches Ref. [183]). Our results, however, indicate that whether the flux gap is fine-tuned or not does not imply that the other aspects of the signal are fine-tuned.

TDMFT, as applied to the Kitaev model, still faces several challenges. We used the second exact approach as the starting point, $2S_i^\alpha = ib_i^0 b_i^\alpha$, but we have made no mention of the projection operator P. In applying mean-field theory, many works handle the projection by imposing the constraint on average [81, 26, 222, 135, 173, 151, 44], arguing that the effect is higher-order [49], using a different transformation without a gauge issue [133, 130], or ignoring the effect altogether [124, 111, 169]. In TDMFT, in zero-field, we automatically satisfy the constraints, on average, as expressed in [151]. Still, better accounting for the effect of P may be important in future work.

Furthermore, TDMFT exhibits several "unphysical" features such as $S^{\alpha\alpha}(\boldsymbol{q}, \omega) < 0$. Though this violation of exact bounds is concerning, it is a product of the approximate nature of the approach. Given the small fraction of support that violates the exact bounds, we still believe our conclusions are sound and correct.

In the next chapter we will use TDMFT as well as spin-wave theory, an approach for computing quantities in a spin "solid" state, to discuss the experimental situation of Kitaev materials and α-$RuCl_3$, in particular.

Chapter 3

Thermal transport in Kitaev materials

The Kitaev model, as we discussed in the previous chapter, describes spin-1/2's on the honeycomb lattice with a bond-dependent Ising interaction and remarkably has an exact solution in terms of Majorana fermions [94].[1] The ground state has the fascinating property that in a weak magnetic field the low-energy excitations are anyons [94]; beyond the intrinsic interest, these anyons could form the basis for a topological quantum memory device [134].

While the Kitaev model was first introduced without a clear path towards material realization, Jackeli and Khaliluin discovered one such route in $4d/5d$ transition metals [78]. The key ingredients are 1) an octahedral cage around the atom with the localized spin which shares an edge with adjacent octahedron, 2) strong spin-orbit coupling, and 3) strong enough interactions to lead to a Mott transition [198]. An alternative pathway involving the $3d$ transition metal Co has recently been discovered [116, 115, 165], and there are now several candidate materials for realizing Kitaev physics [209, 192] such as Na_2IrO_3 [217, 33, 74, 180, 181, 25, 117], Li_2IrO_3 [181, 207, 16, 210], $H_3LiIr_2O_6$ [95, 192], $Na_2Co_2TeO_6$ [113], and α-$RuCl_3$ [9, 10, 8, 153, 132].

Due to the convenience of an exact solution, the Kitaev model without additional terms is often used to compare against experiments, for instance in inelastic neutron scattering [10, 8] and thermal Hall effect [88] experiments. However, numerous theoretical studies have proposed effective Hamiltonians for α-$RuCl_3$, which have revealed the Kitaev term [210, 208, 90, 91, 202, 68], but include other terms such as a Heisenberg term and the symmetric off-diagonal exchange term Γ [154, 89, 210, 208].

In other candidate materials the microscopic spin Hamiltonian contains non-Kitaev terms [210, 182, 192] such as Heisenberg and "Γ" terms, as we listed above. These terms are symmetry-allowed and predicted from ab-initio studies [210, 208]. In particular, minimal models for a variety of materials appear to be satisfied by variations on the following Hamil-

[1] This chapter, and particularly Sec. 3.1, Sec. 3.2, and Sec. 3.4, are adapted with permission from Tessa Cookmeyer and Joel E. Moore. "Spin-wave analysis of the low-temperature thermal Hall effect in the candidate Kitaev spin liquid $\alpha - RuCl_3$". In: *Phys. Rev. B* 98 (6 Aug. 2018), p. 060412. DOI: 10.1103/PhysRevB.98.060412. URL: https://link.aps.org/doi/10.1103/PhysRevB.98.060412,

tonian

$$H_{\mathrm{KM}} = J\sum_{\langle ij\rangle} \boldsymbol{S}_i \cdot \boldsymbol{S}_j + \sum_i \boldsymbol{h}\cdot\boldsymbol{S}_i + \sum_{\langle ij\rangle_\alpha} K S_i^\alpha S_j^\alpha + \Gamma \sum_{\beta\neq\bar{\beta}\neq\alpha} S_i^\beta S_j^{\bar{\beta}} + \Gamma' \sum_{\beta\neq\alpha} (S_i^\beta S_j^\alpha + S_i^\alpha S_j^\beta). \quad (3.1)$$

For full generality, we would also allow a Dzyaloshinskii-Moriya (DM) term and further-ranged Heisenberg, Kiteav, Γ, and Γ' terms. It is therefore important to have a general method to compute static and dynamic quantities near the pure-Kitaev model point and to know how such terms modify the exact results. Standard methods such as (infinite) density-matrix renormalization group [50, 51, 123], (non-)linear spin-wave theory [24, 123, 35, 214, 80, 211, 220, 8, 153, 84, 100], variational Monte-Carlo [223], quantum Monte-Carlo [219, 167], Monte-Carlo cluster perturbation theory [152], Landau-Lifshitz dynamics [163], and exact diagonalization [85, 65, 103, 211] have been used to approach this problem. Although the existence of the exact solution allows some techniques to be more powerful [223, 219, 167], there are numerous challenges in applying them to a two-dimensional (2D) quantum mechanical system. Instead, one of the most intuitive starting point for taking advantage of and extending the exact result is mean-field theory (MFT) as the conserved quantities in the original model can be thought of as mean fields. Many papers have used MFT in analyzing the Kitaev model with various perturbations [169, 133, 111, 43, 14, 81, 26, 222, 135, 173, 151, 44, 49, 124], but our development of TDMFT in the previous chapter allows us to compute results that agree with exact results.

In the rest of this chapter, we review the experimental situation for α-$RuCl_3$, and we provide two theoretical analyses of thermal transport data. The first is spin-wave theory, which we will derive below and is applicable to ordered spin systems. In the second analysis, we will apply TDMFT to compute the thermal conductivity of the Kiteav model in a magnetic field. In some sense, TDMFT is complementary to spin-wave theory where the former allows for the treatment of perturbations to the Kitaev spin liquid state and the latter allows for treating fluctuations on top of the classical ordering in ordered spin states.

3.1 Experiments on α-$RuCl_3$

Of the candidate materials listed above, α-$RuCl_3$ has generated significant excitement due to several experimental results. Although at low temperatures, the spins enter into a zigzag ordering, in a large in-honeycomb-plane field a putative spin liquid state emerges [7, 10, 153, 104, 87].

Raman scattering results on α-$RuCl_3$ reveal a continuum of excitations that exists above and below the magnetic transition temperature [164]; after subtracting a bosonic background, the excitations appear to be fermionic, which suggests fractionalization and proximity to a spin liquid state [132]. Experiments with terahertz spectroscopy [114, 203, 212] and electron spin resonance [149] above and below the field induced transition further demonstrate the existence of interesting features in the excitation spectrum that might also be a sign of the Kitaev spin liquid. The continuum of excitations is also seen in inelastic neutron scattering

data and seem to be qualitatively similar to that expected from the pure Kitaev model [8, 10], and linear spin wave theory fits to inelastic neutron scattering data suggest a significant Kitaev interaction [8, 153].

The "smoking-gun" signature of the Kitaev model is a half-quantized thermal Hall effect due to the Majorana bands acquiring a non-zero Chern number in a small magnetic field [94]. Thermal transport on the α-$RuCl_3$ has revealed "unusual" results in both κ_{xx} and κ_{xy} [88, 87, 62, 63, 104]. When compared with the theoretical predictions of the thermal Hall conductivity of a pure Kitaev model at non-zero temperature [131], these results perhaps suggest the Kitaev-magnet nature of α-$RuCl_3$. Additionally, in the case of a large in-plane magnetic field, κ_{xy}/T reportedly is quantized at $\pi k_B^2/(12\hbar)$ [87, 218, 20] as would be expected from the pure Kitaev model [94]. However, attempts to reproduce the result have run into considerable sample dependence [215, 39, 107]. Furthermore, recent work has seen intriguing features of κ_{xx} in a magnetic field, which at first appeared to have a quantum oscillation-like dependence on the magnetic field [38] but further studies suggest the oscillations are due to a sequence of magnetic field transitions [187, 108, 19].

In total, the experimental situation for α-$RuCl_3$ remains complicated and marred by sample-dependent quantities. Furthermore, as we mention above, our above TDMFT results appear inconsistent with α-$RuCl_3$ being in a Kitaev spin liquid phase. It is still worth investigating what aspects of the thermal transport signatures either are supportive or challenging of the Kitaev spin-liquid interpretation. In the subsequent sections, we will compute thermal Hall conductivity in the ordered phase, to be compared with the results of Ref. [88] to constrain the effective Hamiltonian, and we will set up the computation of the longitudinal thermal conductivity for the Kitaev model in a magnetic field to be compared, qualitatively, with Refs. [38, 187, 108, 19].

3.2 Thermal transport from spin-wave theory

As we discussed in the previous section, α-$RuCl_3$ is not, by itself, a spin liquid. Its low-temperature state has ordered moments. In fact, due to the presence of other terms besides the Kitaev one in the Hamiltonian, it is not uncommon for the candidate materials to be ordered. In this regime, we can apply spin-wave theory, a standard technique allowing for a systematic expansion around the classical ordered state.[2].

Spin wave theory: the general approach

Let us consider a general spin Hamiltonian, which for simplicity, we will restrict to involving two-spin terms only

$$H = \sum_{i,j,\alpha,\beta} S_i^\alpha T_{ij}^{\alpha\beta} S_j^\beta. \tag{3.2}$$

[2]For a thorough introductory reference, see Ref. [83]

where i, j are site indices and $\alpha, \beta \in \{x, y, z\}$ are direction indices. The only restriction on T_{ij} is translation invariance $T_{i+a,j+a} = T_{ij}$. If we interpret these spins as vectors, we can find the classical lowest energy state for this Hamiltonian. The classical solution can be determined e.g. numerically using minimization algorithms and trying many different configurations and sublattice sizes. The solution will have M sublattices, which form a (potentially) larger unit cell, and the spins will point in directions that we specify with the polar coordinate angles ϕ_m and θ_m for $m \in \{1, 2, ..., M\}$.

Spin-wave theory gives us a systematic expansion to compute beyond the classical solution. We first introduce rotated spin variables

$$\begin{aligned} \boldsymbol{S}_i &= R(\theta_i, \phi_i)\boldsymbol{\Omega}_i \\ R(\theta, \phi) &= \begin{pmatrix} \cos(\theta)\cos(\phi) & -\sin(\phi) & \sin(\theta)\cos(\phi) \\ \cos(\theta)\sin(\phi) & \cos(\phi) & \sin(\theta)\sin(\phi) \\ -\sin(\theta) & 0 & \cos(\theta) \end{pmatrix} \end{aligned} \tag{3.3}$$

such that $\boldsymbol{\Omega}_i \to (0, 0, S)$ gives the classical solution. The Hamiltonian can then be written

$$\begin{aligned} H &= \sum_{i,j,\alpha,\beta} \Omega_i^a Q_{ij}^{ab} \Omega_j^b \\ Q_{ij} &= B^T R(\theta_{\mathcal{X}(i)}, \phi_{\mathcal{X}(i)})^T T_{i,j} R(\theta_{\mathcal{X}(j)}, \phi_{\mathcal{X}(j)}) B \\ B &= \begin{pmatrix} \frac{1}{2} & \frac{1}{2} & 0 \\ \frac{1}{2i} & -\frac{1}{2i} & 0 \\ 0 & 0 & 1 \end{pmatrix} \end{aligned} \tag{3.4}$$

where $\mathcal{X}(i)$ returns the sublattice label for site i, $a, b \in \{+, -, z\}$, and the B matrix converts from the x, y, z spin basis to the $+, -, z$ basis.

Now, we represent $\boldsymbol{\Omega}_i$ in terms of Holstein-Primakoff bosons

$$\begin{aligned} \Omega_i^z &= S - b_i^\dagger b_i \\ \Omega_i^- &= b_i^\dagger \sqrt{2S - b_i^\dagger b_i} \\ \Omega_i^+ &= \sqrt{2S - b_i^\dagger b_i}\, b_i. \end{aligned} \tag{3.5}$$

This transformation respects the commutation relation of the spins but comes with the added restriction that $b_i^\dagger b_i \leq 2S$.

We can now do an expansion in $b_i^\dagger b_i/(2S)$, whose smallness is a self-consistency check. Writing out the first few terms, we get

$$\begin{aligned} H^{(0)} &= S^2 \sum_{i,j} Q_{ij}^{zz} \\ H^{(1)} &= \sqrt{2} S^{3/2} \sum_{i,j} b_i^\dagger (Q_{ij}^{-z} + Q_{ji}^{z-}) + b_i (Q_{ij}^{+z} + Q_{ji}^{z+}) \\ H^{(2)} &= S \sum_{i,j} 2(b_i b_j^\dagger Q_{ij}^{+-} + b_i^\dagger b_j Q_{ij}^{-+} + b_i b_j Q_{ij}^{++} + b_i^\dagger b_j^\dagger Q_{ij}^{--}) - b_i^\dagger b_i (Q_{ij}^{zz} + Q_{ji}^{zz}) \end{aligned} \tag{3.6}$$

The $\mathcal{O}(S^2)$ term will recover the classical energy, and, alternatively, can be considered a function of the θ_n and minimized accordingly. The $\mathcal{O}(S^{3/2})$ vanishes as a self-consistent check that the classical energy is indeed a minimum. Finally, the $\mathcal{O}(S)$ term describes free bosons, termed magnons or spin waves, that describe the low-energy excitations above the ground state. Cutting off the approximation here is termed linear spin-wave theory. Higher order terms in this expansion leads to interactions between the bosons.

In order to diagonalize $H^{(2)}$, we introduce sublattice dependent Fourier transforms. That is, we have M flavors/bands of bosons

$$b_{\boldsymbol{k},m} = \frac{1}{\sqrt{N_u}} \sum_{i:\mathcal{X}(i)=m} e^{-i\boldsymbol{k}\cdot\boldsymbol{x}_i} b_i \tag{3.7}$$

where $\boldsymbol{x}_i$ is the displacement vector to site i, and N_u is the number of unit cells in the system. We then find

$$\begin{aligned} H^{(2)} = 2S \sum_{\boldsymbol{k},m,n} & b_{\boldsymbol{k}m} Q^{+-,(\boldsymbol{k})}_{mn} b^\dagger_{\boldsymbol{k}n} + b^\dagger_{\boldsymbol{k}m} Q^{-+,(-\boldsymbol{k})}_{mn} b_{\boldsymbol{k}n} + b_{-\boldsymbol{k}m} Q^{++,(\boldsymbol{k})}_{mn} b_{\boldsymbol{k},n} + b^\dagger_{\boldsymbol{k}m} Q^{--,(-\boldsymbol{k})}_{mn} b^\dagger_{-\boldsymbol{k}n} \\ & - b^\dagger_{\boldsymbol{k}m} \frac{Q^{zz,(\boldsymbol{0})}_{mn} + Q^{zz,(\boldsymbol{0})}_{nm}}{2} b_{\boldsymbol{k}m} \end{aligned} \tag{3.8}$$

where

$$Q^{ab,(\boldsymbol{k})}_{mn} = \sum_j e^{-\boldsymbol{k}\cdot(\boldsymbol{x}_j + \boldsymbol{r}_n - \boldsymbol{r}_m)} Q^{ab}_{\boldsymbol{r}_m, \boldsymbol{x}_j + \boldsymbol{r}_n} \tag{3.9}$$

where $\boldsymbol{r}_m$ is the location of the mth sublattice within the unit cell, and we use the notation so that $Q^{ab}_{\boldsymbol{x}_i,\boldsymbol{x}_j} = Q^{ab}_{ij}$.

We now average the $\boldsymbol{k}$ and $-\boldsymbol{k}$ terms in this expression, and rearrange to be in terms of $\psi^\dagger_{\boldsymbol{k}} = (b^\dagger_{\boldsymbol{k},1}, b^\dagger_{\boldsymbol{k},2}, ..., b^\dagger_{\boldsymbol{k},M}, b_{-\boldsymbol{k},1}, ..., b_{-\boldsymbol{k},M})$. The Hamiltonian becomes

$$\begin{aligned} H^{(2)} &= S \sum_{\boldsymbol{k}} \psi^\dagger_{\boldsymbol{k}} \underbrace{\begin{pmatrix} \mathcal{A}(\boldsymbol{k}) & \mathcal{B}(\boldsymbol{k}) \\ \mathcal{B}(-\boldsymbol{k})^* & \mathcal{A}(-\boldsymbol{k})^T \end{pmatrix}}_{\mathcal{M}(\boldsymbol{k})} \psi_{\boldsymbol{k}} + \mathcal{C} \\ \mathcal{A}_{mn}(\boldsymbol{k}) &= Q^{+-,(\boldsymbol{k})}_{nm} + Q^{-+,(-\boldsymbol{k})}_{mn} - \frac{1}{2}\delta_{mn} \sum_p Q^{zz,(\boldsymbol{0})}_{mp} + Q^{zz,(\boldsymbol{0})}_{pm} \\ \mathcal{B}_{mn}(\boldsymbol{k}) &= Q^{++,(\boldsymbol{k})}_{mn} + Q^{++,(-\boldsymbol{k})}_{nm} \\ \mathcal{C} &= S \sum_{\boldsymbol{k},m,n} \frac{Q^{zz,(\boldsymbol{0}}_{mn} + Q^{zz,(\boldsymbol{0})}_{nm}}{2} + Q^{+-,(\boldsymbol{k})}_{mn} - Q^{-+,(\boldsymbol{k})}_{mn} \end{aligned} \tag{3.10}$$

Now we can diagonalize the above matrix for each value of $\boldsymbol{k}$. In order to respect the boson commutation relations, we cannot diagonalize this matrix by a unitary. Instead, we must diagonalize it with respect to a paraunitary matrix, $\psi_{\boldsymbol{k}} = \mathcal{T}_{\boldsymbol{k}} \phi_{\boldsymbol{k}}$ that satisfies

$$\begin{aligned} I_{2M} &= \mathcal{T}_{\boldsymbol{k}} \sigma_3 \mathcal{T}^\dagger_{\boldsymbol{k}} \sigma_3 \\ \sigma_3 &= \begin{pmatrix} I_M & 0 \\ 0 & I_M \end{pmatrix} \end{aligned} \tag{3.11}$$

where I_N is the $N \times N$ identity matrix. One approach to numerically completing this task is noting that

$$\frac{1}{2}\psi_{\boldsymbol{k}}^\dagger \mathcal{M}(\boldsymbol{k})\psi_{\boldsymbol{k}} = \frac{1}{2}\phi_{\boldsymbol{k}}\sigma_3 \mathcal{T}_{\boldsymbol{k}}^{-1}\sigma_3 \mathcal{M}(\boldsymbol{k})\mathcal{T}_{\boldsymbol{k}}\phi_{\boldsymbol{k}} = \sum_{m=1}^{M}\omega_{\boldsymbol{k},m}\left(\gamma_m^\dagger\gamma_m + \frac{1}{2}\right) \tag{3.12}$$

where $\phi_{\boldsymbol{k}}^\dagger = (\gamma_{\boldsymbol{k},1}^\dagger, ..., \gamma_{\boldsymbol{k},M}^\dagger, \gamma_{-\boldsymbol{k},1}, ..., \gamma_{-\boldsymbol{k},M})$. This calculations implies that $\mathcal{T}_{\boldsymbol{k}}$ is the matrix of eigenvectors of $\sigma_3\mathcal{M}(\boldsymbol{k})$.

Up to the $H^{(2)}$ order, we are left with a quadratic Hamiltonian, so any quantity should be describable in terms of $\mathcal{T}_{\boldsymbol{k}}$ and the $\omega_{\boldsymbol{k},n}$. The two important quantities we will focus on are the spin reduction and the thermal Hall coefficient. The spin reduction on the ith lattice is given by

$$\Delta S_{0,i} = \langle b_i^\dagger b_i\rangle = \frac{1}{V_{1\mathrm{BZ}}}\int_{1\mathrm{BZ}} d^2k \left(\sum_{j=1}^{2M}|\mathcal{T}_{\boldsymbol{k},ij}|^2 n_{\mathrm{BE}}(|\omega_{\boldsymbol{k},j}|) + \sum_{j=M}^{2M}|\mathcal{T}_{\boldsymbol{k},ij}|^2\right), \tag{3.13}$$

where we have specialized to (quasi)two-dimensional systems, and $n_{BE}(x)$ is the Bose-Einstein distribution and $V_{1\mathrm{BZ}}$ is the volume of the first Brillouin zone. If the spin reduction is small, that is $\Delta S_0/S \ll 1$, LSWT is expected to be valid. The thermal Hall coefficient is given by [122]

$$\begin{aligned}\frac{\kappa_{xy}}{k_B^2 T/\hbar} &= -\frac{1/d_c}{(2\pi)^2}\int_{1\mathrm{BZ}} d^2k \sum_{n=1}^{M}\left(c_2(n_{\mathrm{BE}}(\omega_{\boldsymbol{k},n})) - \frac{\pi^2}{3}\right)\Omega_{nn}(\boldsymbol{k}) \\ \Omega_{nn}(\boldsymbol{k}) &= \left(i\epsilon_{\mu\nu c}\sigma_3\frac{\partial\mathcal{T}_k^\dagger}{\partial k_\mu}\sigma_3\frac{\partial\mathcal{T}_k}{\partial k_\nu}\right)_{nn}.\end{aligned} \tag{3.14}$$

Here, ϵ_{ijk} is the Levi-Civita symbol, d_c is the distance between 2D planes (assuming well separated layers), $\Omega_{nn}(\boldsymbol{k})$ is the Berry curvature of the nth magnon band, and, with $\mathrm{Li}_2(z)$ being the dilogarithm, $c_2(x) = (1+x)(\ln(1+x) - \ln(x))^2 - (\ln x)^2 - 2\mathrm{Li}_2(-x)$.

Notice how κ_{xy} is purely due to the Berry Curvature. None of the bands need to have non-zero Chern number, but they must have non-zero Berry Curvature.

In the next section, we will evaluate κ_{xy} for the model relevant to the α-$RuCl_3$ and other Kitaev materials.

LSWT for Kitaev materials

We now specify the parameters in Eq. (3.1) to perform the calculation. We consider many different parameter sets as have been proposed in the literature, which are summarized in Table 3.1, but we always take $\Gamma' = 0$ even if the model has $\Gamma' \neq 0$. Though there is some experimental disagreement in the g-factor [101, 213], susceptibility measurements [198, 172, 120] give the paramagnetic moment to be $\gtrsim 2\mu_B$, with $S = 1/2$. We therefore fix $g = 2.3$ to

Name	J_1	K	Γ	Γ'	J_2	J_3	K_3	Ref.
HK	-4.6	7.0	–	–	–	–	–	[8]
KΓ	–	-6.8	9.5	–	–	–	–	[153]
1(HKΓJ3)	-1.7	-6.7	6.6	–	–	2.7	–	[210]
2(HKΓJ3)	-5.5	7.6	8.4	–	–	2.3	–	[210]
3(HKΓJ3)	-0.5	-5.0	2.5	–	–	0.5	–	[208]
4(HKΓJ3)	0.1	-5.5	7.6	–	–	0.1	–	[202]
5(HKΓJ3)	-0.3	-10.9	6.1	–	–	0.03	–	[202]
6(HKΓJ3)	-3.5	4.6	6.4	–	–	0.8	–	[90]
(HKΓΓ')	-1	-8	4	-0.95	–	–	–	[90]
HKΓ	-12	17	12	–	–	–	–	[91]
HKΓK3	-1.8	-10.6	3.8	–	–	1.25	0.65	[68]
HKΓJ2	1.2	-5.6	1.0	–	0.3	0.3	–	[213]
7(HKΓJ3)	-0.5	-5.0	2.5	–	–	0.1125	–	this work

Table 3.1: This information is primarily drawn from Table 1 in Ref. [79] with some models added. All values are in meV. For this analysis, we ignore the K_3, J_2 values, which are there for completeness. Some groups propose different models within the same paper depending on the space group symmetry. For the HK and KΓ model, we add a small Γ and J_3 term, respectively to help the numerics.

get the correct order of magnitude as in Refs. [210, 208, 212, 110], and $S = 1/2$. According to Refs. [88, 82], the interplanar distance is $d_c = 5.72$ Å.

The results of our SWT calculation are presented in Figs. 3.1. We have compared our code with the results of Refs. [123, 138] to verify correctness. We have also plotted the data from Ref. [88]. We do not plot 5(HKΓJ3) or HKΓJ2 since the spin wave solution is not stable (i.e. there are complex eigenvalues) above some critical field $\mu_0 H_c < 10$ T.

We see rather poor agreement between the models and the theory. Although most models do predict κ_{xy} of the correct sign, models HK, KΓ, 4(HKΓJ3) do not. Further notice that all models with $K > 0$ predict $\kappa_{xy} \gtrsim 0$.

To investigate why there is such a large discrepancy between the theoretical κ_{xy} and the data of Ref. [88], we try to find a large κ_{xy} in a minimal $J_1 - K - \Gamma - J_3$ model. It is worth noting that there is not much freedom. From Curie-Weiss temperature data $|K| \sim 100$ K $= 8.6$ meV [198, 67], which is similar to the estimate of Ref. [88] and is commonly seen in almost all of the models in Table 3.1. Furthermore, it has been observed that the magnetic moments lie in the ac plane and make an angle of approximately 35° [21], which requires a particular Γ/K. Minimizing the classical energy assuming the moments are in the $[xxz]$ direction, in the $J_1 - K - \Gamma - J_3$ model, we obtain an expression equivalent to one in Ref.

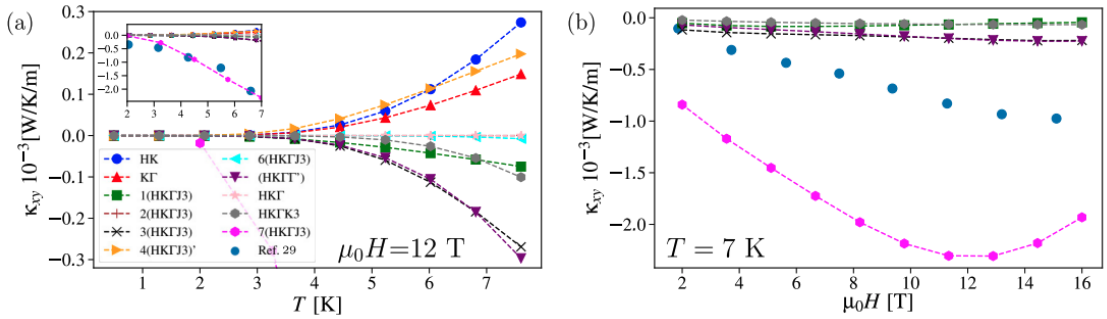

Figure 3.1: We plot κ_{xy} as computed from Eq. (3.14) for the various models in Table 3.1 as a function of (a) temperature and (b) magnetic field. We also plot the data from Ref. [88] as blue dots. The inset of (a) shows a zoomed-out version of the same graph. In (b), models with $\kappa_{xy} \gtrsim 0$ were removed. Our model, which agrees well with the data in (a), does not agree with the data in (b). Since the data of Ref. [88] shows $\kappa_{xy} > 0$ at $T > T_N$ and excitations in the pure Kitaev model contribute to $\kappa_{xy} > 0$ [131], it is expected that at $T \approx T_N \approx 7$ K the contribution from just the magnons should be *below* the experimental data, as is true for our model. We do not plot 5(HKΓJ3) or HKΓJ2 since the zigzag spin wave solution becomes unstable for some critical magnetic field $\mu_0 H < 10$ T. Our proposed model, 7(HKΓJ3) has a large spin reduction $\Delta S_0/S \sim 0.9$ at $T = 7$ K. Copyright © 2018 by the American Physical Society. Reproduced from Ref. [35] with permission.

[79]:

$$\frac{\Gamma}{K} = \frac{2}{\sqrt{2}\tan(\theta) + 1 - \sqrt{2}\cot(\theta)}, \tag{3.15}$$

where $z = \cos(\theta)$ and we assume $x > 0$. Two minima of the classical energy can be found with $K < 0; \Gamma/K \approx -0.82$ and $K > 0; \Gamma/K \approx 0.0065$.

Therefore, for two values of Γ/K with differing signs of K, we have only freedom in J_1 and J_3. $J_1 < 0$ and $J_3 > 0$ help stabilize the zigzag order, so we place these constraints. In the $K > 0$ case with large enough $|J_1|$ to stabilize the zigzag order, we always found $\kappa_{xy} \gtrsim 0$, though a more thorough search of the parameter space might be needed.

In the $K < 0$ case, we instead start with the results of the meta-analysis of *ab initio* models from Ref. [208]: $\Gamma/|K| \approx 0.5$ and $J_1/|K| \approx 0.1$. Fixing $K = -5$ meV as in their proposed model, we scan possible values of J_3. We find that sufficiently low J_3 leads to large enough κ_{xy} to explain all but the lowest temperature point of Ref. [88]. As a representative model, we find that $J_3 = 0.1125$ does well to reproduce the temperature data, as is shown in Fig. 3.1. Note that this model is *representative* not *unique*. Generically, with -5 meV $\gtrsim K \gtrsim -8$ meV, there is a value of $J_3 \gtrsim |K|/200$ that provides an order-of-magnitude fit to the data. For small J_3, though, we find a large spin reduction with $\Delta S_0/S \sim 0.9$; similar to more recent spin-wave approaches to fitting updated inelastic neutron scattering data [163].

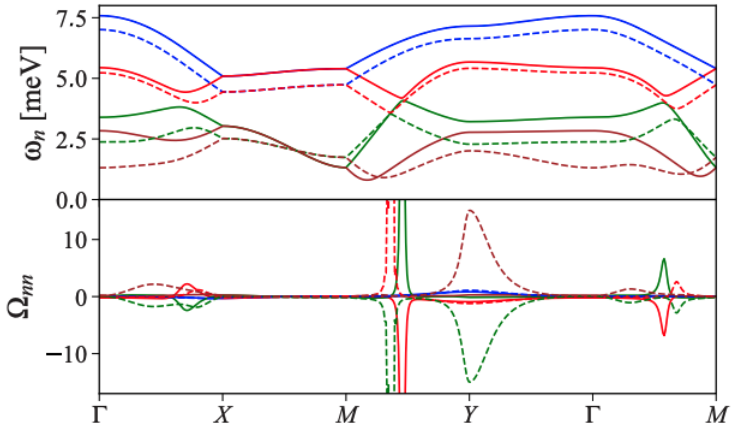

Figure 3.2: We plot the SWT bands, ω_n, and the Berry curvature, Ω_{nn}, for the 3(HKΓJ3) model (solid lines) and the 7(HKΓJ3) model (dashed lines) at $\mu_0 H = 12$ T for various points in the first Brillouin zone (1BZ). The latter model has a much larger κ_{xy} as seen in Fig. 3.1 due to the fact that a) the gap between the lower two bands around the Y point is smaller and at lower energy and b) the gap between the green and red band is at a lower energy. Note that the Berry curvature is largest where the band gap is smallest, and the lower energy means that the effect of $-c_2(n_{\mathrm{BE}}(\omega_n))$ is more significant. (For Ω_{nn}, the path is changed to be slightly inside the 1BZ as opposed to being on the boundary, when applicable.) Reproduced from Ref. [35] with permission.

Further, these models predict much larger κ_{xy} at $T = 7$ K than is measured in Ref. [88] as is seen in Fig. 3.1(b). Because of the proximity to the temperature at which long range order is lost, it is perhaps expected that whatever process is creating a large positive κ_{xy} above $T_N \sim 7$ K is beginning to affect the conductivity at $T = 7$ K. We are not claiming that our model explains the considerable existing data from other experiments (e.g. inelastic neutron scattering, electron spin resonance, etc.); the model is to demonstrate that, theoretically, the thermal Hall effect data could be described solely through SWT while still satisfying the conditions from Ref. [208].

To see why the κ_{xy} increased, we plot in Fig. 3.2 an example of the linear SWT bands and Berry curvature for a particular path through the 1BZ for our model 7(HKΓJ3) vs. the similar model 3(HKΓJ3) on which it is based. It is worth noting that even though the bands are qualitatively similar, the Berry curvature of the two models is quite different. For example, there is a large enhancement of the Berry curvature around the Y point.

The difference in magnitude of κ_{xy} can be understood as follows. The function $f(\omega_n) = -(c_2(n_{\mathrm{BE}}(\omega_n)) - \pi^2/3)$ scaling the Berry curvature in the κ_{xy} integrand essentially serves as a high-pass filter with frequency $\omega_{Hi} = k_B T$. That is, if $\omega_n \ll k_B T$, $f(\omega_n) \sim T/\omega_n$ and if $\omega_n \gg k_B T, f(\omega_n) \sim \pi^2/3$. Since the sum of the Berry curvature integrated over the 1BZ is

zero [122], then $k_BT \gtrsim \omega_n$ for κ_{xy} to be significant. Furthermore, we can see from Fig. 3.2 that the Berry curvature is largest when there is a small gap between the bands. To make the largest possible κ_{xy}, there must be small gaps in the bands at energies $\omega_n \lesssim k_BT$.

Our analysis tends to favor J_3 smaller than has been proposed. As can be seen in plots in Refs. [210, 213], decreasing J_3 tends to move closer to a transition out of the zigzag order. Since smaller band gaps lead to larger Berry curvature, this result makes sense as SWT would predict a magnetic ordering phase transition when a gap in two bands close: assuming the energies of the bands have the form $\omega_\pm = a \pm \sqrt{b}$, a transition occurs at $b = 0$ since $b < 0$ leads to instability of the spin wave solution.

These observations, however, call into question whether the magnon thermal Hall effect is indeed responsible or if the low temperature data is accurate. Denoting $x \equiv \omega_n/T$, we see that $f(\omega_n) = \pi^2/3 - e^{-x}(2 + 2x + x^2) + \mathcal{O}(e^{-2x})$ for $x \gg 1$. Since the mass of the magnons has been estimated to be ~ 2 meV from inelastic neutron scattering [153], κ_{xy}, as predicted from linear SWT, should be exponentially decreasing in $1/T$ at $T \ll 2$ meV ≈ 23 K. All the predictions of magnon thermal Hall effect shown in Fig. 3.1 show such a dependence but the data does not.

Another interpretation of our results is that the models in Table 3.1 are consistent with the data if the magnons are not the dominant source of the κ_{xy} at low temperatures. Phonons could in principle give a larger contribution than ordinarily observed, as has been recently argued by Ref. [107]. To elaborate, in past experiments, although $\kappa_{xy} \lesssim 10^{-4}$ W/K/m, the Hall angle was measured at $\mu_0 H \sim 10$ T to be $\kappa_{xy}/\kappa_{xx} \sim 1 - 5 \times 10^{-4}$ [188, 75]. Since $\kappa_{xx} \sim 2 - 6$ W/K/m for $\alpha-\mathrm{RuCl_3}$ at $T \lesssim 10$ K [88, 104, 62, 63], we would then estimate $\kappa_{xy} \sim 3 \times 10^{-4} \kappa_{xx} \approx 1.2 \times 10^{-3}$ W/K/m, which is of the correct order. Furthermore, a phonon thermal Hall effect would have a power-law temperature dependence as $T \to 0$ which better matches the data than the expected exponential scaling predicted by SWT. Regarding contributions in the ordered phase by Kitaev-like excitations from fluctuations, note that since the pure Kitaev model predicts $\kappa_{xy} > 0$ [131], and the experimental data shows that κ_{xy} switches sign at $T \sim T_N$ [88], these observations would be inconsistent with having fluctuations into the Kitaev model explain the discrepancy between the predicted and observed low temperature κ_{xy}.

Finally, we should emphasize that our results focus on linear SWT. Since the condition $\Delta S_0/S \ll 1$ is not met in a rigorous sense, our results should be treated as a first-order estimate. A more detailed calculation using non-linear SWT keeping interaction terms between the magnons would be an important addition in the future, though such a calculation would be difficult with known techniques.

3.3 Thermal transport from TDMFT

In this section, we focus on predicting κ_{xx} for the Kitaev model in the presence of a magnetic field. For the pure Kitaev model, κ_{xx} has been predicted for both the isotropic and anisotropic case using Monte Carlo methods [131, 148]. In Ref. [131], the effect of a magnetic field is

included; however, to maintain exact solvability, only the term third order in the field is heuristically kept. Perturbatively, the linear term vanishes, but there is a second order term which does not vanish [94].

Instead of relying on a perturbative Hamiltonian, we can use the methods of TDMFT which provide an alternative approach to analyzing the system in a magnetic field. In particular, we are interested in the low-temperature calculation of κ_{xx}/T and whether it reproduces the oscillatory features seen in Ref. [38].

Thermal TDMFT

Before computing in TDMFT, it is useful to review how we would compute a thermal average for the Kitaev model since TDMFT generalizes the exact solution. Any thermal expectation can be written

$$\langle \mathcal{O}_1(t)\mathcal{O}_2\rangle = \frac{1}{\mathrm{Tr}\left[e^{-\beta H}\right]}\sum_m \langle m|e^{-\beta H}\mathcal{O}_1(t)\mathcal{O}_2|m\rangle \tag{3.16}$$

where $|m\rangle$ is any complete set of states. In the Kitaev case, as we discuss in Sec. 2.1, there are an extensive number of conserved quantities which split the spectrum. In the language of the JW transformation, setting the flux configuration, η_i specifies the value of the $i\bar{c}_i\bar{c}_{i+z}$, and then we can trace over the c_i degrees of freedom. We then can write

$$\langle \mathcal{O}_1(t)\mathcal{O}_2\rangle = \sum_{\{\eta_i\}}\frac{1}{Z}\mathrm{Tr}_c\left[e^{-\beta H_K(\{\eta_i\})}\mathcal{O}_1(t)\mathcal{O}_2\right] \tag{3.17}$$

where $H_K(\{\eta_i\})$ is the Kitaev Hamiltonian where the conserved quantities are specified, Tr_c indicates a trace only over the c degrees of freedom, and $Z = \sum_{\{\eta_i\}}\mathrm{Tr}_c\left[e^{-\beta H_K(\{\eta_i\})}\right]$.

For TDMFT to be rigorously valid, as we establish above, there must exist an extensive set of conserved quantities that are precisely a subset of the mean-field parameters. In this case, we can do the same division of the Hilbert space into a summation of the different conserved quantity sectors and a trace over the remaining degrees of freedom. Letting $\{\eta_i'\}$ be this set of self-consistent mean-field distributions, we can write the very similar expression

$$\begin{aligned}\langle \mathcal{O}_1(t)\mathcal{O}\rangle &= \frac{1}{Z}\sum_{\{\eta_i'\}}\sum_{|\gamma_{\{\eta_i'\}}\rangle}\langle\gamma_{\{\eta_i'\}}|e^{(it-\beta)H}\mathcal{O}_1e^{-iHt}\mathcal{O}_2|\gamma_{\{\eta_i'\}}\rangle \\ &\approx \frac{1}{Z}\sum_{\{\eta_i'\}}\sum_{|\gamma_{\{\eta_i'\}}\rangle}e^{(it-\beta)E_{|\gamma_{\{\eta_i'\}}\rangle}}\langle\gamma_{\{\eta_i'\}}|\mathcal{O}_1\mathcal{U}_{|\mathcal{O}_2|\gamma_{\{\eta'\}_i}}(t)\mathcal{O}_2|\gamma_{\{\eta_i'\}}\rangle\end{aligned} \tag{3.18}$$

where the $|\gamma_{\{\eta_i'\}}\rangle$ are the excitation in the non-approximately conserved quantities with energy $E_{|\gamma_{\{\eta_i'\}}\rangle}$, which depend on $\{\eta_i'\}$, and $\mathcal{U}_{\mathcal{O}_2|\gamma_{\{\eta_i'\}}\rangle}$ is the approximate time evolution of the state $\mathcal{O}_2|\gamma_{\{\eta_i'\}}\rangle$ determined with TDMFT.

This expression is significantly unwieldy in practice as for each state, $|\gamma_{\{\eta_i'\}}\rangle$, one must find the self-consistent mean-field solution energy and use TDMFT to time evolve $\mathcal{O}_2|\gamma_{\{\eta_i'\}}\rangle$.

However, since we are interested in low-temperature physics, the calculation can be greatly simplified.

Firstly, due to the flux gap Δ_F [94], there is a temperature $T \lesssim \Delta_F$ below which only the ground state flux sector will contribute. If we are only interested in those low-temperatures, we can ignore all other flux configurations. Secondly, the introduction of a finite number of low-energy excitations of the itinerant c Majoranas will not change the mean-field parameters. This feature arises because the excitations have well-defined momentum and therefore the their effect will be to change the mean-field parameters by a negligible amount in the thermodynamic limit [34]. Therefore, we can approximately replace the sum over the $|\gamma_{\{\eta_i'\}}\rangle$ with a trace over the non-conserved degrees of freedom if we focus on low temperature and we only need to evaluate the approximate time-evolution operator $\mathcal{U}(t)$ using $\mathcal{O}_2|v\rangle$ for $|v\rangle$ the ground state of the system. Finally, we are most interested in the case of the Kitaev model in a magnetic field. In this case, the itinerant c_i and localized $\bar{c}_i$ Majoranas are intermixed. However, the excitations in the $\bar{c}_i$ are gapped in the mean-field Hamiltonian at approximately an energy of $4\Delta_F$ [98]. If we trace over all Majoranas in the ground state, instead of just the c_i, we will incur an error of $e^{-4\Delta_F/T}$, which is parametrically smaller than the error from restricting to the ground state sector. Putting all of these pieces together, we will evaluate thermal correlators at $T \lesssim \Delta_F$ as

$$\langle \mathcal{O}_1(t)\mathcal{O}\rangle \approx \frac{1}{\mathrm{Tr}\left[e^{-\beta H_{\mathrm{MF},0}}\right]}\mathrm{Tr}\left[e^{(it-\beta)H_{\mathrm{MF},0}}\mathcal{O}_1\mathcal{U}_{\mathcal{O}_2|v\rangle}(t)\mathcal{O}_2\right] \tag{3.19}$$

where the trace is over all Majorana degrees of freedom and $H_{\mathrm{MF},0}$ is the mean-field Hamiltonian decoupled with respect to the ground state.

We should verify numerically the presence of the flux gap and the negligible change in the mean-field parameters away from the Kitaev point. If we want to account for the scale between Δ_F and $4\Delta_F$, we can further include a similar expression for the two-flux sectors, but the number of approximate time-evolution operators that will need to be evaluated will then scale with the system size.

Evaluation of thermal transport

From one version of the Kubo formula, we are able to compute κ_{xx} via [148]

$$\kappa_{\alpha\alpha} = \frac{\beta}{2\omega V}(1-e^{-\beta\omega})\int_{-\infty}^{\infty} dt e^{i\omega t}\langle J_\alpha(t)J_\alpha\rangle. \tag{3.20}$$

In this writing, we only need to compute the time-dependent current-current correlator at finite temperature, which we can achieve with TDMFT as described above.

An algorithmic way to derive the current operator is to first assume open boundary conditions, and then

$$J_\alpha = i[H, P_\alpha] \tag{3.21}$$

where P_α is the energy polarization operator given by

$$\boldsymbol{P} = \sum_{i,j} \frac{\boldsymbol{r}_i + \boldsymbol{r}_j}{2} h_{ij} \tag{3.22}$$

if $H = \sum_{i,j} h_{ij}$. In our case, $h_{ij} = -K \sum_{j:j\in\langle ij\rangle_\alpha} S_i^\alpha S_j^\alpha + \delta_{ij} \sum_\beta h_\beta S_i^\beta = K \sum_{j:j\in\langle ij\rangle_\alpha} i c_i c_j b_i^\alpha b_j^\alpha + i\delta_{ij} \sum_\beta h_\beta c_i b_i^\beta$. We therefore get the current operator to be

$$\boldsymbol{J} = \sum_{i,\alpha\beta\gamma} \sigma_i \boldsymbol{\beta} \epsilon_{\alpha\beta\gamma} \left(-2K^2 S^\alpha_{i+\sigma_i\boldsymbol{\alpha}} S^\beta_{i+\sigma_i\boldsymbol{\beta}} S_i^\gamma + h_i^\alpha S^\beta_{i+\sigma_i\boldsymbol{\beta}} S_i^\gamma \right) \tag{3.23}$$

where $\alpha, \beta, \gamma \in \{x, y, z\}$ and the vectors $\boldsymbol{x}$, $\boldsymbol{y}$, and $\boldsymbol{z}$ connect the A sites of the honeycomb to the B sites along the named bonds. Furthermore $\sigma_i = \pm 1$ depending on whether i is in the A sublattice (1) or B sublattice (-1). Notice this has terms that flip the flux configuration now, meaning we should use [34, 97, 98, 199].

In order to handle an arbitrary field, we substitute $S_i^\alpha = i b_i^0 b_i^\alpha$ into Eq. 3.23 and make use of $D_i = b_i^0 b_i^x b_i^y b_i^z = 1$ to find

$$\boldsymbol{J} = \sum_{\langle\langle ij\rangle\rangle_{\alpha\beta}} \boldsymbol{R}_{ij} 2i b_i^0 b_j^0 b_i^\alpha b_k^\alpha b_j^\beta b_k^\beta + \sum_i h_i^z (\sigma_i \boldsymbol{x} b^0_{i+\sigma_i\boldsymbol{x}} b_i^0 b^x_{i+\sigma_i\boldsymbol{x}} b_i^y - \sigma_i \boldsymbol{y} b^0_{i+\sigma_i\boldsymbol{y}} b_i^0 b^y_{i+\sigma_i\boldsymbol{y}} b_i^x) \tag{3.24}$$

where k is the intermediate site connecting i to j and i (j) and k are connected via an α (β) bond and $\boldsymbol{R}_{ij}$ is the vector from i to j. Although there appear to be many terms, each necessitating their own TDMFT computation, we can reduce the number with symmetry. Due to translation symmetry, A and B sublattice symmetry, and $x \leftrightarrow y$ symmetry (if $h^x = h^y$), there are only three prototypical terms:

$$\boldsymbol{T}_1 = (\boldsymbol{y} - \boldsymbol{x}) 2i b_i^0 b_j^0 b_i^x b_k^x b_j^y b_k^y; \qquad \boldsymbol{T}_2 = (\boldsymbol{y} - \boldsymbol{z}) 2i b_i^0 b_j^0 b_i^y b_k^y b_j^z b_k^z \qquad \boldsymbol{T}_3 = h_i^z \boldsymbol{x} b^0_{i+\sigma_i\boldsymbol{x}} b_i^0 b^x_{i+\sigma_i\boldsymbol{x}} b_i^y. \tag{3.25}$$

We then have to compute the overlap with all the other terms. Notice that the vector components of each term will not impact the TDMFT calculation, so we can compute both κ_{xx} and κ_{yy} by scaling appropriately. Notice that only the term $\boldsymbol{T}_3$ will require the use of TDMFT since the other two terms do not change the approximately conserved quantities [34], though it is likely a more self-consistent approach to apply TDMFT to all three terms.

One major computational hurtle is that in an arbitrary magnetic field, we will need to contract 14 Majoranas in order to compute the mean-field expectation values and 12 during the TDMFT calculation to compute $\langle J_\alpha(t) J_\alpha \rangle$. The resulting $13!! = 135135$ and $11!! = 10395$ terms, respectively, may make numerical calculation infeasible. In Ref. [38], the most important component of the magnetic field is in the **a** crystal direction, and there can be a component of the field in the **c** direction too. Conveniently, due to the orientation of the spin axes relative to the crystal axes, we can take a magnetic field $h^x = h^y = 0$ and $h^z \neq 0$, which will be at a 45° angle between the **a** and **c** axes. Restricting to only $h^z \neq 0$ will greatly simplify the number of contractions necessary when carrying out the TDMFT calculation.

Evaluation of correlators and parity

Before we are ready to numerically evaluate these expressions, there are two complications. The first is how we evaluate thermal traces. All of the necessary details are in [199]. We can rewrite

$$\begin{aligned}&\mathrm{Tr}\left[e^{H(M)}c_1\cdots c_N e^{H(N)}c_{N+1}\cdots c_{N+M}\right]\\&\quad=\sum_{i_1,\ldots,i_N}(e^N)_{1i_1}\cdots(e^N)_{N,i_N}\mathrm{Tr}\left[e^{H(M)}e^{H(N)}c_{i_1}\cdots c_{i_N}c_{N+1}\cdots c_{N+M}\right].\end{aligned}\tag{3.26}$$

We can then use $e^{H(M)}e^{H(N)}=e^{\log(e^Me^N)}$ and, using the notation where $\langle e^{H(M)}\mathcal{O}\rangle_{\mathrm{Tr}}=\mathrm{Tr}[e^{H(M)}\mathcal{O}]/\mathrm{Tr}[e^{H(M)}]$ [199]

$$\begin{aligned}\langle e^{H(M)}c_1c_2\cdots c_N\rangle_{\mathrm{Tr}}&=2\mathcal{M}_{12}^{-1}\langle e^{H(M)}c_3\cdots c_N\rangle_{\mathrm{Tr}}\\&\quad-2\mathcal{M}_{13}^{-1}\langle e^{H(M)}c_2c_4\cdots c_N\rangle_{\mathrm{Tr}}+\ldots+2\mathcal{M}_{1N}^{-1}\langle e^{H(M)}c_2c_3\cdots c_{N-1}\rangle_{\mathrm{Tr}}\end{aligned}\tag{3.27}$$

for even N and where $\mathcal{M}=1+e^M$. Finally, we simply need $\mathrm{Tr}\left[e^{H(M)}\right]=\sqrt{\det(1+e^M)}$.

The second major complication is parity. The projector to the physical sector $P=\prod_i(1+D_i)/2$ takes care of any gauge complications. Since $D_i^2=1$, we can arrange $P=(1+\mathcal{D})(\sum'_{\{i\}}\prod_{j\in\{i\}}D_j)$ where $\sum'_{\{i\}}$ is a restricted sum including only either the set $\{i\}$ or $\{1,2,\ldots,\mathcal{N}\}\backslash\{i\}$ (where $\mathcal{N}$ is the number of sites). As explained in [199, 34], unphysical states correspond to when $\mathcal{D}=\prod_{i=1}^{2N}c_ib_i^xb_i^yb_i^z=-1$, which are projected out by P. We can take this into account by following [199].

For all other terms in P, besides $(1+\mathcal{D})$, a massive simplification occurs in the case where $h_x=h_y=0$. We can note that each D_i will change the occupation of the x and y bond fermions making the state orthogonal to the original [12, 34]. The only exception is if we have a collection of D_i along sites that travel all the way around the system and therefore there are no dangling x or y bonds. In this case, though, there must be $\sim\sqrt{\mathcal{N}}$ dangling z bond-fermions since we can't have the collection of all sites since we have pulled out $\mathcal{D}$. Although not strictly orthogonal to the original, when we imagine computing the expectation, we will end up contracting all but a fixed number of these $c_ib_i^z$ Majoranas with each other. All of those contractions scale with h_z, so if $h_z<1$, these terms do not contribute in the thermodynamic limit.[3]

Numerical implementation

In future work we will numerically evaluate these expressions. If we estimate $K\sim 5$ meV, as is relevant for α-$RuCl_3$, the flux gap will be $\Delta_F=0.065\times K=0.325$ meV corresponding to $T=4$ K. In Ref. [38], they go to temperatures of about $T/K\approx 0.0065$, which is well below

[3] Alternatively, if we use the JW transformation, there are no complications with parity. We are unable to use periodic boundary conditions, however, but this fact further implies that the effect of the gauge transformation, besides projecting out unphysical states, must vanish in the thermodynamic limit.

the gap. Therefore, we will take $T = \Delta_F/10$. As we mention above, we will need to verify that the gap persists even in the presence of a magnetic field.

One of the likely biggest hurdles will be the convergence at low ω. It is important to remember that the order of limits should be $\mathcal{N} \to \infty$ and then $\omega \to 0$ [5]. Being at finite temperature, though, seems like it will help in convergence [199] as compared to the zero-temperature INS calculations carried out above.

We will carry out the calculation for both a ferromagnetic and antiferromagnetic Kitaev interaction. If we ignore that we are outside the rigorous range of validity, we can also apply the same approach to the intermediate spin-liquid state seen in the antiferromagnetic Kitaev model [130, 225, 65]. In this way, we can probe the behavior of κ_{xx} as the system moves through successive phase transitions, which has been put forth as a non-exotic explanation for the oscillations in Ref. [38].

3.4 Discussion

Due to the clear experimental implication of the single Majorana edge mode predicted in the Kitaev spin liquid [94], thermal transport experiments in α-$RuCl_3$ are perhaps the most direct avenue for confirming the presence of a Kitaev spin-liquid phase. However, the experimental situation is not so clear cut since some experiments claim to detect a quantized plateau [87, 218, 20] while others do not [215, 39, 107]. Future experiments might consider other geometrical set ups such as an interferometry set up [96] or one similar to the set up used to confirm the non-abelian anyonic nature of the $\nu = 5/2$ fractional quantum Hall state [11].

Nevertheless, even current thermal transport experiments can provide important insights. In this chapter, we saw that a SWT calculation is able to capture the low-temperature thermal Hall effect data and provide a candidate approximate Hamiltonian. It is worth noting that exact diagonalization studies of similar Hamiltonians fail to predict a spin liquid phase where the experiments purportedly measure one [56, 211], perhaps adding more evidence against the interpretation of α-$RuCl_3$ as a Kitaev spin liquid. In the future, my TDMFT approach will allow us to calculate the longitudinal thermal transport predicted from the Kitaev model in the presence of a magnetic field to be compared with recent experiments [38].

Chapter 4

$CeCoIn_5$ and an exotic critical point

Starting in this chapter, we move away from spin liquids and α-$RuCl_3$, and we instead begin to focus on our second class of quantum materials: heavy fermion materials.[1] As we discussed in the introduction, the properties of heavy fermion materials (HFMs), like their T-linear resistivity near quantum critical points, have been a continued source of fascination, calling fundamental concepts of solid state physics into question [178]. $CeCoIn_5$, a HFM, exhibits remarkably similar properties to high-temperature superconductors [147, 15, 139, 129, 177, 99, 179, 224, 186, 197], including signatures of an underlying quantum critical point (QCP) and a 'strange' metallic phase extending to temperatures well above the superconducting transition temperature. In many of the high-temperature superconductors, the identity of the putative QCP is unclear, and their behavior is difficult to reconcile with conventional theories of quantum criticality. For example, there is often no clear symmetry-breaking phase in proximity, or no clear evidence for fluctuations of a symmetry-breaking order parameter as would be expected of a conventional QCP. This has stimulated theoretical studies of unconventional QCPs that either weakly break symmetry [200, 105], or break no symmetries at all [175]. In this chapter, we argue that $CeCoIn_5$ is proximate to a QCP where the density of itinerant electrons (i.e. the Fermi volume) changes discontinuously, and apparently without symmetry-breaking.

At the microscopic level, HFMs including $CeCoIn_5$, are described by a Kondo lattice model, where a half filled f-electron valence shell from cerium contributes localized spin-1/2 moments that coexist with a sea of itinerant conduction electrons. In the conventional metallic ground state of a HFM, the f-electrons, in spite of being spatially localized, appear to become an integral part of the itinerant metal. In particular, they contribute their full share to the total Fermi volume as prescribed by Luttinger's theorem [137]. This phenomenon occurs through the formation of Kondo singlet correlations between the local f moments and the conduction electrons, which effectively hybridize the f level with the conduction sea.

[1] This chapter is adapted from Nikola Maksimovic et al. "Evidence for a delocalization quantum phase transition without symmetry breaking in CeCoIn5". In: *Science* 375.6576 (2022), pp. 76–81. Reproduced with permission from AAAS.

A long-standing challenge has been to characterize a QCP in which the f-electrons recover their localized character and withdraw from the itinerant Fermi volume. Superficially, the remaining Fermi volume without f-electrons is in apparent violation of Luttinger's theorem. The loss of Fermi volume is therefore conventionally accompanied by a transition to a (antiferromagnetic) spin-density wave state, whereby Luttinger's theorem is recovered in the appropriately folded Brillouin zone associated with translational symmetry breaking [178]. Indeed, in almost all prominent HFMs where such an f-electron delocalization transition has been observed, it is accompanied by translational symmetry breaking [140, 170, 46, 37]. Without symmetry breaking, the only known way to reconcile Luttinger's theorem with localized f-electron charge is to form a fractionalized Fermi liquid [175, 176]. In this theoretically predicted phase, the f-electron charge remains localized to the cerium site, while the spin excitations of the f moments are itinerant and form a neutral Fermi surface [175, 29, 45].

In this chapter, we discuss transport and quantum oscillation measurements of $CeCoIn_5$ with small levels of chemical substitution, and compare the experimental data to the above fractional fermi surface model. The results provide evidence that $CeCoIn_5$ is near an f-electron delocalization critical point induced by small levels of electron-doping. Conductivity calculations in the context of the fractionalized Fermi liquid model are able to qualitatively capture the remarkable behavior of the experimentally measured electrical Hall coefficient, providing indirect evidence for an exotic quantum critical point associated with fractionalization of f-electrons.

4.1 Recent experiments

My collaborators have recently carried out detailed experiments on $CeCoIn_5$ as a function of Sn substitution (electron doping) and Cd substitution (hole doping). The first quantity is the Hall coefficient $R_H = -\rho_{xy}/B$. At large fields, ρ_{xy} becomes completely linear in B and measure the total carrier density. Therefore, $R_H(B \to \infty, T \to 0) = 1/n$ where n is the carrier density. As seen in Fig. 4.1, my colleagues were able to reach the high-field limit and as $CeCoIn_5$ is doped, n seems to rapidly increase.

At the naivest level, as it has been presented above, it appears that some previously localized electrons are suddenly contributing to the conductivity once $CeCoIn_5$ has been slightly electron doped. In such a case, there must be a new feature in the Fermi surface to account for the change in carrier density. By carrying out angle-resolved photo-emission spectroscopy (ARPES), the Fermi surface can be directly mapped, and my colleagues indeed find such a new feature for the electron-doped samples as seen in Fig. 4.2(a)-(b). Remarkably, this feature appears to disappear at a relatively low temperature (compared to the Fermi energy) of $T = 100$K as Fig. 4.2(c) shows.

Beyond ARPES, the new feature is additionally seen in quantum oscillation measurements [121]. Starting from Kondo physics, which is known to be applicable to $CeCoIn_5$, we

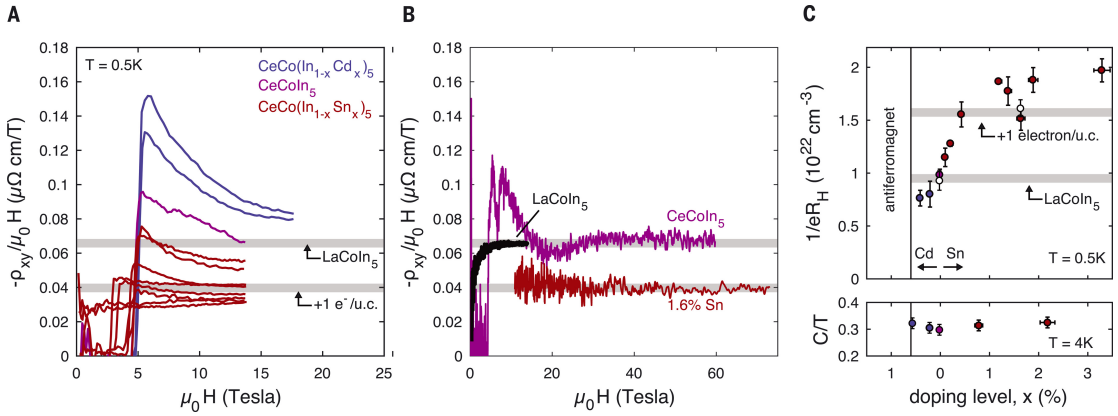

Figure 4.1: (a) Hall resistivity versus magnetic field at 2.5 Kelvin. (b) Net carrier density (n_{tot}) per unit cell, extracted from the linear slope of the Hall resistance between 11-13 Tesla at 2.5 K. (c) $n_{\rm tot}$ exhibits a step when the material is electron-doped. The dashed black line indicates the expected $n_{\rm tot}$ including and excluding the f-electrons, as evaluated from measurements of $LaCoIn_5$ (see Ref. [121]). In the bottom panel, heat capacity coefficient is plotted at 2.5 Kelvin. Error bars are derived primarily from uncertainties in the measurements of geometric factors for transport samples, and sample masses for the heat capacity measurements. Adapted from Ref. [121]. Reproduced with permission from AAAS.

will interpret this data as implying the existence of a Fermi surface reconstruction quantum critical point without symmetry breaking.

4.2 Kondo physics and small-to-large critical point

Fermi surface reconstruction is not uncommon but is usually associated with an AFM transition. The increase in the size of the unit cell and hence decrease of size of the Brillouin zone leads to a restructuring of the Fermi surface to continue to obey Luttinger's theorem [160, 178]. In this case, however, there is no apparent symmetry breaking.

The non-symmetry breaking case was first suggested by Ref. [176]. As discussed at the start of this chapter, the analysis begins with the Kondo lattice model [176, 175, 77, 76]

$$H_{\rm KLM} = \sum_{\boldsymbol{k},\alpha} \epsilon_{\boldsymbol{k}} c^\dagger_{\boldsymbol{k},\alpha} c_{\boldsymbol{k},\alpha} + \frac{J_K}{2} \sum_{i,\alpha\beta} \boldsymbol{S}_i \cdot c^\dagger_{i\alpha} \boldsymbol{\sigma}_{\alpha\beta} c_{i\beta} + J_H \sum_{\langle ij \rangle} \boldsymbol{S}_i \cdot \boldsymbol{S}_j \tag{4.1}$$

where $\alpha, \beta \in \{\uparrow, \downarrow\}$ and $\boldsymbol{\sigma}$ is the vector of Pauli matrices. We now rewrite the spin degrees of freedom in terms of Abrikosov fermions

$$\boldsymbol{S}_i = f^\dagger_{i\alpha} \boldsymbol{\sigma}_{\alpha\beta} f_{i\beta} \tag{4.2}$$

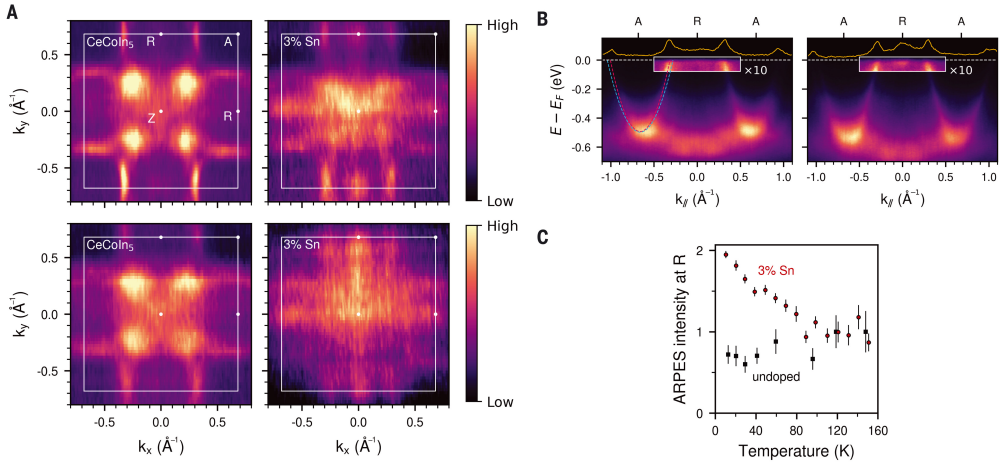

Figure 4.2: (A) Fermi surface maps in pure and 3% Sn-substituted $CeCoIn_5$ at the Brillouin zone top (RZA plane). A new Fermi surface sheet appears at the zone top in the Sn-substituted sample. Each of the four subpanels represents measurements on a different cleave. (B) A-R-A dispersion cuts. Parabolic α and β bands are labeled by red and blue dotted lines, respectively. The new Fermi surface in the Sn-substituted sample is observed as an increase in spectral intensity at the Fermi level at R. The spectral intensity within the white box has been enhanced by a factor of 10 for clarity. E is the energy, E_F is the Fermi energy, and $E - E_F$ denotes the energy relative to the Fermi energy. (C) Comparison of temperature-dependent intensity at the R point normalized to the average value between 120 and 160 K. Adapted from Ref. [121]. Reproduced with permission from AAAS.

with the constraint of single occupancy [175]. In the standard approach, the spin index α is taken to sum over a large N number of parameters (formally we are envisioning the spins as a representation of $SU(N)$ instead of $SU(2)$) [30]. In that case, we are able to decouple the four-fermion terms in the Hamiltonian in terms of two auxiliary fields b and χ [175]. Importantly, the Kondo lattice interaction is rewritten as an interaction between the b, c, and f:

$$\frac{J_K}{2}\sum_{i,\alpha\beta}\boldsymbol{S}_i\cdot c^\dagger_{i\alpha}\boldsymbol{\sigma}_{\alpha\beta}c_{i\beta}\rightarrow -\sum_{r,\alpha}b_r c^\dagger_{r\alpha}f_{r\alpha}+\text{H.c.}. \tag{4.3}$$

In the large N limit, only the mean-field value of b and χ matter. There is then a QCP where $\langle b\rangle$ changes from a zero to non-zero expectation value. When $\langle b\rangle = 0$ in the FL* phase, the conduction electrons, c, and the f fermions are decoupled and only the c electrons form the Fermi surface. Once $\langle b\rangle \neq 0$ in the FL phase, the f fermions hybridize with the c electrons and form a large Fermi surface and, due to the weak dispersion of the f fermions, the resulting band contains heavy fermions [175].

To analyze this transition in more detail, we move beyond mean-field theory. We allow

b to be a proper bosonic field and the fluctuations of the phase of $\chi = \langle\chi\rangle e^{ia}$ are controlled by an emergent internal gauge field, a [175]. By integrating out the c and f degrees of freedom far from the Fermi surface, the b field will gain a dispersion and will be coupled to the internal gauge field a. The timelike component of a, which used to enforce the single occupancy constraint on just the f field, now enforces the constraint $\sum_{i\alpha} f^\dagger_{i\alpha} f_{i\alpha} + b^\dagger_i b_i = 1$. Our resulting simplified model, then, is

$$H = \sum_{\boldsymbol{k},\lambda\in\{c_\alpha,f_\alpha,b\}} (\epsilon_{\lambda,\boldsymbol{k}} - \mu_\lambda)\lambda^\dagger_{\boldsymbol{k}}\lambda_{\boldsymbol{k}} - \sum_{r,\alpha} b_r c^\dagger_{r\alpha} f_{r\alpha} + \text{H.c.} \tag{4.4}$$

with the internal gauge field connecting b and f and enforcing the constraint. The quantum critical point is signified by the condensation of the bosonic field, which occurs as its chemical potential, μ_b, is tuned [175].

This scenario is similar to an approach used to study the Hubbard or t-J model [77, 76]. One of the key differences is that a transition in those models arises due to the tuning of the number of bosons and not the tuning of the boson chemical potential [175] However, in both cases, the b and f species obey the Ioffe-Larkin composition rule [77, 76]

$$\boldsymbol{\sigma}^{-1}_{bf} = \boldsymbol{\sigma}^{-1}_f + \boldsymbol{\sigma}^{-1}_b. \tag{4.5}$$

That is, the conductivity of the b and f add in series and not in parallel. This rule is a straightforward consequence of the internal gauge field's enforcement of the constraint since the b and f currents must be equal and opposite [76].

This model and quantum critical point explains the core features of the experiment. The total conductivity of the system is given by $\boldsymbol{\sigma}_c + \boldsymbol{\sigma}_{bf}$. When the bosons are not condensed, only the c electrons contribute to the conductivity since the bosons are bad conductors. When the bosons condense, the f fermions start to contribute to the conductivity hence the rapid increase in the number of carriers seen in Fig. 4.1(c). Additionally, due to the hybridization of the c and f bands, a new feature should appear in the Fermi surface, exactly as seen in quantum oscillation and ARPES [Fig. 4.2(a)-(b)]. The relatively low-energy at which the feature disappears, Fig. 4.2(c), is due to needing to overcome the boson condensation temperature, which is much lower than the Fermi energy.

4.3 Boltzmann calculation of conductivity

As the discussion in the previous section makes clear, this model captures the key aspects of the experiment. One observed feature we have not discussed yet, however, is the low-field R_H data. As seen in Fig. 4.3, there is a low-temperature peak in R_H for small fields that disappears rapidly as a function of doping. In this section, we will see that this feature is naturally explained by the model.

Since we are interested at points near the critical point, we imagine that the bosons are a bad conductor $\sigma^b_{xx} \ll \sigma^c_{xx}, \sigma^f_{xx}$, which implies that the longitudinal conductivity is due

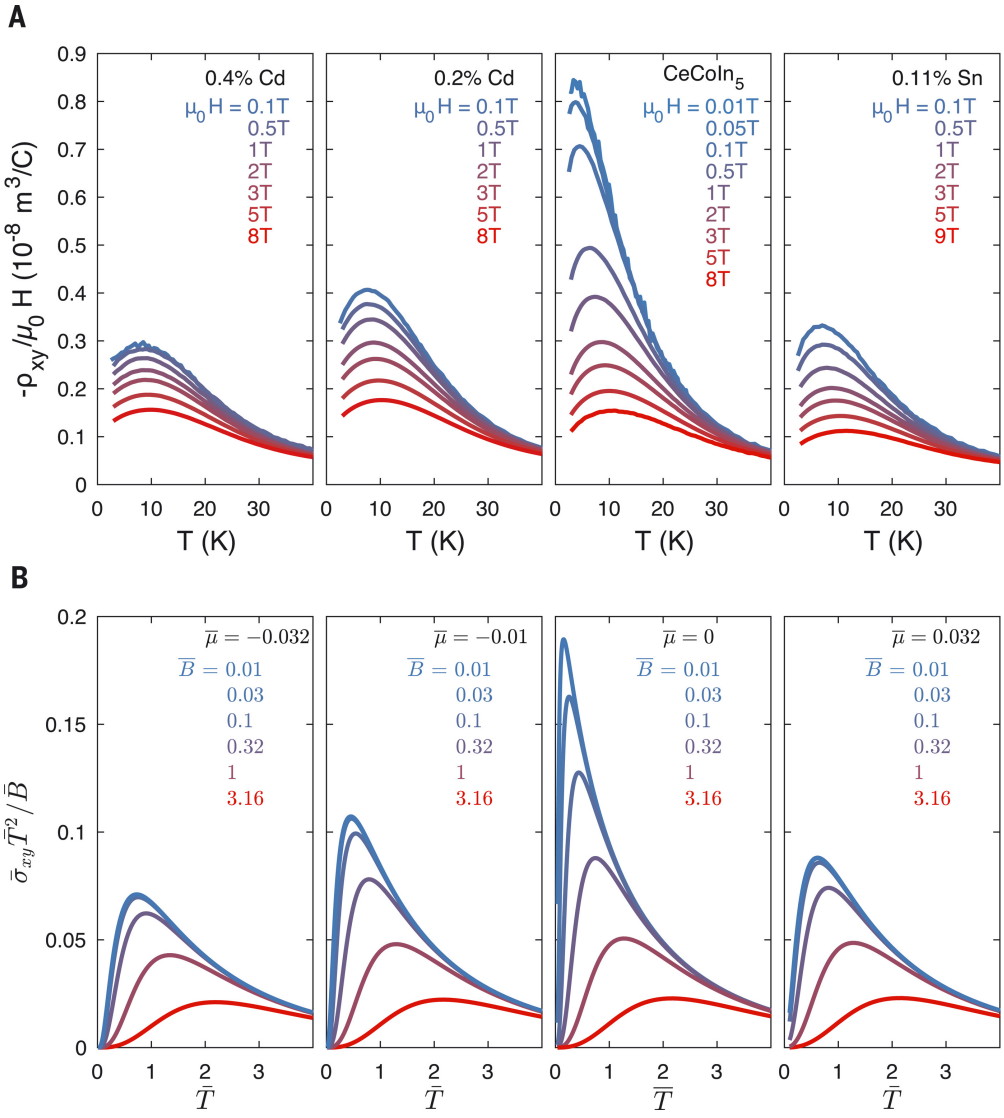

Figure 4.3: (a) Experimentally measured Hall resistivity, divided by the applied magnetic field, for samples with different compositions. Different traces are taken at different applied magnetic fields (0.1, 1, 3, 6, 9 T). Each panel is labeled by the substitution level. (b) The theoretically predicted Hall effect due to bosonic valence fluctuations of the fractionalized Fermi liquid model. Each panel is labeled by the chemical potential in the theory corresponding to the doping level in the experiment, where $\mu < 0$ corresponds to hole-doping and $\mu > 0$ corresponds to electron-doping. Curves labeled by the normalized magnetic field value ($\bar{B} = 0.01$, 0.032, 0.1, 0.32, 1, 3.2) and all theory data includes a parametrization of impurity scattering, $\bar{C} = 4$. Adapted from Ref. [121]. Reproduced with permission from AAAS.

primarily to the conduction electrons. However, we will assume the bosons can substantial contribute to σ_{xy} due to their critical behavior. We will also take the observed $\rho_{xx} \sim T$ as an experimental fact, but in the next chapter, we will discuss a similar model where $\rho_{xx} \sim T$ is predicted from the model.

We consider a semi-classical approximation for the bosonic contribution of the Hall coefficient based on the critical theory of Ref. [175] as described above. Due to the Ioffe-Larkin composition rule, $\boldsymbol{\sigma}^{bf} \approx \boldsymbol{\sigma}^{b}$ and therefore the boson and f-electron contribution is approximately given by

$$R_{H,b} = \sigma_{xy}^{bf}\rho_{xx}^2/(\mu_0 H) \sim T^2\sigma_{xy}^{b}/(\mu_0 H), \tag{4.6}$$

where in the last step we substituted the observed $\rho_{xx} \sim T$.

Following Ref. [175], we take the bosons to have a mass m_b and charge $-e < 0$, a dispersion $\epsilon = k^2/(2m_b) - \mu$, and a quartic interaction with strength u. The chemical potential μ is the tuning parameter in the transition at $T = 0$ with $\mu = 0$ corresponding to the critical point. For comparison with the experiment, we expect that μ is proportional to the doping, x. We will solve a semi-classical Boltzmann equation in the relaxation-time approximation for the bosons while holding μ fixed. The number of bosons is consequently *not* constant, as would be expected since the term in the Lagrangian leading to hybridization of the f-spinon and c-electron also leads to the exchange of c-electrons, fermionic spinons and bosons ($c \leftrightarrow f + b$).

The scattering time has two contributions: scattering off of impurities (the dominant source of which is the dopants) and scattering off of low-energy gauge fluctuations. The impurity scattering relaxation time is given by the usual expression $\tau_i^{-1} = n_i v(k)\sigma(k)$ for velocity $v(k)$ scattering cross-section $\sigma(k)$ and impurity concentration $n_i = |\delta|$. We will assume, for simplicity, that $\tau_i^{-1} = n_i K_1 = K|\mu|$ for constants K_1 and K. The gauge-field scattering has relaxation time $\tau_g = A\beta^{3/2}/\sqrt{\beta k^2/(2m_b)}$ as in Ref. [175]. Since the two scattering mechanisms are independent, the total scattering is given by $\tau^{-1} = \tau_i^{-1} + \tau_g^{-1}$.

We now solve the Boltzmann equation in an arbitrary magnetic field. We are imagining a semi-classical calculation, which implies that we do not consider the effect of quantization of the orbitals. From Ashcroft and Mermin, we have the general form [4]

$$\sigma_{\alpha\beta} = e^2 \int \frac{d\boldsymbol{k}}{4\pi^2} v_\alpha(\boldsymbol{k}) \left(-\frac{\partial n_B(\epsilon_{\boldsymbol{k}})}{\partial \epsilon}\right) \int_{-\infty}^{0} dt v_\beta(\boldsymbol{k}'(t)) e^{t/\tau_{\boldsymbol{k}'(t)}} \tag{4.7}$$

where $\epsilon_{\boldsymbol{k}}$ is the dispersion relation, $n_B(\epsilon)$ is the Bose-Einstein distribution, τ is the scattering time, which can depend on the wave number, $\boldsymbol{k}$. The second wave vector, $\boldsymbol{k}'(t)$ has the boundary condition $\boldsymbol{k}'(t = 0) = \boldsymbol{k}$ and otherwise satisfies the semi-classical equation of motion

$$\frac{d\boldsymbol{k}'}{dt} = e\left[\boldsymbol{E}(\boldsymbol{r}, t) + \frac{d\epsilon_{\boldsymbol{k}'}}{d\boldsymbol{k}'} \times \boldsymbol{B}\right] \tag{4.8}$$

where e is the signed charge.

In this case, we have two massive simplifications. Firstly, the isotropic quadratic dispersion allows us to easily solve the classical equation of motion in the presence of an arbitrary

magnetic field. We have

$$\boldsymbol{k}'(t) = k\cos(\omega t + \phi)\hat{x} + k\sin(\omega t + \phi)\hat{y} \tag{4.9}$$

such that $\boldsymbol{k} = k\cos(\phi)\hat{x} + k\sin(\phi)$.

Secondly, the dependence of $\tau_{\boldsymbol{k}}$ only on the magnituede τ_k and the fact that $|\boldsymbol{k}'(t)| = k$ allows us to can carry out the internal integral

$$\bar{v}_x = \frac{1}{\tau_k}\int_{-\infty}^{0} dt v_x(\boldsymbol{k}'(t))e^{t/\tau_k} = \frac{1}{1+\omega^2\tau_k^2}\left(\frac{k_x}{m} + \frac{k_y}{m}\omega\tau_k\right). \tag{4.10}$$

We have used the fact that $\boldsymbol{v} = \boldsymbol{k}/m$ for our dispersion relation.

Plugging in the scattering τ_k, the expression for the velocity, and changing variables, we arrive at the boson contribution to the Hall conductivity

$$\sigma_{xy}^b = -\frac{A^2\omega_c e^2(2m_b)^{3/2}}{6\pi^2 m_b}\beta^{3/2}\int_0^\infty y^{3/2}dy\left[\frac{e^{y+a}}{(e^{y+a}-1)^2}\frac{1}{(\sqrt{y}+C|\mu|\beta^{3/2})^2+\omega_c^2A^2\beta^3}\right] \tag{4.11}$$

where $y = \beta k^2/(2m_b), a = -\mu\beta + \beta\Sigma_b(0,0)$, and $\omega_c = e\mu_0 H/m_b$, and $C = AK$. The self-energy, $\Sigma_b(0,0)$ is given by [175]

$$\Sigma_b(0,0) = \frac{u(2m_bT)^{3/2}}{2\pi^2}\int_0^\infty \sqrt{y}dy\left[\frac{1}{e^{y-\beta\mu}-1} - \frac{1}{y-\beta\mu} + \frac{1}{y}\right]. \tag{4.12}$$

This calculation will certainly break down at the temperature scale where $\mu > 0$ and $\Sigma_b(0,0) \leq \mu$. In a conventional bose liquid this would signal a transition to a superfluid phase of the bosons, which is precluded in our system if the compact $U(1)$ gauge field fluctuations are taken into account. Nevertheless the temperature scale at which $\Sigma_b(0,0) \leq \mu$ still represents a crossover scale below which the boson resistivity is expected to drop sharply, thus our approximations are not valid below that scale. For the small $|\mu|$ we consider below, that crossover temperature is an order of magnitude below the peak of the graph.

We fix $1 = (\bar{u})^{-2} = (u(2m_b)^{3/2}/(2\pi^2))^{-2}$ as setting our energy scale, and we switch to dimensionless parameters: $\bar{T} = \bar{u}^2T, \bar{\mu} = \bar{u}^2\mu, \bar{C} = \bar{u}C, \bar{B} = \omega_c A\bar{u}^3 \propto \mu_0 H$, and $\bar{\sigma}_{xy} = \sigma_{xy}^b/\mathcal{C}$ with $\mathcal{C} = Ae^2(2m_b)^{3/2}/(6\pi^2 m_b)$. We numerically evaluate $\bar{\sigma}_{xy}\bar{T}^2/\bar{B}$ vs. $\bar{T}$ for several choices of parameters $\bar{B}$, $\bar{\mu}$, and $\bar{C}$, and show some plots to compare with the experiment in Figs. 4.3(b).

We notice that the graphs qualitatively capture the critical curves. The temperature of the peak increases and the peak decreases with increasing $|\mu|$ (i.e. increasing doping) or increasing H. The asymmetry of the experiment, where the peak height decays faster for smaller electron doping than hole doping, could be explained by a difference in the value of $\bar{C}$ coming from a difference in scattering off of impurities.

For the critical curve, we can easily evaluate the limiting behavior for large and small T. In the $a \ll 1$ limit, the integrand is dominated by $y \ll 1$. In the $a \gg 1$ limit, we can

approximate $e^{y+a} - 1 \approx e^{y+a}$. We find,

$$\lim_{H\to 0} -\frac{\bar{\sigma}_{xy}(\mu = 0)}{\bar{B}} = \frac{1}{\bar{T}^{3/2}} \int_0^\infty dy y^{1/2} \frac{e^{y+a}}{(e^{y+a}-1)^2} \sim \begin{cases} \frac{1}{\sqrt{a}\bar{T}^{3/2}} & \text{if } a \ll 1 \\ \frac{1}{e^a \bar{T}^{3/2}} & \text{if } a \gg 1 \end{cases}. \tag{4.13}$$

Since $a(\mu = 0) = \bar{T}^{1/2}\zeta$ for ζ an order 1 constant, we see that $|\bar{\sigma}_{xy}| \sim \bar{T}^{-7/4}$ at low temperatures and $|\bar{\sigma}_{xy}| \sim e^{-\zeta\sqrt{\bar{T}}}$ at high temperatures. As we move to $\mu < 0$ and $H \to 0$, the divergence of $\bar{\sigma}_{xy}$ at low $\bar{T}$ will be cut off. Assuming as above that $\rho_{xx} \sim \bar{T}$, it then follows that $R_{H,b} \sim \lim_{H\to 0} \bar{\sigma}_{xy}(\mu = 0)\rho_{xx}^2/\bar{B}$ does not diverge as $\bar{T} \to 0$. Instead, the curve has a peak structure as the $R_{H,b}$ interpolates between the $\bar{T}^{1/4}$ behavior at low $\bar{T}$ and the $e^{-\zeta\sqrt{\bar{T}}}$ behavior at high $\bar{T}$. If on the other hand we assume $\rho_{xx} = \rho_0 + DT$ with a finite zero temperature resistivity ρ_0, then $R_{H,b}$ will diverge as $T \to 0$ at the critical point $\mu = 0$.

4.4 Discussion

As we argued in this chapter, the phenomenology of a Fermi surface reconstruction transition without symmetry breaking [175, 176] captures the essential features of recent experiments on $CeCoIn_5$. We started from a phenomenological description of this transition that, due to universality, should apply in some vicinity of the quantum critical point. T-linearity in $CeCoIn_5$ exists only up to 20 K, about 10 times its superconductivity transition temperature [92]. Due to its absence at large temperatures, it may be the case that the T-linearity is entirely due to the quantum critical point, as opposed to other materials where criticality cannot be the sole explanation [57]. However, the small-to-large Fermi surface transition we have described may be relevant to a recent transition seen in the cuprates, and these two systems bearing the same QCP may explain their similarities [121].

One consequence of our interpretation of $CeCoIn_5$ bearing this QCP is that when hole-doped, in the FL* phase, the localized spins have been fractionalized. When there is symmetry-breaking, these spins antiferromagnetically order, but in this case there is an absence of order. Finding direct evidence for the fractionalization through e.g. INS experiments would further support evidence for this QCP and would also imply that the spins are forming a spin liquid.

A major caveat to our work in this chapter, though, is that we made a series of approximations in analyzing the Hamiltonian, Eq. (4.4), in order to reproduce the features seen in R_H. Notably, we assumed T-linear resistivity for the total longitudinal conductivity, and we used a Boltzmann analysis, which captures only a subset of the diagrams relevant to conductivity. If the f and c Fermi surfaces coincide, T-linearity is expected for this model [145], a scenario which may be favored energetically [1]. Due to the absence of analytic control in this model, it remains a question if our Boltzmann analysis is providing the correct qualitative picture. In the next chapter, we will introduce a similar model where we are able to exactly solve for the conductivity.

Chapter 5

An exactly solvable model of a strongly-coupled critical point

In the introduction, we discussed the ubiquity of strange metal behavior for heavy-fermion compounds near a quantum critical point.[1] Usually, the quantum critical point is related to an antiferromagnetic transition but the above experiments on $CeCoIn_5$ seem to indicate criticality without a magnetic ordering transition. In our semiclassical approach above, we failed to capture the T-linear resitivity and therefore the strange metal phase but instead assumed the T-linearity was present. Furthermore, the approximations we made above are not rigorously controlled making our conclusions questionable.

One possibility of producing strange metal physics, as we discuss briefly in the introduction, is the SYK model. In this chapter, we will introduce a model inspired by Kondo lattice physics that is exactly solvable in the same way as the SYK model. Our model will reproduce the marginal Fermi liquid (MFL) phenomenology, Eq. (1.4), at the critical point while still capturing many of the experimental features that $CeCoIn_5$ exhibits.

Although it is easy to get lost in the calculations since many expressions appear unwieldy, the sketch of the solution is as follows: obtain the Schwinger-Dyson equations, solve them to obtain the exact Green's functions, and use the Kubo formula to compute the conductivity. Due to the large-N limit we consider, there are a finite number of terms for both the Schwinger-Dyson equations and the Kubo formula, which allows us to obtain exact expressions. We can carry out this procedure analytically in certain limits, but for a generic point, we need to evaluate the expressions numerically.

[1] This chapter is adapted with permission from Erik E. Aldape et al. "Solvable theory of a strange metal at the breakdown of a heavy Fermi liquid". In: *Phys. Rev. B* 105 (23 June 2022), p. 235111. DOI: 10.1103/PhysRevB.105.235111. URL: https://link.aps.org/doi/10.1103/PhysRevB.105.235111,

5.1 The model and its solution

As we showed above, the Kondo lattice model can be manipulated to include the interaction between three species of the form

$$H_{\rm KL} \sim g \sum_{r,\sigma} c^\dagger_{r\sigma} f_{r\sigma} b_r + \text{H.c.} \tag{5.1}$$

To make our model reminiscent of SYK physics, we can introduce a large-N number of flavors and make the couplings random

$$H_{\rm SYK,KL} = \sum_{r,ijk,\sigma} g^r_{ijk} c^\dagger_{r\sigma,i} f_{r\sigma,j} b_{r,k} + \text{H.c.} \tag{5.2}$$

where g^r_{ijk} are Gaussian distributed complex random variables that are site dependent, $\langle\langle g^r_{ijk} g^{r'}_{ijk}\rangle\rangle$; the translationally-invariant site-independent disorder model can additionally be solved [1] but is more challenging to analyze away from the critical point. Our model is then described by the following Hamiltonian

$$\begin{aligned} H &= \sum_{\lambda\in\{c_\sigma, f_\sigma, b\}} H_\lambda + H_{\rm int}, \\ H_y &= \sum_{i=1}^{N} \sum_{k} (\epsilon_{\lambda,k} - \mu_\lambda) \lambda^\dagger_{k,i} \lambda_{k,i}, \\ H_{\rm int} &= \frac{1}{N} \sum_{i,j,l=1}^{N} \sum_{r,\sigma} (g^r_{ijl} c^\dagger_{r,\sigma,i} f_{r,\sigma,j} b_{r,l} + \text{H.c.}), \end{aligned} \tag{5.3}$$

Importantly, similar to the Kondo lattice constraint of one boson or spinon per site, we have the constraint

$$\sum_{i=1}^{N} \left(b^\dagger_{r,i} b_{r,i} + \sum_\sigma f^\dagger_{r,i,\sigma} f_{r,i,\sigma} \right) = N\kappa. \tag{5.4}$$

As we will see below, the constraint allows for the tuning across the quantum critical point. Furthermore, the f and b couple to an internal $U(1)$ gauge field as above, coming from the constraint, and enforcing the Ioffe-Larkin composition rules. We will discuss this point more below, but we set the gauge field coupling to be $1/\sqrt{N}$ to ensure that the effect of the gauge field is controlled.

For simplicity, we will take $\epsilon_{\lambda,k} = k^2/(2m_\lambda)$. We are imagining that the masses are relevant to heavy fermion physics. Since the f fermions will enhance the mass of the conduction electrons, $m_c \ll m_f$, and the dispersion of b is a higher-order effect, implying that $m_f \ll m_b$.

In the next section, we will reduce this model to a set of self-consistency equations whose solution is readily available.

Schwinger-Dyson equations and their solution

We can combine all of this information into the following thermal path integral [30]

$$\begin{aligned}
\mathcal{Z} &= \int \mathcal{D}[c,f,b,\alpha] e^{-S};\\
S &= \sum_{\lambda\in\{c_\sigma,f_\sigma,b\}} S_\lambda + S_{\text{int}} + S_{\text{con.}}\\
S_\lambda &= \sum_i^N \frac{1}{\beta}\sum_{i\omega_n,k} (-i\omega_n + \epsilon_{\lambda,k} - \mu_\lambda)\lambda^\dagger_{k,i}\lambda_{k,i};\\
S_{\text{int}} &= \int_0^\beta d\tau \frac{1}{N}\sum_{r,ijk,\sigma} (g^r_{ijl} c^\dagger_{r\sigma,i} f_{r\sigma,j} b_{r,l} + h.c.)\\
S_{\text{con.}} &= \int_0^\beta d\tau \sum_r i\alpha_r \left(\sum_{i\sigma} f^\dagger_{r\sigma,i} f_{r\sigma,i} + \sum_i b^\dagger_{r,i} b_{r,i} - \kappa N\right)
\end{aligned} \tag{5.5}$$

where N, the number of flavors, is large. Note that this sets the convention $c(\tau) = T\sum_{i\omega_n} e^{-i\omega_n\tau} c(i\omega_n)$. We have suppressed the τ and $i\omega_n$ dependence of c, b, and f, but it is clear from context. We will also suppress the r dependence.

To address the random on-site interaction g^r_{ijk}, we want to disorder average the Free energy. The standard approach is to use the "replica trick" where we replace

$$\ln(\mathcal{Z}) = \lim_{n\to 0} \frac{\mathcal{Z}^n - 1}{n}. \tag{5.6}$$

When n is an integer, we can compute the average of $\mathcal{Z}^n$. As we will argue below, $\overline{(\mathcal{Z}^n)} = (\bar{\mathcal{Z}})^n$ where the overline indicates disorder averaging. There is no rigorous justification for why this approach would extend to non-integer n, but it is the standard assumption made with the replica trick. With this assumption, we have $\overline{\ln(\mathcal{Z})} = \ln(\overline{\mathcal{Z}})$ as seen in other SYK models [28, 144].

Since g^r_{ijk} is Gaussian distributed $\langle\langle g^r_{ijk} g^{r'}_{ijk}\rangle\rangle = \frac{g^2}{2}\delta_{rr'}$, and letting $A^{r\sigma}_{ijk} = c^\dagger_{r\sigma i}(\tau) f_{r\sigma j}(\tau) b_{rk}(\tau)$, we see the interaction term becomes

$$\begin{aligned}
&\int \mathcal{D}[g] e^{-\sum_{r,ijk,\sigma}\left(\frac{(g^r_{ijk})^2}{g^2} + \int_0^\beta d\tau (g^r_{ijk} A^{r\sigma}_{ijk} + h.c.)\right)}\\
&\quad = (\pi g^2)^{\mathcal{N}N^3} e^{\frac{g^2}{2N^2}\sum_{\sigma,\sigma'}\int_0^\beta\int_0^\beta d\tau d\tau' (A^{r\sigma,*}_{ijk}(\tau') A^{r\sigma'}_{ijk}(\tau) + A^{r\sigma}_{ijk}(\tau) A^{r\sigma',*}_{ijk}(\tau'))}\\
&\quad = (\pi g^2)^{\mathcal{N}N^3} e^{-\frac{g^2}{N^2}\sum_{r,\sigma\sigma'}\int_0^\beta\int_0^\beta d\tau d\tau' (c_{i\sigma}(\tau')\bar{c}_{i\sigma'}(\tau) f_{j\sigma'}(\tau)\bar{f}_{j\sigma}(\tau') b_k(\tau)\bar{b}_k(\tau'))}
\end{aligned} \tag{5.7}$$

where $\mathcal{N}$ is the number of sites. Now we use the definition of the Green's functions $NG^r_y(\tau - \tau') = -\sum_i y_i(\tau)\bar{y}_i(\tau')$ and introduce the self-energy fields enforcing the definition of the

Green's functions

$$\int \mathcal{D}[\Sigma^y] e^{\sum_r \int_0^\beta d\tau d\tau' \Sigma_r^y(\tau'-\tau)(\eta(x) N G_y^r(\tau-\tau') + \sum_i \bar{y}_i(\tau') y_i(\tau)} \tag{5.8}$$

with $\eta(y) = \pm 1$ for boson and fermion parity. We are not interested in the case where the anomalous Green's functions are non-zero, though future work may consider this. Additionally, if we consider the case where we are averaging $(\mathcal{Z})^n$ instead of $\mathcal{Z}$, we will similarly only see a change to this calculation if the Green's functions connecting different replicas are non-zero (i.e. if spontaneous replica-symmetry breaking occurs). The diagrams corresponding to non-replica-symmetric processes are suppressed in the large-N limit, similarly to Ref. [28]. We therefore will only consider the case where replica symmetry is maintained and then $\overline{(\mathcal{Z}^n)} = (\bar{\mathcal{Z}})^n$.

$$\begin{aligned}
S_{\text{tot}} = &\sum_i^N \frac{1}{\beta} \sum_{i\omega_n,k,y} (-i\omega_n + \epsilon_{y,k} - \mu_y) \bar{y}_{k,i} y_{k,i} \\
&+ \int_0^\beta d\tau \sum_r i\alpha_r \left(\sum_i f_{r\sigma i}^\dagger f_{r\sigma i} + \sum_i b_{ri}^\dagger b_{ri} - \kappa M \right) \\
&- g^2 N \sum_\sigma \int_0^\beta d\tau d\tau' G_{c_\sigma}(\tau'-\tau) G_{f_\sigma}(\tau-\tau') G_b(\tau-\tau') \\
&+ \sum_r \int_0^\beta d\tau d\tau' \Bigg[\sum_\sigma \Sigma_{c_\sigma}^r \left(-N G_{c_\sigma}^r(\tau-\tau') + \sum_i \bar{c}_{r\sigma i}(\tau') c_{r\sigma i}(\tau) \right) \\
&+ \Sigma_{f_\sigma}^r \left(-N G_{f_\sigma}^r(\tau-\tau') + \sum_i \bar{f}_{r\sigma i}(\tau') f_{r\sigma i}(\tau) \right) \\
&+ \Sigma_b^r \left(N G_b^r(\tau-\tau') + \sum_i \bar{b}_i(\tau') b_i(\tau) \right) \Bigg]
\end{aligned} \tag{5.9}$$

Everything is extensive in N, so we can replace the path-integral by the value of the action at the stationary point. Assuming spatial (and spin) uniformity in Σ_x^r, G_x^r, and α_r we integrate out the f, c, and b fields. Varying the action with respect to G_x, Σ_x, and α, we find:

$$
\begin{aligned}
\frac{\delta S}{\delta i\alpha} &\implies \beta M(2G_f(0) - G_b(0) - \kappa) = 0 \\
\frac{\delta S}{\delta \Sigma_x} &\implies G_x(i\omega_n)\mathcal{N} + \sum_k \frac{1}{-i\omega_n + \epsilon_{x,k} - \mu_x + \Sigma_x(i\omega_n) + i\alpha} = 0 \qquad \text{for } x \in \{f, b\} \\
\frac{\delta S}{\delta \Sigma_c} &\implies G_c(i\omega_n)\mathcal{N} + \sum_k \frac{1}{-i\omega_n + \epsilon_{c,k} - \mu_c + \Sigma_c(i\omega_n)} = 0 \\
\frac{\delta S}{\delta G_c} &\implies \Sigma_c(i\omega_n) + g^2 \frac{1}{\beta} \sum_{i\omega'_m} G_f(i\omega'_m) G_b(i\omega_n - i\omega'_m) = 0 \\
\frac{\delta S}{\delta G_b} &\implies -\Sigma_b(i\omega_n) + 2g^2 \frac{1}{\beta} \sum_{i\omega'_m} G_c(i\omega'_m) G_f(i\omega'_m - i\omega_n) = 0 \\
\frac{\delta S}{\delta G_f} &\implies \Sigma_f(i\omega_n) + g^2 \frac{1}{\beta} \sum_{i\omega'_m} G_c(i\omega'_m) G_b(i\omega'_m - i\omega_n) = 0
\end{aligned}
\tag{5.10}
$$

where we used the convention

$$
F_x(\tau - \tau') = \frac{1}{\beta} \sum_{i\omega_n} F_x(i\omega_n) e^{-i\omega_n(\tau - \tau')} \tag{5.11}
$$

for functions of $\tau - \tau'$ for x Fermionic and the opposite for x Bosonic.

These are exactly the Schwinger-Dyson equations that can be more easily derived diagrammatically [1, 28, 144, 27], but with the added influence of the fixed-length constraint. The mean-field value of $\Delta_b = i\alpha - \mu_b$ is the boson thermal mass. We assume that the bandwidth of the fermions is large, so the small shift in μ_f from Δ_b will be seen to be negligible. In this limit, we have the result [144]

$$
G_x(i\omega_n) = -i\frac{\nu_x}{2}\text{sgn}(\omega_n) \tag{5.12}
$$

for $x = \{c, f\}$ if $\text{Im}[\Sigma_x(i\omega)] = -\text{sgn}(\omega_n)$, which we will verify, where ν_x is the density of states at the Fermi surface. This simplification will allow us to straightforwardly solve the Schwinger-Dyson equations.

The boson self-energy becomes

$$
\begin{aligned}
\Sigma_b(i\omega_n) &= 2g^2 T \sum_{i\omega'_m} G_c(i\omega'_m) G_f(i\omega'_m - i\omega_n) = \gamma|\omega_n| + C_b, \\
\gamma &= g^2 \nu_c \nu_f / (2\pi).
\end{aligned}
\tag{5.13}
$$

and we absorb the cutoff dependent constant C_b into Δ_b. From here, the boson Green's function is straightforwardly obtained as

$$\begin{aligned} G_b(i\omega_n) &= \int \frac{d^dk}{(2\pi)^d} \frac{1}{i\omega_n - k^2/2m_b - \gamma|\omega| - \Delta_b} \\ &\approx -\frac{m_b}{2\pi} \ln\left(\frac{\Lambda}{-i\omega_n + \gamma|\omega| + \Delta_b}\right), \quad d = 2, \end{aligned} \tag{5.14}$$

where have introduced a cutoff $\Lambda = \pi^2/(2m_b)$, and we ensure that $\Lambda \gg \Delta_b, |\omega_n|, \gamma|\omega_n|$. A similar expression can be obtained for $d = 3$, but specializing to $d = 2$ is necessary to obtain T-linear resistivity. For now, we will specialize to a fully two-dimensional model, and we will comment more on this choice in the discussion.

The last step is to evaluate the fermion self-energies. We do so with the Lehmann representation of the Schwinger-Dyson equations

$$\Sigma_c(i\omega_n, T) = g^2 \int \frac{d\epsilon d\epsilon'}{(2\pi)^2} A_f(\epsilon) A_b(\epsilon') \frac{n_B(\epsilon') + n_F(-\epsilon)}{\epsilon' + \epsilon - i\omega_n}, \tag{5.15}$$

where $A_f(\epsilon) = -2\mathrm{Im}[G_f^R(\epsilon)] = \nu_f$ is the fermion spectral function, and $A_b(\epsilon) = -2\mathrm{Im}[G_b^R(\epsilon)]$. Importantly, we analytically continue $i\omega \to \omega + i\delta$ to obtain

$$\mathrm{Im}[\Sigma_{c,R}(\omega, T)] = g^2 \nu_f \int \frac{d\epsilon}{4\pi} A_b(\epsilon)(n_B(\epsilon) + n_F(\epsilon - \omega)) \tag{5.16}$$

and a similar expression for $\mathrm{Im}[\Sigma_{f,R}(\omega, T)]$ with $\nu_f \leftrightarrow \nu_c$ and $\omega \leftrightarrow -\omega$.

Solution in a magnetic field

In principle, once we account for the constraint equation which provides an expression for Δ_b, we will have solved the Schwinger-Dyson equations, as we will simply need to carry out numerous integrals numerically or analytically. Before doing so, though, we are interested in computing all components of the conductivity tensor, which requires that we perform these calculations in the presence of a magnetic field, $\boldsymbol{B} = B\hat{z}$. We can take the $B \to 0$ limit at any time to recover the proper expressions in the absence of field.

Our choice of quadratic dispersion allows us to switch to the Landau level basis in the $x - y$ plane given by the wavefunctions

$$\begin{aligned} \psi_{n,k}(x, y) &= \frac{1}{\sqrt{L_x \ell}} e^{ikx} \phi_{n,k}(y/\ell); \\ \phi_{n,k}(z) &= \frac{\pi^{-1/4}}{\sqrt{2^n n!}} H_n(z + k\ell) \exp\left(-\frac{(z + k\ell)^2}{2}\right), \end{aligned} \tag{5.17}$$

where $\ell = 1/\sqrt{e_\lambda B_\lambda}$ and $H_n(x)$ are the (physicist's) Hermite polynomials satisfying the recursion relation $H_{n+1}(x) = 2xH_n(x) - H_n'(x)$. The energy of the states is $\omega_{c\lambda}(n + 1/2)$

where $\omega_{c\lambda} = |e_\lambda|B_\lambda/m_\lambda$, where $\lambda \in \{c, f, b\}$. The charge, e_λ and (effective) magnetic field, B_λ, for each of the three species is left unspecified for now.

The change of basis is accomplished by rewriting the operators $\lambda_r(\tau) = \sum_{nk} \psi_{nk}(r)\lambda_{nk}(\tau)$ for $\lambda \in \{c_\sigma, f_\sigma, b\}$ where the $\psi(nk)$ for each species is different because each ℓ is different. Because $\mu_c, \mu_f \gg \omega_{c,c/f}$, we still have the original result for the fermion Green's function that $G_{c,f}(i\omega_n) = -i(\nu_{c,f}/2)\mathrm{sgn}(\omega_n)$. That is, the fermions are less affected by the Landau level quantization than the bosons, and, consequently, the boson self-energy calculation above is unaffected.

However, the boson's Green function must be calculated by summing over the Landau levels instead of integrating over momentum. Instead of the Green's function, we will evaluate the spectral function directly with the result being

$$\begin{aligned} A_b(\omega) &= -\frac{1}{\ell^2 2\pi}\sum_m \frac{2\gamma\omega}{(\omega - (m+1/2)\omega_{cb} - \Delta_b)^2 + \gamma^2\omega^2} \\ &= \frac{m_b}{\pi}\mathrm{Im}\left[\psi_0\left(\frac{1}{2} - \frac{-\Delta_b + \omega + i\gamma\omega}{\omega_{bc}}\right)\right] \\ &\xrightarrow{B\to 0} -\frac{m_b}{\pi}\left[\pi\Theta(\omega - \Delta_b) + \tan^{-1}\left(\frac{\gamma\omega}{\Delta_b - \omega}\right)\right], \end{aligned} \tag{5.18}$$

where $\Theta(x)$ is the Heaviside step function, $\psi_0(z)$ is the digamma function. Note that the temperature dependence of A_b comes entirely from its dependence on $\Delta(T)$.

Now, with an explicit expression, we return to the self consistency needed above

$$\mathrm{Im}\left[\Sigma_c(i\omega_n)\right] = \omega_n g^2 \nu_f \int \frac{d\epsilon d\epsilon'}{(2\pi)^2}\frac{n_B(\epsilon') + n_F(-\epsilon)}{(\epsilon' + \epsilon)^2 + \omega_n^2} A_b(\epsilon') \tag{5.19}$$

Note that $A_b(\epsilon')$ is odd in ϵ' (as is $n_B(\epsilon')$, so the $n_F(-\epsilon)$ term vanishes once we integrate over ϵ'. The rest of the integrand has the same sign as $A_b(\epsilon')n_B(\epsilon') < 0$ implying that $\mathrm{Im}[\Sigma_x(i\omega)] = -\mathrm{sgn}(\omega_n)$

The boson thermal mass

Now we obtain an expression for $\Delta_b(T)$, after which we will have solved the Schwinger-Dyson equations. It can be easily checked that the change in the number of f fermions in response to a shifting chemical potential is suppressed by $\Delta\mu_f/\Lambda_f$ where Λ_f, the f fermion bandwidth, is assumed to be large. Therefore, the constraint can be written as

$$\kappa - \kappa_c = (G_b(\tau = 0^-, \Delta_b(T)) - G_b(\tau = 0^-, \Delta_{b,c}(0)), \tag{5.20}$$

and Δ_b depends on both temperature and κ, but we suppress the κ dependence generally. When we are at criticality, $\kappa = \kappa_c$, $\Delta_b = \Delta_{b,c}$, and $\Delta_{b,c}(T = 0) = 0$. This is reminiscent of the $O(N)$ rotor model [159] and the calculation of the thermal mass in [142].

Although we can do this calculation carefully in multiple ways, we will recall that $G_b(\tau = 0^-) = -\sum_i \langle b_i^\dagger(\tau = 0^-) b_i(\tau = 0^-)\rangle \equiv -n_b$, which is the number density of bosons. For this number to converge, we choose to regulate it in the usual way (see [119])

$$n_b = -\frac{1}{V}\sum_{nk}\int_{-\infty}^{\infty}\frac{d\omega}{2\pi} n_B(\omega) A_{bn}(\omega, \Delta_b), \tag{5.21}$$

where A_{bn} is the summand seen in (5.18).

Note that

$$\int_{-\infty}^{\infty} d\omega n_B(\omega) A_{bn}(\omega, \Delta_b) = \int_0^{\infty} d\omega n_B(\omega)(A_{bn}(\omega, \Delta_b) - A_{bn}(-\omega, \Delta_b)) - \int_0^{\infty} d\omega A_{bn}(-\omega, \Delta_b), \tag{5.22}$$

and that the first integral on the right-hand side is 0 when $T = 0$. Recalling the form of the boson's spectral function from (5.18), we will find

$$\begin{aligned} -2\pi(\kappa - \kappa_c) = \frac{\omega_{cb} m_b}{2\pi}\Bigg[\int_0^{\infty} n_B(\omega)\frac{(A_b(\omega, \Delta_b) - A_b(-\omega, \Delta_b))}{1/(\ell^2 2\pi)} \\ + \frac{2\gamma}{\gamma^2 + 1}\ln\left(\frac{\Gamma(\mathcal{N} + 3/2)\Gamma(1/2 + \Delta_b/\omega_{cb})}{\Gamma(\mathcal{N} + 3/2 + \Delta_b/\omega_{cb})\Gamma(1/2)}\right)\Bigg], \end{aligned} \tag{5.23}$$

where we have cut off the Landau level sum at $\mathcal{N} = \Lambda/\omega_{bc}$ and $\Gamma(n)$ is the Gamma function.

Taking the $B \to 0$ limit of (5.23), we can scale out $\Delta_b = zT$ and $x = \omega/T$ to find

$$\begin{aligned} 2\pi^2(\kappa - \kappa_c)\frac{1}{T m_b} = \int_0^{\infty}\frac{dx}{e^x - 1}\left[\tan^{-1}\left(\frac{\gamma x}{z - x}\right) + \tan^{-1}\left(\frac{\gamma x}{z + x}\right)\right] \\ - \pi\ln\left(1 - e^{-z}\right) - \frac{\gamma}{\gamma^2 + 1} z\ln\left(\frac{\Lambda e}{zT}\right). \end{aligned} \tag{5.24}$$

As $z \to 0$, the first two terms of the left-hand side dominate and as $z \to \infty$, the rightmost term dominates, so we see that there is a solution with z, whose value will change logarithmically, as $T \to \infty$. As expected, there is always a solution, so the bosons are not truly condensed as long as their dispersion is strictly 2D. Instead, for $\kappa > \kappa_c$ the gap becomes exponentially small in $(\kappa - \kappa_c)/T$, i.e. $\Delta_b \sim T\exp\left[-\frac{2\pi(\kappa - \kappa_c)}{T m_b}\right]$.

Fig. 5.1 summarizes the behavior of $\Delta_b(T)$ in the three phases at zero and finite applied field. The important feature is the T-linear (up to logarithmic corrections) growth in the critical region. Low T transport is dictated by the limit of $z = \Delta_b/T$ as $T \to 0$ which shifts from ∞ to zero across the transition.

5.2 Transport

Now that we have the exact Green's functions and self-energies, we can proceed to compute electrical transport.

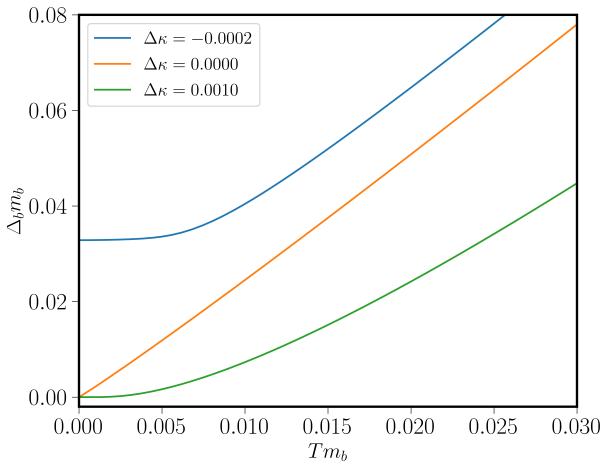

Figure 5.1: We plot Δ_b vs. T for various $\Delta\kappa = \kappa - \kappa_c$ with the color indicating $\Delta\kappa$. All curves become T-linear upon entering the critical region, but are either exponentially suppressed or approach a constant as $T \to 0$ if $\Delta_\kappa > 0$ or $\Delta_\kappa < 0$ respectively. All other parameters are the same as in Fig. 5.4. Copyright © 2022 by the American Physical Society. Reproduced from Ref. [1] with permission.

To do so, we need an expression for the current operator. The locality of the interaction leads to no net effect on the operator, and it is therefore given by the standard expression

$$\boldsymbol{J}(r,\tau) = \sum_{\lambda\in\{c_\sigma,f_\sigma,b\}} \frac{e_\lambda}{2m_\lambda i}\Big[\lambda_r^\dagger(\tau)(\boldsymbol{\nabla} - ie_\lambda \boldsymbol{A}_\lambda)\lambda_r(\tau) - (\boldsymbol{\nabla} + ie_\lambda \boldsymbol{A}_\lambda)\lambda_r^\dagger(\tau)\lambda_r(\tau)\Big] = \sum_\lambda \boldsymbol{J}_\lambda(r,\tau). \tag{5.25}$$

where we have used $e_b + e_f - e_c = 0$ due to charge conservation (discussed more below).

With this expression in hand, we can evaluate $\sigma_{\alpha\beta}$ through the Kubo formula in the Landau level basis. The use of the Landau level basis is possible because the self-energies of all three species are independent of momentum and therefore proportional to the identity matrix in real space, which implies that they are also proportional to the identity matrix in the Landau level basis, greatly simplifying the computation. As before, we may obtain $B = 0$ expressions by taking the $B \to 0$ limit of our expressions here.

In general, when applying the Kubo formula, we would need to consider correlators of the total current, $\langle J(r,\tau)J(r',0)\rangle$. Due to the large N limit, evaluating these correlators reduces to a small set of diagrams, as seen in Fig. 5.2. In our model, however, every diagram except the bubble diagram is zero. In evaluating the bubble diagram, the interspecies Green's functions are zero, and we can therefore compute each species conductivity separately.

Now, our starting point is the Kubo formula in momentum space, which we will transform

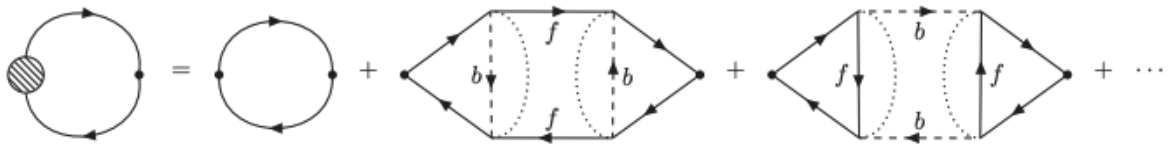

Figure 5.2: The diagrams that contribute to the c conductivity. These diagrams are not suppressed by the large N limit, but only the first (bubble) diagram is nonzero. The dotted lines indicate the averaging over the flavor random couplings g^r_{ijl}, which carry momentum. Consequentially, the momentum integrals in the left and right loops of the correction diagrams are decoupled. The diagrams that contribute to the f and b conductivities are analogous to the ones above. The diagrams that contribute to the cross-correlations of currents of different species are analogous to the vertex diagrams correcting the bubble diagram above, and also vanish. Copyright © 2022 by the American Physical Society. Reproduced from Ref. [1] with permission.

to the Landau Level basis. Recall that [119] $\sigma_{\lambda,\alpha\beta}(\omega,q) = -\mathrm{Im}\Pi^R_{\lambda,\alpha\beta}(\omega,q)/\omega$ where

$$\Pi_{\lambda,\alpha\beta} = -\frac{1}{V}\int dxdx'dydy' e^{iq_x(x-x')}e^{iq_y(y-y')}\int_0^{1/T} d\tau e^{i\omega\tau}\langle T_\tau J^\dagger_{\lambda,\alpha}(r,\tau)J_{\lambda,\beta}(r',0)\rangle, \tag{5.26}$$

where τ is imaginary time. With the above identities, a straightforward calculation will yield the spatially-integrated current as

$$\begin{aligned}\frac{2m_\lambda i}{e_\lambda}\int dxdy \begin{pmatrix} J_{\lambda,x}(r,\tau) \\ J_{\lambda,y}(r,\tau)\end{pmatrix} &\equiv \int dxdy \left(\lambda^\dagger_r(\tau)(\boldsymbol{\nabla} - ie_\lambda \boldsymbol{A}_\lambda)\lambda_r(\tau) - (\boldsymbol{\nabla} + ie_\lambda \boldsymbol{A}_\lambda)\lambda^\dagger_r(\tau)\lambda_r(\tau)\right) \\ &= \frac{2}{\ell}\sum_{k,n}\left(\begin{pmatrix} i \\ 1\end{pmatrix}\sqrt{\frac{n+1}{2}}\lambda^\dagger_{nk}(\tau)\lambda_{n+1,k}(\tau) + \begin{pmatrix} i \\ -1\end{pmatrix}\sqrt{\frac{n}{2}}\lambda^\dagger_{nk}(\tau)\lambda_{n-1,k}(\tau)\right).\end{aligned} \tag{5.27}$$

We now evaluate $\Pi_{\lambda,xx}$ and $\Pi_{\lambda,xy}$ at $q = 0$ using this expression. Using $G_{\lambda nk}(\tau) = -\langle\lambda_{nk}(\tau)\lambda^\dagger_{nk}(0)\rangle$, we get

$$\begin{aligned}\begin{pmatrix}\Pi_{\lambda,xx} \\ \Pi_{\lambda,xy}\end{pmatrix} &= \frac{-\eta e^2}{V\ell^2 m^2_\lambda}\int_0^{1/T} d\tau e^{i\omega\tau}\sum_{nk}\begin{pmatrix} \frac{n+1}{2}G_{\lambda nk}(\tau)G_{\lambda,n+1,k}(-\tau) + \frac{n}{2}G_{\lambda nk}(\tau)G_{\lambda,n-1,k}(-\tau) \\ -i\frac{n+1}{2}G_{\lambda nk}(\tau)G_{\lambda,n+1,k}(-\tau) + i\frac{n}{2}G_{\lambda nk}(\tau)G_{\lambda,n-1,k}(-\tau)\end{pmatrix} \\ &= \frac{-\eta e^2\omega^2_{c\lambda}}{2\pi}T\sum_{i\nu_n}\left(\sum_n \frac{n+1}{2}\begin{pmatrix}1 \\ -i\end{pmatrix}G_{\lambda n}(i\nu_n)G_{\lambda,n+1}(i\nu_n - i\omega)\right. \\ &\left. + \frac{n}{2}\begin{pmatrix}1 \\ i\end{pmatrix}G_{\lambda n}(i\nu_n)G_{\lambda,n-1}(i\nu_n - i\omega)\right).\end{aligned} \tag{5.28}$$

where $\eta = \pm$ for bosons and fermions, respectively, because of time-ordering. In the second step, we switched to Matsubara frequencies, used the fact that $G_{nk}(\tau) \equiv G_n(\tau)$ is independent of k, and there are $L_x L_y/\ell^2/(2\pi)$ terms in the k sum.

In the calculation, we have neglected the vertex corrections to the conductivity, as depicted in Fig. 5.2, which can be shown to vanish even at $B \neq 0$. Since the disordered interactions g^r_{ijk} are uncorrelated between different sites, such corrections can be written as

$$\delta\Pi_\lambda = \left\langle \int dxdy \boldsymbol{J}_\lambda(r,\tau) \int dx_{1,2}dy_{1,2}d\tau_{1,2,3,4}\lambda^\dagger_{r_1}(\tau_1)\lambda_{r_1}(\tau_2)K(\tau_1,\tau_2,\tau_3,\tau_4)\lambda^\dagger_{r_2}(\tau_3)\lambda_{r_2}(\tau_4) \right.$$
$$\left. \int dx'dy' \boldsymbol{J}_\lambda(r',\tau') \right\rangle. \tag{5.29}$$

Since $\lambda_r(\tau) = \sum_{n,k} \psi_{n,k}(r)\lambda_{nk}(\tau)$, and $G_{\lambda nk}(\tau)$ are independent of k, the identity

$$\int dk H_n(z+kl)H_{n\pm1}(z+kl)\exp\left(-(z+kl)^2\right) = 0, \tag{5.30}$$

ensures that these corrections vanish.

Proceeding similarly as to [119], we next switch to the Lehmann representation, analytically continue, take the imaginary part, and expand for small ω. We find

$$\sigma_{\lambda,xx} = -s_\lambda \lim_{\omega\to 0} \frac{\mathrm{Im}[\Pi_{\lambda,xx}(\omega)]}{\omega} = -\frac{s_\lambda e^2 \omega_{c\lambda}^2}{4\pi} \sum_n (n+1) \int \frac{d\epsilon}{(2\pi)} A_{\lambda n}(\epsilon) A_{\lambda,n+1}(\epsilon) \left(\frac{\partial n_\eta(\epsilon)}{\partial \epsilon}\right)$$
$$= -\frac{s_\lambda e^2}{4\pi} \int \frac{d\epsilon}{2\pi} \frac{4\Sigma''_\lambda(\epsilon)\frac{\partial n_\eta(\epsilon)}{\partial\epsilon}}{4[\Sigma''_\lambda(\epsilon)]^2 + \omega^2_{c\lambda}} \left(2\Sigma''_\lambda(\epsilon) + 2(\epsilon+\tilde{\mu}_\lambda)\mathrm{Im}\left[\psi_0\left(\frac{1}{2} + \frac{-\epsilon + i\Sigma''_\lambda(\epsilon) - \tilde{\mu}_\lambda}{\omega_{c\lambda}}\right)\right]\right), \tag{5.31}$$

where s_λ is the spin degeneracy of the species λ. We performed the Landau level sum in terms of the digamma function, ψ_0, and we used $\psi_0(z) = \psi_0(1+z) - 1/z$ and

$$A_{\lambda n}(\epsilon) = \frac{2\eta\Sigma''_\lambda(\epsilon)}{(\epsilon + \tilde{\mu}_\lambda - (n+1/2)\omega_{c\lambda})^2 + [\Sigma''_\lambda(\epsilon)]^2}, \tag{5.32}$$

so that $\Sigma''_\lambda(\epsilon) = \mathrm{Im}[\Sigma_{\lambda,R}(\epsilon)]$ and $\tilde{\mu}_\lambda = \mu_\lambda - \mathrm{Re}[\Sigma_{\lambda,R}(\epsilon)]$.

For $\sigma_{\lambda,xy}$, we convert to relative and center of mass coordinates $\epsilon_c = (\epsilon + \epsilon')/2$ and $\epsilon_r = \epsilon - \epsilon'$. We then symmetrize with respect to ϵ_r in order to get an integral from 0 to ∞.

We find

$$\begin{aligned}
\Pi_{\lambda,xy}(\omega\to 0) &= -i\frac{e_\lambda^2\omega_{c\lambda}^2}{4\pi}\sum_n (n+1)\int \frac{d\epsilon d\epsilon'}{(2\pi)^2}A_{\lambda n}(\epsilon)A_{\lambda,n+1}(\epsilon')(n_\eta(\epsilon)-n_\eta(\epsilon'))\left[\frac{2(\omega+i\delta)}{(\epsilon-\epsilon')^2}\right],\\
\sigma_{\lambda,xy} &= -\frac{s_\lambda e_\lambda^2\omega_{c\lambda}^2}{2\pi}\sum_n (n+1)\int_0^\infty \frac{d\epsilon_r}{2\pi}\int_{-\infty}^\infty \frac{d\epsilon_c}{2\pi}\frac{\sinh\left(\frac{\epsilon_r}{2T}\right)}{\cosh\left(\frac{\epsilon_c}{T}\right)-\eta\cosh\left(\frac{\epsilon_r}{2T}\right)}\frac{1}{\epsilon_r^2}\\
&\quad\times\left[A_{\lambda n}\left(\epsilon_c+\frac{\epsilon_r}{2}\right)A_{\lambda,n+1}\left(\epsilon_c-\frac{\epsilon_r}{2}\right)-A_{\lambda n}\left(\epsilon_c-\frac{\epsilon_r}{2}\right)A_{\lambda,n+1}\left(\epsilon_c+\frac{\epsilon_r}{2}\right)\right]\\
&= -\frac{s_\lambda e_\lambda^2}{(2\pi)^3}\int_0^\infty d\epsilon_r\int_{-\infty}^\infty d\epsilon_c\left(F_\lambda(\epsilon_c,\epsilon_r)-F_\lambda(\epsilon_c,-\epsilon_r)\right)\frac{\sinh\left(\frac{\epsilon_r}{2T}\right)}{\cosh\left(\frac{\epsilon_c}{T}\right)-\eta\cosh\left(\frac{\epsilon_r}{2T}\right)}\frac{1}{\epsilon_r^2},
\end{aligned}\tag{5.33}$$

The sum can be done to give an explicit expression for $F_\lambda(\epsilon_c,\epsilon_r)$ as

$$\begin{aligned}
\frac{F_\lambda\left(\frac{\epsilon+\epsilon'}{2},\epsilon-\epsilon'\right)}{2\Sigma''_\lambda(\epsilon)\Sigma''_\lambda(\epsilon')} &= \mathrm{Im}\left[\frac{\psi_0\left(\frac{2\epsilon-2i\Sigma''_\lambda(\epsilon)-2\tilde{\mu}_\lambda(\epsilon)}{2\omega_{c\lambda}}-\frac{1}{2}\right)\left(2\epsilon-\omega_{c\lambda}-2i\Sigma''_\lambda(\epsilon)-2\tilde{\mu}_\lambda(\epsilon)\right)}{\Sigma''_\lambda(\epsilon)(\Sigma''_\lambda(\epsilon')^2+(\epsilon'-\epsilon+\omega_{c\lambda}+i\Sigma''_\lambda(\epsilon)-\tilde{\mu}_\lambda(\epsilon')+\tilde{\mu}_\lambda(\epsilon))^2)}\right]\\
&+\mathrm{Im}\left[\frac{\psi_0\left(\frac{2\epsilon'+2i\Sigma''_\lambda(\epsilon')-2\tilde{\mu}_\lambda(\epsilon')}{2\omega_{c\lambda}}+\frac{1}{2}\right)\left(2\epsilon'+\omega_{c\lambda}+2i\Sigma''_\lambda(\epsilon')-2\tilde{\mu}_\lambda(\epsilon')\right)}{\Sigma''_\lambda(\epsilon')(\Sigma''_\lambda(\epsilon')^2-\Sigma''_\lambda(\epsilon)^2+2i\Sigma''_\lambda(\epsilon')(\epsilon-\epsilon'-\omega_{c\lambda}+\tilde{\mu}_\lambda(\epsilon')-\tilde{\mu}_\lambda(\epsilon))-(\epsilon-\epsilon'-\omega_{c\lambda}+\mu_\lambda(\epsilon')-\mu_\lambda(\epsilon))^2)}\right].
\end{aligned}\tag{5.34}$$

For the fermions, for small magnetic fields, these expressions give the same result as the expressions derived from the Boltzmann equations in [144] with the identification $v_F^2\nu/(4\pi)\to n/m$ where v_F is the Fermi velocity, n is the density, and m is the mass. However, for large magnetic fields, our expressions will have quantum oscillations that are absent in the Boltzmann treatment.

Ioffe-Larkin composition rule and the effective charge and magnetic field

We left e_f, e_b, e_c, B_b, B_f, and B_c unspecified above. For the conduction electrons, c, $e_c=-1$ is the charge of the electron and $B_c=B$ is the applied field. In order for the interaction term, $c^\dagger fb$, to conserve charge, we must have $e_f+e_b=-1$ as well. How the charge is distributed is a gauge choice, with the emergent gauge field ensuring the physical results are independent of this choice.

We see in Fig. 5.3 that there are three diagrams that contribute to the renormalization of the charge. In the diagrams, the polarization bubbles, $\mathbf{\Pi}$, [2] and propagators are fully renormalized (with the fermionic spin degeneracy included). Any other diagram is either zero because of the locality of the SYK-type interaction or suppressed by $1/N$. We note that

[2]The polarization bubbles $\mathbf{\Pi}_{f,b}$ involve the subtraction of diamagnetic terms not explicitly shown in Fig. 5.3, which render $\mathbf{\Pi}_{f,b}(\omega,q)=\mathbf{\Pi}_{f,b}(\omega,q)-\mathbf{\Pi}_{f,b}(\omega=0,q=0)$. Additionally, they differ from the polarization bubble used in computing the conductivity as we have pulled out the factor of the bare charges.

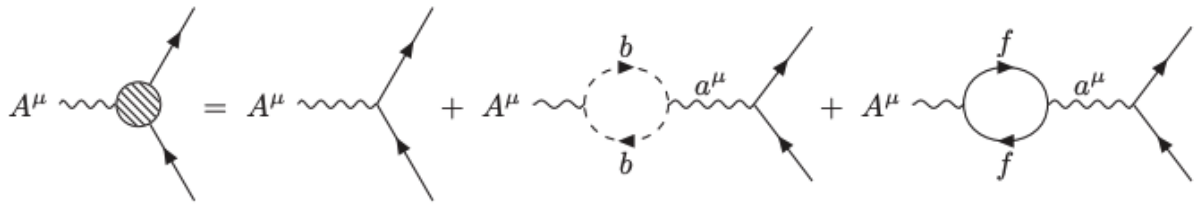

Figure 5.3: The diagrams that contribute to the renormalized charge. The propagators and polarization bubbles are all fully dressed. A^μ is the external gauge field, a^μ is the emergent gauge field, and the lines to the right of the diagrams are either b or f propagators depending on whether the renormalized b charge or renormalized f charge is being computed.

the propagator for the emergent $U(1)$ gauge field is [106]

$$\boldsymbol{D}(\tau - \tau') = -\langle a(\tau)a(\tau')\rangle = -(\boldsymbol{\Pi}_f + \boldsymbol{\Pi}_b)^{-1}, \tag{5.35}$$

and the boldface is indicating tensors, which follows if the inverse bare propagator is taken to be infinitesimal.

Summing these diagrams for, e.g. the f fermions gives

$$\begin{aligned} \boldsymbol{e}_f^r &= e_f - e_f\boldsymbol{\Pi}_f(\boldsymbol{\Pi}_f + \boldsymbol{\Pi}_b)^{-1} + e_b\boldsymbol{\Pi}_b(\boldsymbol{\Pi}_f + \boldsymbol{\Pi}_b)^{-1} \\ &= (e_f + e_b)\boldsymbol{\Pi}_b(\boldsymbol{\Pi}_f + \boldsymbol{\Pi}_b)^{-1} = -\boldsymbol{\Pi}_b(\boldsymbol{\Pi}_f + \boldsymbol{\Pi}_b)^{-1}, \end{aligned} \tag{5.36}$$

where the extra minus sign for $\boldsymbol{\Pi}_b$ comes because f and b are oppositely charged under the emergent gauge field, and all polarization bubbles are evaluated at (ω, q). Switching $f \leftrightarrow b$ will give the boson result. Therefore, the charge renormalizes to become a tensor. It is worth noting that $\boldsymbol{\Pi}_b$, $\boldsymbol{\Pi}_f$, and $\boldsymbol{\Pi}_b + \boldsymbol{\Pi}_f$ are 2×2 antisymmetric matrices and therefore commute with each other. When we compute the total current-current correlator due to the f and b sub-systems after renormalizing the currents using the respective charge renormalizations, we find,

$$\begin{aligned} \boldsymbol{\Pi}_{\text{tot}} &= \boldsymbol{\Pi}_b\boldsymbol{\Pi}_f^2[(\boldsymbol{\Pi}_b + \boldsymbol{\Pi}_f)^{-1}]^2 + \boldsymbol{\Pi}_f\boldsymbol{\Pi}_b^2[(\boldsymbol{\Pi}_b + \boldsymbol{\Pi}_f)^{-1}]^2 \\ &= (\boldsymbol{\Pi}_b^{-1} + \boldsymbol{\Pi}_f^{-1})^{-1}. \end{aligned} \tag{5.37}$$

This expression implies that the f and b resistivity are added in series.

One important point that is glossed over in the above is that the electric and magnetic field are renormalized differently, and $\boldsymbol{\Pi}_b$ and $\boldsymbol{\Pi}_f$ are evaluated for different effective magnetic fields. In our notation, $\boldsymbol{\Pi}(\omega, q) \approx -i\boldsymbol{\sigma}\omega + \boldsymbol{\chi}q^2$, so the renormalization changes depending on whether the vertex is magnetic $A^\mu(\omega = 0, q \to 0)$, or electric, $A^\mu(\omega \to 0, q = 0)$. We find,

for instance for the f fermions

$$E^f_{\rm eff} = \boldsymbol{\sigma}_b(\boldsymbol{\sigma}_f + \boldsymbol{\sigma}_b)^{-1}E, \qquad B^f_{\rm eff} = \frac{\chi_b}{\chi_b + \chi_f}B, \tag{5.38}$$

for a weak magnetic field B. In the magnetic field case, we additionally average over q, which replaces $\boldsymbol{\chi}$ with half its trace $\chi = (\chi_{xx} + \chi_{yy})/2$.

In our derivation, we have neglected contributions to $\boldsymbol{\sigma}$ and $\boldsymbol{\chi}$ from potential cross-correlations $\boldsymbol{\Pi}_{fb} \sim \langle J_f J_b\rangle$. Doing so is valid, as the site-uncorrelated g^r_{ijk} render them of the form

$$\boldsymbol{\Pi}_{fb}(i\omega, q) \sim \int d^2k d^2k' d\Omega d\Omega' v_{f,k} v_{b,k} G_{f,k+q/2}(i\Omega + i\omega/2) G_{f,k-q/2}(i\Omega - i\omega/2) K_{fb}(i\Omega, i\Omega', \omega, q)$$
$$\times G_{b,k'+q/2}(i\Omega' + i\omega/2) G_{b,k'-q/2}(i\Omega' - i\omega/2), \tag{5.39}$$

where $v_{x,k} = \nabla_k \epsilon_{x,k}$. Since $G_{x,k} = G_{x,-k}$, $G_{x,k+q/2}(i\Omega + i\omega/2)G_{x,k-q/2}(i\Omega - i\omega/2) = G_{x,k}(i\Omega + i\omega/2)G_{x,k}(i\Omega - i\omega/2) + \Xi_{x,k}(i\Omega, i\omega)|q|^2$, with $\Xi_{x,k} = \Xi_{x,-k}$, and $v_{x,k} = -v_{x,-k}$, the $\mathcal{O}(\omega)$ and $\mathcal{O}(q^2)$ terms in the expansion of $\boldsymbol{\Pi}_{fb}(\omega, q)$ vanish and we can thus neglect these cross-correlations.

Because of the renormalization of the magnetic field from the internal gauge field, we must find expressions for χ_f and χ_b. To find them, we evaluate $\chi_\lambda q^2 = \Pi_\lambda(\omega = 0, q \to 0) - \Pi_\lambda(\omega = 0, q = 0)$, averaging over the two possible directions. Then, we have the bubble contributions

$$\Pi_\lambda(q \to 0) = \frac{\Pi_{\lambda,xx} + \Pi_{\lambda,yy}}{2} = -\eta \frac{1}{V}\sum_k \frac{k^2}{2m_\lambda^2} T \sum_{i\nu} \left(G_\lambda(k - q/2, i\nu) G_\lambda(k + q/2, i\nu)\right)$$
$$= -2\eta T \int_0^{\tilde{k}_{\rm max}} \frac{d\tilde{k}}{(2\pi)^2} \int_0^{2\pi} d\theta \tilde{k}^3 \left(\sum_{i\nu} \frac{1}{(i\nu/T - \tilde{k}^2 + \tilde{k}\tilde{q}\cos(\theta) - \tilde{q}^2/4 + \mu_\lambda/T - \Sigma_\lambda/T)} \frac{1}{(\tilde{q} \to -\tilde{q})} \right)$$
$$\chi_\lambda = -\eta \frac{1}{2m_\lambda} \int_0^{k_{\rm max}} k^3 \frac{dk}{2\pi} \left(\sum_{i\nu} \frac{(i\nu_\lambda/T + \mu/T - \Sigma_\lambda/T)}{(i\nu/T - k^2 + \mu_\lambda/T - \Sigma_\lambda/T)^4} \right), \tag{5.40}$$

where in the second line of the above, we re-scaled the momenta by a factor of $\tilde{k} = k/\sqrt{2m_\lambda T}$, and we relabeled $\tilde{k} \to k$ in line 3.

We can do the Matsubara sums exactly in the bosonic case since $\Sigma_b(i\omega) = \gamma|\omega|$. We carry them out to find ($z = -\mu/T = \Delta_b/T$):

$$\chi_b = -\frac{1}{2m_b} \int_0^{\sqrt{\Lambda/T}} \frac{dk}{2\pi} k^3 \left(\frac{z}{(k^2 + z)^4} + {\rm Re}\left[\frac{\psi_2\left(\frac{k^2+z}{2\pi\gamma - 2\pi i}\right)}{(2\pi\gamma - 2\pi i)^3} + \frac{k^2}{3} \frac{\psi_3\left(\frac{k^2+z}{2\pi\gamma - 2\pi i}\right)}{(2\pi\gamma - 2\pi i)^4} \right] \right), \tag{5.41}$$

with $\psi_n(z)$ the polygamma function and Λ is the boson bandwidth. This expression diverges as $\chi_b \sim (1/m_b)\ln(\Lambda/\Delta_b)$ when $\Delta_b \to 0$.

For the f fermions, we can transform (5.40) to

$$\begin{aligned}\chi_f &= \frac{1}{2m_f}\int_{-\mu_f}^{\Lambda_f}\frac{d\epsilon}{2\pi}(\epsilon+\mu_f)T\sum_{i\nu}\left(\frac{(i\nu+\mu_f-\Sigma_f(i\nu))}{(i\nu-\epsilon-\Sigma_f(i\nu))^4}\right)\\ &= T\sum_{i\nu}\frac{(\Lambda_f+\mu_f)^2(\Lambda_f-2\mu_f+3\Sigma_f(i\nu)-3i\nu)}{24\pi m_f(\Lambda_f+\Sigma_f(i\nu)-i\nu)^3(\mu_f-\Sigma_f(i\nu)+i\nu)}.\end{aligned} \tag{5.42}$$

We note that T and $|\Sigma_f(i\nu)|$ are always much smaller than the f bandwidth Λ_f and Fermi energy μ_f, for any value of ν, since $|\Sigma_f(i\nu)|$ is bounded by a scale controlled by the boson bandwidth $\Lambda \ll \Lambda_f, \mu_f$. Therefore we can expand the summand of (5.42) in powers of Σ_f and take the $T \to 0$ limit. It may then be seen that the sum of the absolute values of the contributions from all these terms in the expansion is bounded by a quantity that vanishes in the limit of $\Lambda_f, \mu_f \to \infty$, leaving χ_f to take its free fermion value of $1/(24\pi m_f)$, which can be easily verified by inserting the result for $\Sigma_f(i\nu)$ and then numerically integrating over ν in this limit.

5.3 Results

With the above expressions in hand, we are able to now discuss the resulting conductivity. We will first specialize to certain limits to provide analytic results, and then we will consider the general case numerically.

Analytic results: T-linearity, etc.

The QCP is defined by $\Delta_b = 0$; when inserted into (5.14) and (5.10), we obtain MFL self-energies:

$$\begin{aligned}\Sigma_c(i\omega, T=0) &= g^2\int\frac{d\omega'}{2\pi}G_f(i\omega')G_b(i\omega-i\omega')\\ &= \frac{\gamma m_b}{2\pi\nu_c}\left[i\omega\ln\left(\frac{\sqrt{1+\gamma^2}}{e\Lambda/|\omega|}\right)+\cot^{-1}(\gamma)|\omega|\right]+C_c,\end{aligned} \tag{5.43}$$

and a similar expression for $\Sigma_f(i\omega, T=0)$. The constant C_c can be absorbed into μ_c.

The parameter γ, related to the strength of damping of the b bosons, allows us to tune between different physical regimes. In general we expect γ to increase with the strength of the Kondo coupling g. In the limit of $\gamma \gg 1$, the analytic continuation of (5.43) to real frequency gives

$$\mathrm{Im}[\Sigma_{c,f,R}](\omega, T=0) = -\frac{\gamma m_b}{4\nu_{c,f}}|\omega|, \tag{5.44}$$

which is the traditional MFL form [201]. On the other hand, when $\gamma \ll 1$, the fermion self-energies (5.43) are *asymmetric* about $\omega = 0$:

$$\mathrm{Im}[\Sigma_{c,R}](\omega, T=0) = \frac{\gamma m_b}{2\pi\nu_c}|\omega| \left(-\frac{\pi}{2} - \cot^{-1}(\gamma)\mathrm{sgn}(\omega)\right). \tag{5.45}$$

Thus, in this regime, our model provides a concrete example of a "skewed" MFL [47]. This skewed MFL is expected to have a nonvanishing Seebeck coefficient in the $T \to 0$ limit due to the asymmetric inelastic scattering rate in (5.45) [47, 48]. The nonvanishing Seebeck coefficient as $T \to 0$, and the asymmetric frequency dependence of the electron spectral function, provide experimentally detectable signatures of the small γ regime [3].

In the FL* phase, where $\Delta_b(T=0) > 0$, we obtain, in a similar fashion to (5.43),

$$\Sigma_{c,f}(i\omega, T=0) = -\frac{\gamma m_b \ln(\Lambda/\Delta_b(T=0))}{\pi\nu_{c,f}} i\omega + i\frac{\gamma^2 m_b}{2\pi\nu_{c,f}\Delta_b(T=0)}\omega^2. \tag{5.46}$$

The $\mathcal{O}(\omega^2)$ term leads to a Fermi liquid ω^2 scattering rate on the real frequency axis, and hence a scattering rate $\propto \omega^2 + \pi^2 T^2$ upon analytic continuation to the thermal circle for $T > 0$. The $\mathcal{O}(\omega)$ term leads to a renormalization of the Fermi liquid quasiparticle weights, and hence an enhancement of the conduction electron effective mass, given by

$$m_c^* = m_c \left(1 + \frac{\gamma m_b}{\pi\nu_c} \ln\left(\frac{\Lambda}{\Delta_b(T)}\right)\right). \tag{5.47}$$

Here, we extended the result to small nonvanishing temperatures by replacing $\Delta_b(0) \to \Delta_b(T)$. Since $\Delta_b(T=0) \sim \kappa_c - \kappa$ vanishes on approach to the QCP, the zero temperature effective mass diverges, consistent with experimental findings in HFMs [185, 37]. In the critical region $\Delta_b \propto T$ up to logarithmic corrections. Thus, the divergence of m_c^* is cut-off logarithmically by the temperature at criticality.

Moving to non-zero temperature, in the two limits $\gamma \gg \max(1, \Delta_b/T)$ and $\gamma \ll 1$ we obtain explicit expressions for the imaginary parts of the self-energy in the critical region [1]. For large γ we have

$$\mathrm{Im}[\Sigma_{c,R}(\omega, T)] \approx -\frac{\gamma m_b}{2\pi\nu_c} T\left[\frac{\Delta_b}{\gamma T}\ln\left(\frac{\Lambda e}{\Delta_b}\right) + \pi \ln\left(2\cosh\left(\frac{\omega}{2T}\right)\right)\right];\ \Delta_b/(\gamma T) < 1,$$

$$\Delta_b \approx \frac{\pi\gamma T}{\ln\left(\frac{\Lambda}{T\gamma e}\right)} W_0\left(\frac{2\sqrt{e}}{\pi^2}\ln\left(\frac{\Lambda}{T\gamma e}\right)\right), \tag{5.48}$$

where $W_0(z)$ is the Lambert W function. For $\gamma \ll 1$, (5.43) is well approximated by:

$$\mathrm{Im}[\Sigma_{c,R}(\omega, T)] \approx -\frac{\gamma^2 m_b}{2\pi\nu_c} T\left(1 + e^{\omega/T}\right),\ |\omega| \lesssim T. \tag{5.49}$$

[3] The magnitude of the low-temperature Seebeck coefficient is $\sim k_B/e$ when $\gamma \ll 1$, declining to zero as γ is increased to $\gamma \gg 1$.

Like at $T = 0$ (5.45), this self-energy is asymmetric between positive and negative frequencies, and is therefore skewed.

Taking the $B \to 0$ limit of our expression for σ_{xx} above, Eq. (5.31), gives [144] :

$$\rho_{c,xx} = T \left(\frac{n_c}{8m_c} \int_{-\infty}^{\infty} d\omega \frac{\mathrm{sech}^2(\omega/(2T))}{|\mathrm{Im}[\Sigma_{c,R}(\omega, T)]|} \right)^{-1} . \tag{5.50}$$

In the critical region $\mathrm{Im}[\Sigma_{c,R}(\omega, T)] \sim T$ for $|\omega| \lesssim T$, so that the integral in (5.50) is independent of T at leading order. Thus we get nearly T-linear resistivity in the critical strange metal.

In the FL* phase we found in (5.46) that $|\mathrm{Im}[\Sigma_{c,R}(\omega, T)]| \propto \omega^2 + \pi^2 T^2$. Plugging this into (5.46) gives $\rho_{xx} \propto T^2$ as in a normal Fermi liquid.

Planckian dissipation

As we discussed in Chapter 1, It has been proposed that inelastic relaxation times, in most if not all situations, cannot be much smaller than the quantum mechanical "Planckian" time scale $\tau_P = \hbar/(k_B T)$ (see [57] and references therein). There is a growing list of materials, showing strange metal behavior at low temperatures, which seem to be close to this limit, namely they relax on the Planckian time scale up to a constant of order one [18, 109, 128, 22, 143]. Since the self-energies calculated above imply relaxation times proportional to $1/T$, it is interesting to ask how systems described by this model line up with the proposed Planckian bound.

Note however, that the correct quasiparticle relaxation time cannot be extracted directly as the inverse $\mathrm{Im}\Sigma_R$. Rather it is renormalized by the same factor as the mass. To see this, we eliminate the prefactor of the ω term to obtain the standard Fermi liquid form of the Green's function

$$G_{c,R}(\omega, k) = \frac{Z}{\omega - Z\xi_k - iZ\mathrm{Im}\left[\Sigma_{c,R}(\omega)\right]} \tag{5.51}$$

with $Z = m/m_c^*$. From this we can immediately obtain $1/\tau_c = Z\,\mathrm{Im}\left(\Sigma_{c,R}(\omega = 0)\right)$. This is the same timescale extracted from analysis of transport data pertaining to strange metal QCPs [18, 109, 128, 22, 143] using the Drude formula for quasi particle transport $\tau = m^*\sigma_{xx}/(ne^2)$. In the experiments the effective quasiparticle mass is measured slightly away from the critical point. Note that we focus here on the relaxation rates of the conduction electrons because they dominate the transport.

In the strongly damped regime, where $\gamma \gg 1, \Delta_b/T$, equations (5.47) and (5.48) give

$$\begin{aligned} \tau_c &= \left(\frac{\pi \nu_c}{\gamma m_b} + \ln\left(\frac{\Lambda}{\gamma T}\right) \right) \frac{\hbar}{k_B T} \\ &\approx \ln\left(\frac{\Lambda}{\gamma T}\right) \frac{\hbar}{k_B T}, \end{aligned} \tag{5.52}$$

At realistic temperatures τ_c can be viewed as Planckian relaxation modified only by a slowly varying logarithmic function of temperature and nearly independent of the microscopic couplings. The result provides an appealing potential explanation for observation of near Planckian relaxation across different materials, with $\mathcal{O}(1)$ proportionality constants that vary only slightly between materials [18].

In the weakly damped regime $\gamma \ll 1$ equations (5.47) and (5.49) give

$$\tau_c = \frac{1}{\gamma}\left(\frac{\pi\nu_c}{\gamma m_b} + \ln\left(\frac{\Lambda}{T\ln(\pi/\gamma)}\right)\right)\frac{\hbar}{k_B T}, \tag{5.53}$$

which is manifestly nonuniversal. The proposed Planckian lower bound is still obeyed, but exceeded by a large factor of at least $1/\gamma$. Thus we do not expect Planckian transport in the weak damping regime. Such "sub-Planckian" behavior has in fact recently been reported in experiments on HFMs [194].

Numerical approach

In this model, we have the following parameters: m_λ, γ, and $n_{c/f}$. We have already discussed how the various limits of γ can effect the results above, and we take the masses in the scale $m_b \gg m_f \gg m_c$. We can vary the densities n_c, n_f, which implicitly set the μ_f and μ_c, but we fix them to be $n_c = n_f = 1$. We were considering a fully 2D system above, but we have the flexibility to make the conduction electrons c three-dimensional to yield a more physically relevant model in which case the f and b occupy disconnected 2D planes. We use this interpretation below; the only difference is the relationship between ν_c and n_c.

For a given temperature, T, magnetic field, B, and $\Delta\kappa = \kappa - \kappa_c$, in order to evaluate the conductivity, we first need to self-consistently solve for the effective magnetic field $B_{\text{eff}}^{b/f}$ using

$$B_{\text{eff}}^{f} = \frac{\chi_b}{\chi_b + \chi_f}B; \qquad B_{\text{eff}}^{b} = \frac{\chi_f}{\chi_b + \chi_f}B. \tag{5.54}$$

The value of $\chi_f = 1/(24\pi m_f)$ is set, but χ_b, as determined from Eq. (5.41) depends on $z = \Delta_b/T$. In turn, the value of Δ_b is determined by Eq. (5.23), which requires the effective field as input. Note that the effective field is strongly renormalized when $\chi_b/\chi_f \gg 1$, such as when $\Delta\kappa > 0$, and it is worth using the $B \to 0$ expression for Δ_b in this regime.

Once we have found a self-consistent solution, we will know the effective fields and Δ_b. By inserting Eq. (5.18) into Eq. (5.16) (and an equivalent expression for $\text{Im}\,[\Sigma_{f,R}]$ with $\omega \leftrightarrow -\omega$ and $\nu_f \leftrightarrow \nu_c$) and noting $\Sigma_{b,R}(\omega) = -i\gamma\omega$, we will have evaluated all of the self-energy expressions. With $\gamma \ll 1$, we ensure that the real part of the self-energy (derivable via the Kramers-Kronig relation) does not meaningfully renormalize the fermion chemical potentials, but this limit can also be checked numerically. Finally, inserting the self-energies into Eq. (5.31) and Eq. (5.33) (with $e_\lambda^2 = 1$ for all species), we then combine the conductivities via the Ioffe-Larkin composition rule $\boldsymbol{\sigma}_{\text{tot}} = \boldsymbol{\sigma}_c + (\boldsymbol{\sigma}_f^{-1} + \boldsymbol{\sigma}_b^{-1})$.

As a representative point, we set $\gamma = 0.02 \ll 1$, $\Lambda m_b = \pi^2/2$, and $m_b = 5m_f = 50m_c$. As we can see in Fig. 5.4, we have FL like behavior when $\kappa < \kappa_c$ and T-linear (up to logarithmic corrections) behavior in the critical fan.

We also plot R_H vs. κ. We find that there is a small peak at $\kappa = \kappa_c$ with a value of 4/3 [1]. As we move to larger κ, there is an increase in R_H.

We can see this increase more clearly in Fig. 5.5. The enhancement is dominated by the contribution of the boson conductivity $\boldsymbol{\sigma}_b$ to the total conductivity $\boldsymbol{\sigma}$. The strong non-monotonic behavior stems from a competition between two effects. On the one hand the boson gap decreases rapidly with decreasing temperature and becomes exponentially suppressed below the grayed out crossover regime, $\Delta_b \sim T \exp\left[-\frac{2\pi(\kappa-\kappa_c)}{Tm_b}\right]$. This leads to a large $\sigma_{b,xy}$ due to bosons excited above the small gap. On the other hand, the susceptibility χ_b diverges rapidly ultimately leading to vanishing of B_b and hence also of $\boldsymbol{\sigma}_b$ at zero temperature. The interplay between these two effects leads to the sharp peak in $|R_H|$ versus temperature seen in Fig. 5.5.

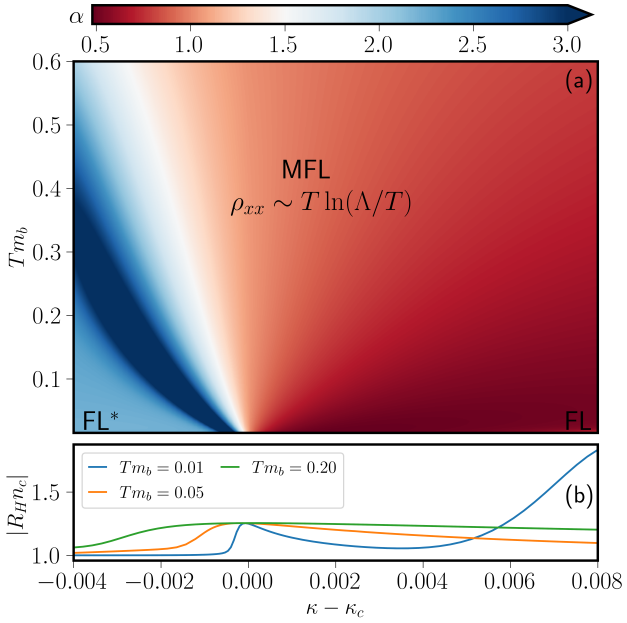

Figure 5.4: (a) The phase diagram for our 2D model. The resistivity is given by $\rho_{xx} - \rho_{xx}(T = 0) \sim T^\alpha \ln(\Lambda/T)$, and the color indicates the value of $\alpha = d\ln(\rho_{xx}/\ln(\Lambda/T))/d\ln(T)$. (b) The plot of the weak-field R_H vs. $\kappa - \kappa_c$. R_H has a peak near the crossover from Fermi-liquid behavior to T-linear resistivity and approaches a constant to either side signaling the change in carrier density. The large peak of R_H seen at low temperatures is occurring as the boson is condensing, as discussed in Fig. 5.5. Here, $\gamma = 0.02$, $nc = nf = 1$, $\Lambda m_b = \pi^2/2$, and $m_b = 5m_f = 50m_c$.

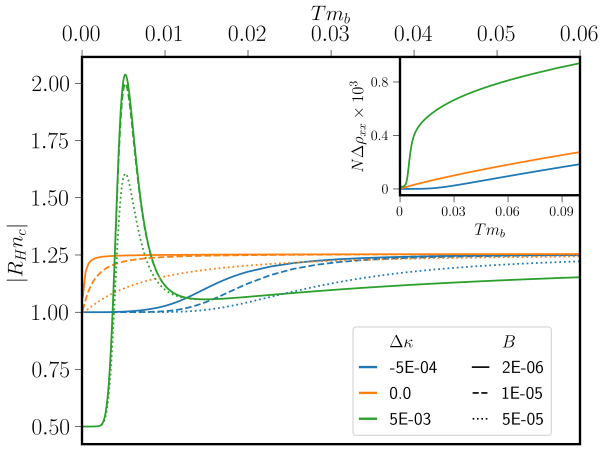

Figure 5.5: R_H vs. T for various B and $\Delta\kappa = \kappa - \kappa_c$, computed numerically without any approximations. R_H is roughly constant within the critical region and is higher than the expected $R_H \approx -1/n_c$ seen in the FL* region (blue and orange curves). A larger B suppresses R_H slightly. There is a large enhancement in the crossover region between the condensed bosons and the quantum critical region, when we ignore inter-layer instabilities for $\kappa > \kappa_c$ (green curve). (Inset) $\Delta\rho_{xx} \equiv \rho_{xx} - \rho_{xx}(T = 0)$ vs. T for different values of $\Delta\kappa$. The other parameters are the same as in Fig. 5.4. Copyright © 2022 by the American Physical Society. Reproduced from Ref. [1] with permission.

3D modification

Using the expressions from the previous sections, we have evaluated ρ_{xx} and R_H for a 2D model (or a 3D model without inter-layer couplings for the f and b fields) for all values of parameters at small B. We have devised this model in thinking about experiments on $CeCoIn_5$, which shows some aspects of 2D physics even as a 3D material (i.e. there is strong anisotropy in the c direction) [147]. Therefore our 2D stacked layers model may be more relevant than a fully 3D model.

However, we must analyze possible instabilities that will take us away from our fully 2D solution. When there is a third spatial dimension present, we should therefore ask what relevant inter-layer interactions are allowed and what their impact on the physics will be.

An important feature of our model is that the b and f partons are deconfined in a stack of independent 2D layers. We can therefore write down the following large N, instability inducing [141], local, gauge-invariant, quartic interactions between adjacent layers l and l',

where r denotes the 2D coordinate of a site within a layer:

$$H_{bb} = -\frac{J_b}{N}\sum_{i,j=1}^{N}\sum_{r} b^\dagger_{r(l),i} b_{r(l'),i} b^\dagger_{r(l'),j} b_{r(l),j},$$
$$H'_{bb} = -\frac{J'_b}{N}\sum_{i,j=1}^{N}\sum_{r} b^\dagger_{r(l),i} b^\dagger_{r(l'),i} b_{r(l'),j} b_{r(l),j}, \tag{5.55}$$

$$H_{ff} = -\frac{J_f}{N}\sum_{i,j=1}^{N}\sum_{\substack{r,\sigma,\sigma',\\ \tau,\tau'}} f^\dagger_{r(l),i,\sigma} f^\dagger_{r(l'),i,\sigma'} f_{r(l'),j,\tau} f_{r(l),j,\tau'},$$
$$H_{bf} = -\frac{J_{bf}}{N}\sum_{i,j=1}^{N}\sum_{r,\sigma}\left[b^\dagger_{r(l),i} b_{r(l'),i} f^\dagger_{r(l),j,\sigma} f_{r(l'),j,\sigma} + \text{H.c}\right].$$

None of these terms contribute directly to the parton self-energies or transport at large N. H_{ff} induces BCS-like inter-layer f fermion pairing instabilities, which occur at exponentially small energy scales, and are therefore not of concern to us. The terms in H_{bb} create inter-layer boson instabilities driven by susceptibilities that scale as $\sim m_b J'_b \ln(\Lambda/\Delta_b)$. In the gapped phase of the boson, and in the quantum critical region, these susceptibilities are thus small at the temperature scales of interest, hence we ignore them. However, for $\kappa > \kappa_c$, $\Delta_b(T)$ starts decreasing rapidly below some temperature scale (Fig. 5.1), which makes these susceptibilities large, causing the onset of instabilities that lead to the condensation of inter-layer boson bilinears. The resulting 3D boson phase will then further have single-boson condensation as temperature is lowered [159]. Once this happens, both the partons will have 3D dispersions as these boson interaction terms will appear like inter-layer hoppings, $b^\dagger_l b^\dagger_{l'} b_l b_{l'} \sim c_b b^\dagger_l b_{l'}$, and H_{bf} will similarly generate inter-layer hopping for the f fermions [4]. This leads to two important changes to the model; first the partons develop an anisotropic dispersion with hopping proportional to the single-boson condensate strength at low temperatures, and second the fermions now scatter off both the $N-1$ critical bosons $b_{2,..,N}$ as well as the condensed mode $\langle b_1 \rangle$.

To model these effects, the dispersion of the partons is changed to be

$$\epsilon_{b/f,k} = \frac{1}{2m_{b/f}}(k_x^2 + k_y^2 + Y_{b/f} k_z^2), \quad Y_{b/f} = 4\pi^2 J_{b/bf} r_0^2, \tag{5.56}$$

where r_0 is the size of the condensate. Rewriting the Schwinger-Dyson equations within the condensed phase, the only changes are to the fermion self-energy and the constraint. The constraint equation becomes

$$\kappa - \kappa_c = r_0^2 + (n_b - n_b^c), \tag{5.57}$$

[4] H'_{bb} will also generate inter-layer boson pairing terms $\sim c'_b b^\dagger_l b^\dagger_{l'}$, but the Hugenholtz-Pines theorem [73] nevertheless ensures a 3D gapless boson phase, with the same effects on the fermions.

where, in this equation, n_b is the number of bosons not participating in the condensate with $\Delta_b = 0$, and using the self-consistently determined dispersion. The self-energy expression is changed to be

$$\mathrm{Im}[\Sigma_{c,R}] = -r_0^2 g^2 \frac{\nu_f}{2} - g^2 \frac{\nu_f}{4\pi} \int_{-\infty}^{\infty} d\epsilon \bar{A}_b(\epsilon)(n_B(\epsilon) + n_F(\epsilon - \omega)),$$

with $\tilde{A}_b$ the spectral function of the uncondensed modes.

To keep the number of f fermions fixed, as the dispersion changes, the Fermi energy shifts which in turn modifies the density of states. In order to connect with the 2D model, we introduce a maximum momentum in the z direction, K. The spinless density of states is then given by

$$\nu_f = \begin{cases} \frac{K m_f}{\pi} & \epsilon_F^0 > \frac{Y_f K^2}{3 m_f} \\ \frac{m_f}{\pi} \left(\frac{3 \epsilon_F^0 K m_f}{c_f} \right)^{1/3} & \epsilon_F^0 < \frac{Y_f K^2}{3 m_f} \end{cases}, \tag{5.58}$$

where $\epsilon_{F,0}$ is the Fermi energy with $Y_f = 0$. Note that we take $K = \pi$ so the density of states in the small condensate regime is $\nu_f = m_f$, the same as in the purely 2D case. We will work in the regime where the second condition of (5.58) is never reached; this is achieved by taking J_{bf} sufficiently small. If the second condition was achieved, $\gamma = g^2 \nu_c \nu_f / (2\pi)$ would change.

The spectral function for the uncondensed modes can be evaluated utilizing the 2D results by replacing $\Delta_b \to \Delta_b + Y_b k_z^2/(2m_b)$ in (5.18) to find

$$\begin{aligned} \frac{2\pi}{m_b} \tilde{A}_b(\omega, 0) = K \mathrm{sgn}(\omega) - \frac{2K}{\pi} \tan^{-1} \left(\frac{Y_b K^2}{4\gamma m_b \omega} - \frac{1}{\gamma} \right) \\ - \frac{4}{\pi Y_b} \mathrm{Im} \left[\sqrt{2(1 + i\gamma)\omega m_b} \tanh^{-1} \left(\frac{Y_b K}{\sqrt{2 m_b (1 + i\gamma)\omega}} \right) \right]. \end{aligned} \tag{5.59}$$

Unlike the $O(N)$ rotor model, the dispersion is also modified as the condensate grows. This changing dispersion results in a different temperature dependence when $T m_b \gg \kappa - \kappa_c$ and also results in multiple self-consistent values of the condensate size r_0 at fixed κ and T. If we assume interactions which generate a 3D instability at $T = 0$, the physical solution for r_0 is the one that approaches a non-zero constant at low temperatures, which is the one we use in our numerical calculations.

Deep in the condensed phase at low temperatures, r_0 will be roughly constant and large. In this regime, the frequency dependence of the spectral function for the uncondensed boson modes then goes as as $\sqrt{\omega}$, leading directly to $\mathrm{Im}[\Sigma_{c,R}(\omega = 0, T)] \sim T^{3/2} + \text{const.}$ behavior. Therefore, in the 3D version of our model, we will recover power-law scaling with temperature when $\kappa > \kappa_c$ as well.

5.4 Discussion

The new large N approach formulated in this chapter captures a strongly coupled QCP, showing linear in T resistivity at a Kondo breakdown transition involving a change of the Fermi surface volume. Such MFL phenomenology, seen ubiquitously in experiments with heavy fermion materials, could not be obtained in a controlled way within previous large N theories [155, 31, 6, 175]. The essential new element in our formulation is that the number of fermions and critical boson species are both scaled with N.

The MFL with linear in T resistivity is obtained for a 3D system only if the QCP and adjacent FL* phase are deconfined in layers, that is deconfined inside 2D planes, yet confined between planes.[5] This model can be tuned between two regimes by a coupling constant γ. In the strong damping limit $\gamma \gg 1$ the system exhibits Planckian dissipation, with a universal electron relaxation time $\tau_{tr} \approx \hbar/(k_B T)$. The strong damping also prevents any significant enhancement of the Hall coefficient R_H in the critical regime. In the weak damping regime, $\gamma \ll 1$, the transport relaxation time is much larger than the Planckian time (by a factor $1/\gamma$), and the Hall coefficient R_H is enhanced in the critical regime. Furthermore, the electron self-energy in this regime is "skewed", with an asymmetry in the damping of particle vs. hole excitations (5.49). We note that strange metallic behavior with a transport relaxation time much larger than the Planckian time has been observed experimentally in HFMs [194].

A testable prediction, which follows is that Planckian dissipation at the QCP cannot be accompanied by enhancement of the Hall coefficient R_H. Enhancement of R_H at the QCP, as has been observed in recent experiments with $CeCoIn_5$ [121], can occur only in the weakly damped regime of our model, where a set of additional features are predicted: first, the QCP and the nearby FL* phase are deconfined only within 2D planes, which would have observable implications on transport. For example, the thermal conductivity is expected to be strongly anisotropic, because in this phase spinons contribute to the in-plane, but not to the out-of-plane thermal transport. The charge conductivity, on the other hand, is dominated by the conduction electrons, which can hop between planes, and would therefore be much more isotropic. Consequently, only the in-plane Lorenz ratio is expected to be significantly enhanced. Another unique property of the weakly damped ($\gamma \ll 1$) MFL, is a skewed fermion spectral function, which is expected to generate a low temperature Seebeck coefficient in the critical regime [47, 144]. Sizeable $T \to 0$ Seebeck coefficients have recently been reported experimentally in 2D strange metals [48, 32], and it would be interesting to investigate whether these arise due to skewed electron self-energies.

Finally, let us return to how well our model captures the QCP in $CeCoIn_5$. The four main experimental signatures are: 1) $1/R_H$ at low temperatures and high fields exhibits a sharp increase, 2) at low fields and low temperatures R_H has a peak in temperature, 3) ARPES and quantum oscillations see new features of the Fermi surface, and 4) T-linear resistivity above the QCP. Just as our model in the previous chapter, we capture points 1 and 3 by the

[5] We can consider a fully 3D model that captures similar effects without the need for deconfined layers if the g^r_{ijk} are site-correlated [1]; however, in that case, the Fermi surfaces of the c and f must be matched.

nature of having a small-to-large Fermi surface transition. The hybridization of the f and c fields by the (nearly) condensed b field when $\kappa > \kappa_c$ and f's non-contribution to $\boldsymbol{\sigma}$ when the bosons are not condensed explains both of these features. Unlike the previous chapter, we are able to address point 4 and describe MFL physics in the critical fan. For point 2, we saw that the boson condensing can lead to a large increase in R_H, which qualitatively matches what is seen in the experiment. In order for the peak height of R_H to decrease as $\kappa > \kappa_c$ (currently it only increases as κ increases), we may need to add an impurity scattering of the bosons as we did in the previous chapter.

In total, this model captures much of the necessary ingredients to understand the QCP of $CeCoIn_5$. Although the model is not the most physical starting point, it does succeed in providing a solvable model that captures much of the phenomenology including the MFL physics. The new large N approach we have introduced to study the Kondo breakdown transition in HFM can also be useful in formulating a controlled theory of other quantum critical states. The high T_c cuprate superconductors, for example, exhibit similar signatures of FS reconstruction near optimal doping [150], accompanied by T-linear resistivity [191]. While there are no local moments to be subsumed in the Fermi sea, a parton model describing a change in FS volume has recently been proposed [221]. Investigating this QCP using the new large N scheme is an interesting problem for future work. Our approach can also be used to address the interplay of these critical fluctuations with superconductivity and magnetism, which appear to be crucial to cuprate phenomenology.

Chapter 6

Conclusion

In this dissertation, I have focused on two materials α-$RuCl_3$ and $CeCoIn_5$. Both compounds are examples of quantum materials, and I analyzed them with a combination of exact and approximate techniques.

α-$RuCl_3$ is a prime candidate for a material realization of the Kitaev spin liquid, which could make it the first definitively identified spin liquid. My analysis of the thermal Hall effect data is consistent with a large Kitaev interaction term in the material's approximate Hamiltonian. However, the INS spectrum seen in experiments on α-$RuCl_3$ is not consistent with my predictions using TDMFT. My results, in combination with the inability for the candidate model Hamiltonians for this material to predict a Kitaev spin liquid phase [56, 211] and the inconsistency of experimental evidence for a quantized thermal Hall plateau [87, 218, 20, 215, 39, 107], do not present a compelling argument that α-$RuCl_3$ will yield a Kitaev spin liquid platform. The main challenge, at this stage, appears to be in achieving consistent experimental results; without them, it is not clear whether we theorists are analyzing signal or noise.

As I discuss, TDMFT is not just applicable to α-$RuCl_3$. My approach can be used to analyze any Kitaev spin liquid candidate. Several other candidates have been put forth over the years, such as Na_2IrO_3 [217, 33, 74, 180, 181, 25, 117], Li_2IrO_3 [181, 207, 16, 210], $H_3LiIr_2O_6$ [95, 192], and $Na_2Co_2TeO_6$ [113]. It has been difficult to grow large enough single-crystal samples of the iridate compounds for INS experiments, but, as that obstacle is overcome, these other candidate materials may provide a more straight-forward avenue to a Kitaev spin liquid. As my analysis shows, the key signature would be an INS signal closely matching that of the pure Kitaev model across the 1BZ.

In $CeCoIn_5$, my experimental colleagues find direct evidence for a Fermi surface reconstruction transition without symmetry breaking. In the context of that theory, I was able to heuristically explain the low-temperature peak of the Hall coefficient, and I developed a model based reminiscent of the SYK model that is exactly solvable and captures much of the qualitative aspects of the experiment. Taken together, my analysis suggests that the strange metallicity of $CeCoIn_5$ is likely due to a quantum critical point (QCP). The presence of a QCP, which may bear some similarity to a QCP found in the cuprates [121], may help

explain why $CeCoIn_5$ bears similarities to the high-temperature superconductors.

A QCP explanation for strange metallicity, however, is not sufficient to explain T-linear resistance in all materials [57]. The SYK model has provided more analytic control in analyzing certain scenarios [27], but new ideas continue to appear. Recent work proposes the idea of an Ersatz Fermi liquid [42], which shares many of the properties of Fermi liquids and may explain why strange metals seem to still possess Fermi liquid-like properties but different dynamics. Despite much progress, connecting recent ideas like the SYK model to material properties in order to guide the search for higher temperature superconductors remains a key theoretical challenge.

Bibliography

[1] Erik E. Aldape et al. "Solvable theory of a strange metal at the breakdown of a heavy Fermi liquid". In: *Phys. Rev. B* 105 (23 June 2022), p. 235111. DOI: 10.1103/PhysRevB.105.235111. URL: https://link.aps.org/doi/10.1103/PhysRevB.105.235111.

[2] Andrea Amoretti. *Condensed matter applications of AdS/CFT: Focusing on strange metals*. Springer, 2017.

[3] P.W. Anderson. "Resonating valence bonds: A new kind of insulator?" In: *Materials Research Bulletin* 8.2 (1973), pp. 153–160. ISSN: 0025-5408. DOI: https://doi.org/10.1016/0025-5408(73)90167-0. URL: http://www.sciencedirect.com/science/article/pii/0025540873901670.

[4] Neil W Ashcroft and N David Mermin. *Solid state physics*. Cengage Learning, 2022.

[5] Assa Auerbach. "Equilibrium formulae for transverse magnetotransport of strongly correlated metals". In: *Phys. Rev. B* 99 (11 Mar. 2019), p. 115115. DOI: 10.1103/PhysRevB.99.115115. URL: https://link.aps.org/doi/10.1103/PhysRevB.99.115115.

[6] Assa Auerbach and K Levin. "Kondo bosons and the Kondo lattice: Microscopic basis for the heavy Fermi liquid". In: *Physical review letters* 57.7 (1986), p. 877. URL: https://journals.aps.org/prl/abstract/10.1103/PhysRevLett.57.877.

[7] S.-H. Baek et al. "Evidence for a Field-Induced Quantum Spin Liquid in α-$RuCl_3$". In: *Phys. Rev. Lett.* 119 (3 July 2017), p. 037201. DOI: 10.1103/PhysRevLett.119.037201. URL: https://link.aps.org/doi/10.1103/PhysRevLett.119.037201.

[8] A Banerjee et al. "Proximate Kitaev quantum spin liquid behaviour in a honeycomb magnet". In: *Nature materials* 15.7 (2016), pp. 733–740.

[9] Arnab Banerjee et al. "Excitations in the field-induced quantum spin liquid state of α-RuCl 3". In: *npj Quantum Materials* 3.1 (2018), pp. 1–7.

[10] Arnab Banerjee et al. "Neutron scattering in the proximate quantum spin liquid α-RuCl3". In: *Science* 356.6342 (2017), pp. 1055–1059. ISSN: 0036-8075. DOI: 10.1126/science.aah6015.

[11] Mitali Banerjee et al. "Observation of half-integer thermal Hall conductance". In: *Nature* 559.7713 (2018), pp. 205–210.

[12] G. Baskaran, Saptarshi Mandal, and R. Shankar. "Exact Results for Spin Dynamics and Fractionalization in the Kitaev Model". In: *Phys. Rev. Lett.* 98 (24 June 2007), p. 247201. DOI: 10.1103/PhysRevLett.98.247201. URL: https://link.aps.org/doi/10.1103/PhysRevLett.98.247201.

[13] Erez Berg et al. "Monte Carlo studies of quantum critical metals". In: *Annual Review of Condensed Matter Physics* 10 (2019), pp. 63–84.

[14] Christoph Berke, Simon Trebst, and Ciarán Hickey. "Field stability of Majorana spin liquids in antiferromagnetic Kitaev models". In: *Phys. Rev. B* 101 (21 June 2020), p. 214442. DOI: 10.1103/PhysRevB.101.214442. URL: https://link.aps.org/doi/10.1103/PhysRevB.101.214442.

[15] A. Bianchi et al. "Avoided antiferromagnetic order and quantum critical point in $CeCoIn_5$". In: *Physical Review Letters* 91.25 (Dec. 2003), p. 257001. ISSN: 0031-9007.

[16] A. Biffin et al. "Noncoplanar and Counterrotating Incommensurate Magnetic Order Stabilized by Kitaev Interactions in $\gamma-Li_2IrO_3$". In: *Phys. Rev. Lett.* 113 (19 Nov. 2014), p. 197201. DOI: 10.1103/PhysRevLett.113.197201. URL: https://link.aps.org/doi/10.1103/PhysRevLett.113.197201.

[17] P. Bonche, S. Koonin, and J. W. Negele. "One-dimensional nuclear dynamics in the time-dependent Hartree-Fock approximation". In: *Phys. Rev. C* 13 (3 Mar. 1976), pp. 1226–1258. DOI: 10.1103/PhysRevC.13.1226. URL: https://link.aps.org/doi/10.1103/PhysRevC.13.1226.

[18] J. A. N. Bruin et al. "Similarity of Scattering Rates in Metals Showing T-Linear Resistivity". In: *Science* 339.6121 (2013), pp. 804–807. ISSN: 0036-8075. DOI: 10.1126/science.1227612. eprint: https://science.sciencemag.org/content/339/6121/804.full.pdf. URL: https://science.sciencemag.org/content/339/6121/804.

[19] JAN Bruin et al. "Origin of oscillatory structures in the magnetothermal conductivity of the putative Kitaev magnet α-$RuCl_3$". In: *arXiv preprint arXiv:2205.15839* (2022).

[20] JAN Bruin et al. "Robustness of the thermal Hall effect close to half-quantization in α-RuCl3". In: *Nature Physics* (2022), pp. 1–5.

[21] H. B. Cao et al. "Low-temperature crystal and magnetic structure of $\alpha - RuCl_3$". In: *Phys. Rev. B* 93 (13 Apr. 2016), p. 134423. DOI: 10.1103/PhysRevB.93.134423. URL: https://link.aps.org/doi/10.1103/PhysRevB.93.134423.

[22] Yuan Cao et al. "Strange metal in magic-angle graphene with near Planckian dissipation". In: *Phys. Rev. Lett.* 124 (7 Feb. 2020), p. 076801. DOI: 10.1103/PhysRevLett.124.076801. URL: https://link.aps.org/doi/10.1103/PhysRevLett.124.076801.

[23] Robert Cava, Nathalie De Leon, and Weiwei Xie. *Introduction: quantum materials.* 2021.

[24] Li Ern Chern, Emily Z. Zhang, and Yong Baek Kim. "Sign Structure of Thermal Hall Conductivity and Topological Magnons for In-Plane Field Polarized Kitaev Magnets". In: *Phys. Rev. Lett.* 126 (14 Apr. 2021), p. 147201. DOI: 10.1103/PhysRevLett.126.147201. URL: https://link.aps.org/doi/10.1103/PhysRevLett.126.147201.

[25] S. K. Choi et al. "Spin Waves and Revised Crystal Structure of Honeycomb Iridate Na_2IrO_3". In: *Phys. Rev. Lett.* 108 (12 Mar. 2012), p. 127204. DOI: 10.1103/PhysRevLett.108.127204.

[26] Wonjune Choi et al. "Topological superconductivity in the Kondo-Kitaev model". In: *Phys. Rev. B* 98 (15 Oct. 2018), p. 155123. DOI: 10.1103/PhysRevB.98.155123. URL: https://link.aps.org/doi/10.1103/PhysRevB.98.155123.

[27] Debanjan Chowdhury et al. "Sachdev-Ye-Kitaev models and beyond: Window into non-Fermi liquids". In: *Rev. Mod. Phys.* 94 (3 Sept. 2022), p. 035004. DOI: 10.1103/RevModPhys.94.035004. URL: https://link.aps.org/doi/10.1103/RevModPhys.94.035004.

[28] Debanjan Chowdhury et al. "Translationally invariant non-fermi-liquid Metals with critical fermi surfaces: solvable models". In: *Phys. Rev. X* 8 (3 July 2018), p. 031024. DOI: 10.1103/PhysRevX.8.031024. URL: https://link.aps.org/doi/10.1103/PhysRevX.8.031024.

[29] P. Coleman. "Theories of non-Fermi liquid behavior in heavy fermions". In: *Physica B* 259-261 (Jan. 1999), pp. 353–358.

[30] Piers Coleman. "Heavy fermions: electrons at the edge of magnetism". In: *Handbook of magnetism and advanced magnetic materials* (2007). URL: https://onlinelibrary.wiley.com/doi/abs/10.1002/9780470022184.hmm105.

[31] Piers Coleman. "New approach to the mixed-valence problem". In: *Physical Review B* 29.6 (1984), p. 3035. URL: https://journals.aps.org/prb/abstract/10.1103/PhysRevB.29.3035.

[32] C. Collignon et al. "Thermopower across the phase diagram of the cuprate $La_{1.6-x}Nd_{0.4}Sr_xCuO_4$: Signatures of the pseudogap and charge density wave phases". In: *Phys. Rev. B* 103 (15 Apr. 2021), p. 155102. DOI: 10.1103/PhysRevB.103.155102. URL: https://link.aps.org/doi/10.1103/PhysRevB.103.155102.

[33] R. Comin et al. "Na_2IrO_3 as a Novel Relativistic Mott Insulator with a 340-meV Gap". In: *Phys. Rev. Lett.* 109 (26 Dec. 2012), p. 266406. DOI: 10.1103/PhysRevLett.109.266406. URL: https://link.aps.org/doi/10.1103/PhysRevLett.109.266406.

[34] Tessa Cookmeyer and Joel E Moore. "Dynamics of fractionalized mean-field theories: consequences for Kitaev materials". In: *arXiv arXiv:2206.04788* (2022).

[35] Tessa Cookmeyer and Joel E. Moore. "Spin-wave analysis of the low-temperature thermal Hall effect in the candidate Kitaev spin liquid $\alpha - RuCl_3$". In: *Phys. Rev. B* 98 (6 Aug. 2018), p. 060412. DOI: 10.1103/PhysRevB.98.060412. URL: https://link.aps.org/doi/10.1103/PhysRevB.98.060412.

[36] Tessa Cookmeyer, Johannes Motruk, and Joel E. Moore. "Four-Spin Terms and the Origin of the Chiral Spin Liquid in Mott Insulators on the Triangular Lattice". In: *Phys. Rev. Lett.* 127 (8 Aug. 2021), p. 087201. DOI: 10.1103/PhysRevLett.127.087201. URL: https://link.aps.org/doi/10.1103/PhysRevLett.127.087201.

[37] J. Custers et al. "The break-up of heavy electrons at a quantum critical point". In: *Nature* 424.6948 (July 2003), pp. 524–527. ISSN: 1476-4687. DOI: 10.1038/nature01774. URL: https://doi.org/10.1038/nature01774.

[38] Peter Czajka et al. "Oscillations of the thermal conductivity in the spin-liquid state of α-RuCl3". In: *Nature Physics* 17.8 (2021), pp. 915–919.

[39] Peter Czajka et al. "Planar thermal Hall effect of topological bosons in the Kitaev magnet α-RuCl3". In: (2022).

[40] P. A. M. Dirac. "Note on Exchange Phenomena in the Thomas Atom". In: *Mathematical Proceedings of the Cambridge Philosophical Society* 26.3 (1930), pp. 376–385. DOI: 10.1017/S0305004100016108.

[41] Seung-Hwan Do et al. "Majorana fermions in the Kitaev quantum spin system α-RuCl3". In: *Nature Physics* 13.11 (2017), pp. 1079–1084.

[42] Dominic V. Else, Ryan Thorngren, and T. Senthil. "Non-Fermi Liquids as Ersatz Fermi Liquids: General Constraints on Compressible Metals". In: *Phys. Rev. X* 11 (2 Apr. 2021), p. 021005. DOI: 10.1103/PhysRevX.11.021005. URL: https://link.aps.org/doi/10.1103/PhysRevX.11.021005.

[43] Lucas R. D. Freitas and Rodrigo G. Pereira. "Gapless excitations in non-Abelian Kitaev spin liquids with line defects". In: *Phys. Rev. B* 105 (4 Jan. 2022), p. L041104. DOI: 10.1103/PhysRevB.105.L041104. URL: https://link.aps.org/doi/10.1103/PhysRevB.105.L041104.

[44] Yong Hao Gao et al. "Thermal Hall signatures of non-Kitaev spin liquids in honeycomb Kitaev materials". In: *Phys. Rev. Research* 1 (1 Aug. 2019), p. 013014. DOI: 10.1103/PhysRevResearch.1.013014. URL: https://link.aps.org/doi/10.1103/PhysRevResearch.1.013014.

[45] P. Gegenwart, Q. Si, and F. Steglich. "Quantum criticality in heavy-fermion metals". In: *Nature Physics* 4.3 (Mar. 2008), pp. 186–197.

[46] P. Gegenwart et al. "Breakup of heavy fermions on the brink of "Phase A" in $CeCu_2Si_2$". In: *Phys. Rev. Lett.* 81.7 (1998), pp. 1501–1504. ISSN: 10797114. DOI: 10.1103/PhysRevLett.81.1501.

[47] Antoine Georges and Jernej Mravlje. "Skewed Non-Fermi Liquids and the Seebeck Effect". In: *arXiv e-prints*, arXiv:2102.13224 (Feb. 2021), arXiv:2102.13224. arXiv: 2102.13224 [cond-mat.str-el].

[48] Bhaskar Ghawri et al. "Excess entropy and breakdown of semiclassical description of thermoelectricity in twisted bilayer graphene close to half filling". In: *arXiv e-prints*, arXiv:2004.12356 (Apr. 2020), arXiv:2004.12356. arXiv: 2004.12356.

[49] Ara Go, Jun Jung, and Eun-Gook Moon. "Vestiges of Topological Phase Transitions in Kitaev Quantum Spin Liquids". In: *Phys. Rev. Lett.* 122 (14 Apr. 2019), p. 147203. DOI: 10.1103/PhysRevLett.122.147203. URL: https://link.aps.org/doi/10.1103/PhysRevLett.122.147203.

[50] Matthias Gohlke, Roderich Moessner, and Frank Pollmann. "Dynamical and topological properties of the Kitaev model in a [111] magnetic field". In: *Phys. Rev. B* 98 (1 July 2018), p. 014418. DOI: 10.1103/PhysRevB.98.014418. URL: https://link.aps.org/doi/10.1103/PhysRevB.98.014418.

[51] Matthias Gohlke et al. "Dynamics of the Kitaev-Heisenberg Model". In: *Phys. Rev. Lett.* 119 (15 Oct. 2017), p. 157203. DOI: 10.1103/PhysRevLett.119.157203. URL: https://link.aps.org/doi/10.1103/PhysRevLett.119.157203.

[52] Shou-Shu Gong, Wei Zhu, and D. N. Sheng. "Emergent chiral spin liquid: Fractional quantum Hall effect in a kagome Heisenberg model". In: *Scientific reports* 4 (2014), p. 6317.

[53] Shou-Shu Gong et al. "Chiral spin liquid with spinon Fermi surfaces in the spin-$\frac{1}{2}$ triangular Heisenberg model". In: *Phys. Rev. B* 100 (24 Dec. 2019), 241111(R). DOI: 10.1103/PhysRevB.100.241111. URL: https://link.aps.org/doi/10.1103/PhysRevB.100.241111.

[54] Shou-Shu Gong et al. "Global phase diagram and quantum spin liquids in a spin-$\frac{1}{2}$ triangular antiferromagnet". In: *Phys. Rev. B* 96 (7 Aug. 2017), p. 075116. DOI: 10.1103/PhysRevB.96.075116. URL: https://link.aps.org/doi/10.1103/PhysRevB.96.075116.

[55] Shou-Shu Gong et al. "Global phase diagram of competing ordered and quantum spin-liquid phases on the kagome lattice". In: *Phys. Rev. B* 91 (7 Feb. 2015), p. 075112. DOI: 10.1103/PhysRevB.91.075112. URL: https://link.aps.org/doi/10.1103/PhysRevB.91.075112.

[56] Jacob S Gordon et al. "Theory of the field-revealed Kitaev spin liquid". In: *Nature communications* 10.1 (2019), pp. 1–8.

[57] Sean A. Hartnoll and Andrew P. Mackenzie. "Colloquium: Planckian dissipation in metals". In: *Rev. Mod. Phys.* 94 (4 Nov. 2022), p. 041002. DOI: 10.1103/RevModPhys.94.041002. URL: https://link.aps.org/doi/10.1103/RevModPhys.94.041002.

[58] Ian M Hayes et al. "Scaling between magnetic field and temperature in the high-temperature superconductor BaFe2 (As1- x P x) 2". In: *Nature Physics* 12.10 (2016), pp. 916–919.

[59] Wen-Yu He et al. "Spinon Fermi Surface in a Cluster Mott Insulator Model on a Triangular Lattice and Possible Application to $1T-TaS_2$". In: *Phys. Rev. Lett.* 121 (4 July 2018), p. 046401. DOI: 10.1103/PhysRevLett.121.046401. URL: https://link.aps.org/doi/10.1103/PhysRevLett.121.046401.

[60] Yin-Chen He, D. N. Sheng, and Yan Chen. "Chiral Spin Liquid in a Frustrated Anisotropic Kagome Heisenberg Model". In: *Phys. Rev. Lett.* 112 (13 Apr. 2014), p. 137202. DOI: 10.1103/PhysRevLett.112.137202. URL: https://link.aps.org/doi/10.1103/PhysRevLett.112.137202.

[61] Yin-Chen He et al. "Signatures of Dirac Cones in a DMRG Study of the Kagome Heisenberg Model". In: *Phys. Rev. X* 7 (3 July 2017), p. 031020. DOI: 10.1103/PhysRevX.7.031020. URL: https://link.aps.org/doi/10.1103/PhysRevX.7.031020.

[62] Richard Hentrich et al. "Large Thermal Hall Effect in α-$RuCl_3$: Evidence for Heat Transport by Kitaev-Heisenberg Paramagnons". In: *arXiv preprint arXiv:1803.08162* (2018).

[63] Richard Hentrich et al. "Unusual Phonon Heat Transport in $\alpha-RuCl_3$: Strong Spin-Phonon Scattering and Field-Induced Spin Gap". In: *Phys. Rev. Lett.* 120 (11 Mar. 2018), p. 117204. DOI: 10.1103/PhysRevLett.120.117204. URL: https://link.aps.org/doi/10.1103/PhysRevLett.120.117204.

[64] Maria Hermanns, Itamar Kimchi, and Johannes Knolle. "Physics of the Kitaev model: fractionalization, dynamic correlations, and material connections". In: *Annual Review of Condensed Matter Physics* 9 (2018), pp. 17–33.

[65] Ciarán Hickey and Simon Trebst. "Emergence of a field-driven U (1) spin liquid in the Kitaev honeycomb model". In: *Nature communications* 10.1 (2019), pp. 1–10.

[66] Yukio Hirano and Yoshiyuki Ono. "Photogeneration dynamics of nonlinear excitations in polyacetylene". In: *Journal of the Physical Society of Japan* 69.7 (2000), pp. 2131–2144.

[67] Daichi Hirobe et al. "Magnetic thermal conductivity far above the Néel temperature in the Kitaev-magnet candidate $\alpha-RuCl_3$". In: *Phys. Rev. B* 95 (24 June 2017), p. 241112. DOI: 10.1103/PhysRevB.95.241112. URL: https://link.aps.org/doi/10.1103/PhysRevB.95.241112.

[68] Y. S. Hou, H. J. Xiang, and X. G. Gong. "Unveiling magnetic interactions of ruthenium trichloride via constraining direction of orbital moments: Potential routes to realize a quantum spin liquid". In: *Phys. Rev. B* 96 (5 Aug. 2017), p. 054410. DOI: 10.1103/PhysRevB.96.054410. URL: https://link.aps.org/doi/10.1103/PhysRevB.96.054410.

[69] Shijie Hu et al. "Dirac Spin Liquid on the Spin-1/2 Triangular Heisenberg Antiferromagnet". In: *Phys. Rev. Lett.* 123 (20 Nov. 2019), p. 207203. DOI: 10.1103/PhysRevLett.123.207203.

[70] Wen-Jun Hu et al. "Competing spin-liquid states in the spin-$\frac{1}{2}$ Heisenberg model on the triangular lattice". In: *Phys. Rev. B* 92 (14 Oct. 2015), 140403(R). DOI: 10.1103/PhysRevB.92.140403. URL: https://link.aps.org/doi/10.1103/PhysRevB.92.140403.

[71] Wen-Jun Hu et al. "Variational Monte Carlo study of a chiral spin liquid in the extended Heisenberg model on the kagome lattice". In: *Phys. Rev. B* 91 (4 Jan. 2015), 041124(R). DOI: 10.1103/PhysRevB.91.041124. URL: https://link.aps.org/doi/10.1103/PhysRevB.91.041124.

[72] Edwin W Huang et al. "Strange metallicity in the doped Hubbard model". In: *Science* 366.6468 (2019), pp. 987–990.

[73] N. M. Hugenholtz and D. Pines. "Ground-state energy and excitation spectrum of a system of interacting bosons". In: *Phys. Rev.* 116 (3 Nov. 1959), pp. 489–506. DOI: 10.1103/PhysRev.116.489. URL: https://link.aps.org/doi/10.1103/PhysRev.116.489.

[74] Sae Hwan Chun et al. "Direct evidence for dominant bond-directional interactions in a honeycomb lattice iridate Na2IrO3". In: *Nature Physics* 11.6 (2015), pp. 462–466.

[75] A. V. Inyushkin and A. N. Taldenkov. "On the phonon Hall effect in a paramagnetic dielectric". In: *JETP Letters* 86.6 (Nov. 2007), pp. 379–382. ISSN: 1090-6487. DOI: 10.1134/S0021364007180075. URL: https://doi.org/10.1134/S0021364007180075.

[76] L. B. Ioffe and G. Kotliar. "Transport phenomena near the Mott transition". In: *Phys. Rev. B* 42 (16 Dec. 1990), pp. 10348–10359. DOI: 10.1103/PhysRevB.42.10348. URL: https://link.aps.org/doi/10.1103/PhysRevB.42.10348.

[77] L. B. Ioffe and A. I. Larkin. "Gapless fermions and gauge fields in dielectrics". In: *Phys. Rev. B* 39 (13 May 1989), pp. 8988–8999. DOI: 10.1103/PhysRevB.39.8988. URL: https://link.aps.org/doi/10.1103/PhysRevB.39.8988.

[78] G. Jackeli and G. Khaliullin. "Mott Insulators in the Strong Spin-Orbit Coupling Limit: From Heisenberg to a Quantum Compass and Kitaev Models". In: *Phys. Rev. Lett.* 102 (1 Jan. 2009), p. 017205. DOI: 10.1103/PhysRevLett.102.017205. URL: https://link.aps.org/doi/10.1103/PhysRevLett.102.017205.

[79] Lukas Janssen, Eric C. Andrade, and Matthias Vojta. "Magnetization processes of zigzag states on the honeycomb lattice: Identifying spin models for $\alpha-RuCl_3$ and Na_2IrO_3". In: *Phys. Rev. B* 96 (6 Aug. 2017), p. 064430. DOI: 10.1103/PhysRevB.96.064430. URL: https://link.aps.org/doi/10.1103/PhysRevB.96.064430.

[80] Lukas Janssen, Stefan Koch, and Matthias Vojta. "Magnon dispersion and dynamic spin response in three-dimensional spin models for $\alpha-RuCl_3$". In: *Phys. Rev. B* 101 (17 May 2020), p. 174444. DOI: 10.1103/PhysRevB.101.174444. URL: https://link.aps.org/doi/10.1103/PhysRevB.101.174444.

[81] Ming-Hong Jiang et al. "Tuning Topological Orders by a Conical Magnetic Field in the Kitaev Model". In: *Phys. Rev. Lett.* 125 (17 Oct. 2020), p. 177203. DOI: 10.1103/PhysRevLett.125.177203. URL: https://link.aps.org/doi/10.1103/PhysRevLett.125.177203.

[82] R. D. Johnson et al. "Monoclinic crystal structure of $\alpha - RuCl_3$ and the zigzag antiferromagnetic ground state". In: *Phys. Rev. B* 92 (23 Dec. 2015), p. 235119. DOI: 10.1103/PhysRevB.92.235119. URL: https://link.aps.org/doi/10.1103/PhysRevB.92.235119.

[83] D H Jones, Q A Pankhurst, and C E Johnson. "Spin-wave theory of anisotropic antiferromagnets in applied magnetic fields". In: *Journal of Physics C: Solid State Physics* 20.31 (1987), p. 5149. URL: http://stacks.iop.org/0022-3719/20/i=31/a=017.

[84] Darshan G. Joshi. "Topological excitations in the ferromagnetic Kitaev-Heisenberg model". In: *Phys. Rev. B* 98 (6 Aug. 2018), p. 060405. DOI: 10.1103/PhysRevB.98.060405. URL: https://link.aps.org/doi/10.1103/PhysRevB.98.060405.

[85] David A. S. Kaib, Stephen M. Winter, and Roser Valentí. "Kitaev honeycomb models in magnetic fields: Dynamical response and dual models". In: *Phys. Rev. B* 100 (14 Oct. 2019), p. 144445. DOI: 10.1103/PhysRevB.100.144445. URL: https://link.aps.org/doi/10.1103/PhysRevB.100.144445.

[86] Ryui Kaneko, Satoshi Morita, and Masatoshi Imada. "Gapless Spin-Liquid Phase in an Extended Spin 1/2 Triangular Heisenberg Model". In: *Journal of the Physical Society of Japan* 83.9 (2014), p. 093707. DOI: 10.7566/JPSJ.83.093707. URL: https://doi.org/10.7566/JPSJ.83.093707.

[87] Y Kasahara et al. "Majorana quantization and half-integer thermal quantum Hall effect in a Kitaev spin liquid". In: *Nature* 559.7713 (2018), pp. 227–231.

[88] Y. Kasahara et al. "Unusual Thermal Hall Effect in a Kitaev Spin Liquid Candidate α-$RuCl_3$". In: *Phys. Rev. Lett.* 120 (21 May 2018), p. 217205. DOI: 10.1103/PhysRevLett.120.217205. URL: https://link.aps.org/doi/10.1103/PhysRevLett.120.217205.

[89] Vamshi M Katukuri et al. "Kitaev interactions between j = 1/2 moments in honeycomb Na 2 IrO 3 are large and ferromagnetic: insights from ab initio quantum chemistry calculations". In: *New Journal of Physics* 16.1 (2014), p. 013056. URL: http://stacks.iop.org/1367-2630/16/i=1/a=013056.

[90] Heung-Sik Kim and Hae-Young Kee. "Crystal structure and magnetism in $\alpha - RuCl_3$: An ab initio study". In: *Phys. Rev. B* 93 (15 Apr. 2016), p. 155143. DOI: 10.1103/PhysRevB.93.155143. URL: https://link.aps.org/doi/10.1103/PhysRevB.93.155143.

[91] Heung-Sik Kim et al. "Kitaev magnetism in honeycomb $RuCl_3$ with intermediate spin-orbit coupling". In: *Phys. Rev. B* 91 (24 June 2015), p. 241110. DOI: 10.1103/PhysRevB.91.241110. URL: https://link.aps.org/doi/10.1103/PhysRevB.91.241110.

[92] Stefan Kirchner et al. "Colloquium: Heavy-electron quantum criticality and single-particle spectroscopy". In: *Rev. Mod. Phys.* 92 (1 Mar. 2020), p. 011002. DOI: 10.1103/RevModPhys.92.011002. URL: https://link.aps.org/doi/10.1103/RevModPhys.92.011002.

[93] A Yu Kitaev. "Fault-tolerant quantum computation by anyons". In: *Annals of physics* 303.1 (2003), pp. 2–30.

[94] Alexei Kitaev. "Anyons in an exactly solved model and beyond". In: *Annals of Physics* 321.1 (2006). January Special Issue, pp. 2–111. ISSN: 0003-4916. DOI: https://doi.org/10.1016/j.aop.2005.10.005. URL: http://www.sciencedirect.com/science/article/pii/S0003491605002381.

[95] K Kitagawa et al. "A spin–orbital-entangled quantum liquid on a honeycomb lattice". In: *Nature* 554.7692 (2018), pp. 341–345.

[96] Kai Klocke et al. "Thermal Probes of Phonon-Coupled Kitaev Spin Liquids: From Accurate Extraction of Quantized Edge Transport to Anyon Interferometry". In: *Phys. Rev. X* 12 (1 Feb. 2022), p. 011034. DOI: 10.1103/PhysRevX.12.011034. URL: https://link.aps.org/doi/10.1103/PhysRevX.12.011034.

[97] J. Knolle et al. "Dynamics of fractionalization in quantum spin liquids". In: *Phys. Rev. B* 92 (11 Sept. 2015), p. 115127. DOI: 10.1103/PhysRevB.92.115127. URL: https://link.aps.org/doi/10.1103/PhysRevB.92.115127.

[98] Johannes Knolle, Subhro Bhattacharjee, and Roderich Moessner. "Dynamics of a quantum spin liquid beyond integrability: The Kitaev-Heisenberg-Γ model in an augmented parton mean-field theory". In: *Phys. Rev. B* 97 (13 Apr. 2018), p. 134432. DOI: 10.1103/PhysRevB.97.134432. URL: https://link.aps.org/doi/10.1103/PhysRevB.97.134432.

[99] Y. Kohori et al. "NMR and NQR studies of the heavy fermion superconductors $CeTIn_5$ (T = Co and Ir)". In: *Physical Review B* 64.13 (Sept. 2001), p. 134526.

[100] Shinnosuke Koyama and Joji Nasu. "Field-angle dependence of thermal Hall conductivity in a magnetically ordered Kitaev-Heisenberg system". In: *Phys. Rev. B* 104 (7 Aug. 2021), p. 075121. DOI: 10.1103/PhysRevB.104.075121. URL: https://link.aps.org/doi/10.1103/PhysRevB.104.075121.

[101] Yumi Kubota et al. "Successive magnetic phase transitions in $\alpha - RuCl_3$: XY-like frustrated magnet on the honeycomb lattice". In: *Phys. Rev. B* 91 (9 Mar. 2015), p. 094422. DOI: 10.1103/PhysRevB.91.094422. URL: https://link.aps.org/doi/10.1103/PhysRevB.91.094422.

[102] Kenneth C. Kulander. "Time-dependent Hartree-Fock theory of multiphoton ionization: Helium". In: *Phys. Rev. A* 36 (6 Sept. 1987), pp. 2726–2738. DOI: 10.1103/PhysRevA.36.2726. URL: https://link.aps.org/doi/10.1103/PhysRevA.36.2726.

[103] Pontus Laurell and Satoshi Okamoto. "Dynamical and thermal magnetic properties of the Kitaev spin liquid candidate α-RuCl 3". In: *npj Quantum Materials* 5.1 (2020), pp. 1–10.

[104] Ian A. Leahy et al. "Anomalous Thermal Conductivity and Magnetic Torque Response in the Honeycomb Magnet $\alpha-RuCl_3$". In: *Phys. Rev. Lett.* 118 (18 May 2017), p. 187203. DOI: 10.1103/PhysRevLett.118.187203. URL: https://link.aps.org/doi/10.1103/PhysRevLett.118.187203.

[105] S. Lederer et al. "Superconductivity and non-Fermi liquid behavior near a nematic quantum critical point". In: *PNAS* 114.19 (May 2017), pp. 4905–4910. ISSN: 1091-6490. DOI: 10.1073/pnas.1620651114. URL: http://www.ncbi.nlm.nih.gov/pubmed/28439023%20http://www.pubmedcentral.nih.gov/articlerender.fcgi?artid=PMC5441715.

[106] Patrick A. Lee and Naoto Nagaosa. "Gauge theory of the normal state of high-T_c superconductors". In: *Phys. Rev. B* 46 (9 Sept. 1992), pp. 5621–5639. DOI: 10.1103/PhysRevB.46.5621. URL: https://link.aps.org/doi/10.1103/PhysRevB.46.5621.

[107] É Lefrançois et al. "Evidence of a Phonon Hall Effect in the Kitaev Spin Liquid Candidate α-$RuCl_3$". In: *arXiv preprint arXiv:2111.05493* (2021).

[108] Étienne Lefrançois et al. "Oscillations in the magnetothermal conductivity of α-$RuCl_3$: Evidence of transition anomalies". In: *arXiv preprint arXiv:2301.05254* (2023).

[109] A Legros et al. "Universal T-linear resistivity and Planckian dissipation in overdoped cuprates". In: *Nature Physics* 15.2 (2019), pp. 142–147.

[110] Han Li et al. "Identification of magnetic interactions and high-field quantum spin liquid in α-RuCl3". In: *Nature Communications* 12.1 (2021), p. 4007.

[111] Heqiu Li, Yong Baek Kim, and Hae-Young Kee. "Magnetic-field Induced Topological Transitions and Thermal Conductivity in a Generalized Kitaev Model". In: *arXiv preprint arXiv:2202.12315* (2022).

[112] S. Licciardello et al. "Coexistence of orbital and quantum critical magnetoresistance in $FeSe_{1-x}S_x$". In: *Phys. Rev. Res.* 1 (2 Sept. 2019), p. 023011. DOI: 10.1103/PhysRevResearch.1.023011. URL: https://link.aps.org/doi/10.1103/PhysRevResearch.1.023011.

[113] Gaoting Lin et al. "Field-induced quantum spin disordered state in spin-1/2 honeycomb magnet Na2Co2TeO6". In: *Nature communications* 12.1 (2021), pp. 1–8.

[114] A. Little et al. "Antiferromagnetic Resonance and Terahertz Continuum in $\alpha-RuCl_3$". In: *Phys. Rev. Lett.* 119 (22 Nov. 2017), p. 227201. DOI: 10.1103/PhysRevLett.119.227201. URL: https://link.aps.org/doi/10.1103/PhysRevLett.119.227201.

[115] Huimei Liu, Ji ři Chaloupka, and Giniyat Khaliullin. "Kitaev Spin Liquid in $3d$ Transition Metal Compounds". In: *Phys. Rev. Lett.* 125 (4 July 2020), p. 047201. DOI: 10.1103/PhysRevLett.125.047201. URL: https://link.aps.org/doi/10.1103/PhysRevLett.125.047201.

[116] Huimei Liu and Giniyat Khaliullin. "Pseudospin exchange interactions in d^7 cobalt compounds: Possible realization of the Kitaev model". In: *Phys. Rev. B* 97 (1 Jan. 2018), p. 014407. DOI: 10.1103/PhysRevB.97.014407. URL: https://link.aps.org/doi/10.1103/PhysRevB.97.014407.

[117] X. Liu et al. "Long-range magnetic ordering in Na_2IrO_3". In: *Phys. Rev. B* 83 (22 June 2011), p. 220403. DOI: 10.1103/PhysRevB.83.220403. URL: https://link.aps.org/doi/10.1103/PhysRevB.83.220403.

[118] A. H. MacDonald, S. M. Girvin, and D. Yoshioka. "$\frac{t}{U}$ expansion for the Hubbard model". In: *Phys. Rev. B* 37 (16 June 1988), pp. 9753–9756. DOI: 10.1103/PhysRevB.37.9753. URL: https://link.aps.org/doi/10.1103/PhysRevB.37.9753.

[119] Gerald D Mahan. *Many-particle physics*. Springer Science & Business Media, 2013. URL: https://www.springer.com/gp/book/9780306434235.

[120] M. Majumder et al. "Anisotropic $Ru^{3+}4d^5$ magnetism in the $\alpha - RuCl_3$ honeycomb system: Susceptibility, specific heat, and zero-field NMR". In: *Phys. Rev. B* 91 (18 May 2015), p. 180401. DOI: 10.1103/PhysRevB.91.180401. URL: https://link.aps.org/doi/10.1103/PhysRevB.91.180401.

[121] Nikola Maksimovic et al. "Evidence for a delocalization quantum phase transition without symmetry breaking in CeCoIn5". In: *Science* 375.6576 (2022), pp. 76–81.

[122] Ryo Matsumoto, Ryuichi Shindou, and Shuichi Murakami. "Thermal Hall effect of magnons in magnets with dipolar interaction". In: *Phys. Rev. B* 89 (5 Feb. 2014), p. 054420. DOI: 10.1103/PhysRevB.89.054420. URL: https://link.aps.org/doi/10.1103/PhysRevB.89.054420.

[123] P. A. McClarty et al. "Topological magnons in Kitaev magnets at high fields". In: *Phys. Rev. B* 98 (6 Aug. 2018), p. 060404. DOI: 10.1103/PhysRevB.98.060404. URL: https://link.aps.org/doi/10.1103/PhysRevB.98.060404.

[124] Jia-Wei Mei. "Possible Fermi Liquid in the Lightly Doped Kitaev Spin Liquid". In: *Phys. Rev. Lett.* 108 (22 May 2012), p. 227207. DOI: 10.1103/PhysRevLett.108.227207. URL: https://link.aps.org/doi/10.1103/PhysRevLett.108.227207.

[125] Laura Messio, Bernard Bernu, and Claire Lhuillier. "Kagome Antiferromagnet: A Chiral Topological Spin Liquid?" In: *Phys. Rev. Lett.* 108 (20 May 2012), p. 207204. DOI: 10.1103/PhysRevLett.108.207204. URL: https://link.aps.org/doi/10.1103/PhysRevLett.108.207204.

[126] Tetsuya Minakawa et al. "Majorana-Mediated Spin Transport in Kitaev Quantum Spin Liquids". In: *Phys. Rev. Lett.* 125 (4 July 2020), p. 047204. DOI: 10.1103/PhysRevLett.125.047204.

[127] Connie H Mousatov, Erez Berg, and Sean A Hartnoll. "Theory of the strange metal Sr3Ru2O7". In: *Proceedings of the National Academy of Sciences* 117.6 (2020), 2852–2857.

[128] Y. Nakajima et al. "Planckian dissipation and scale invariance in a quantum-critical disordered pnictide". In: *arXiv e-prints* (Feb. 2019). arXiv: 1902.01034.

[129] Y. Nakajima et al. "Unusual Hall effect in quasi two-dimensional strongly correlated metal $CeCoIn_5$". In: *Physica C* 460-462 (Sept. 2007), pp. 680–681. ISSN: 0921-4534. DOI: 10.1016/J.PHYSC.2007.03.082. URL: https://www.sciencedirect.com/science/article/pii/S0921453407002146.

[130] Joji Nasu and Yukitoshi Motome. "Nonequilibrium Majorana dynamics by quenching a magnetic field in Kitaev spin liquids". In: *Phys. Rev. Research* 1 (3 Oct. 2019), p. 033007. DOI: 10.1103/PhysRevResearch.1.033007. URL: https://link.aps.org/doi/10.1103/PhysRevResearch.1.033007.

[131] Joji Nasu, Junki Yoshitake, and Yukitoshi Motome. "Thermal Transport in the Kitaev Model". In: *Phys. Rev. Lett.* 119 (12 Sept. 2017), p. 127204. DOI: 10.1103/PhysRevLett.119.127204.

[132] Joji Nasu et al. "Fermionic response from fractionalization in an insulating two-dimensional magnet". In: *Nature Physics* 12.10 (2016), pp. 912–915.

[133] Joji Nasu et al. "Successive Majorana topological transitions driven by a magnetic field in the Kitaev model". In: *Phys. Rev. B* 98 (6 Aug. 2018), p. 060416. DOI: 10.1103/PhysRevB.98.060416. URL: https://link.aps.org/doi/10.1103/PhysRevB.98.060416.

[134] Chetan Nayak et al. "Non-Abelian anyons and topological quantum computation". In: *Rev. Mod. Phys.* 80 (3 Sept. 2008), pp. 1083–1159. DOI: 10.1103/RevModPhys.80.1083. URL: https://link.aps.org/doi/10.1103/RevModPhys.80.1083.

[135] Satoshi Okamoto. "Global phase diagram of a doped Kitaev-Heisenberg model". In: *Phys. Rev. B* 87 (6 Feb. 2013), p. 064508. DOI: 10.1103/PhysRevB.87.064508. URL: https://link.aps.org/doi/10.1103/PhysRevB.87.064508.

[136] Joseph Orenstein. "Ultrafast spectroscopy of quantum materials". In: *Physics Today* 65.44 (2012), p. 570.

[137] M. Oshikawa. "Topological Approach to Luttinger's Theorem and the Fermi Surface of a Kondo Lattice". In: *Physical Review Letters* 84.15 (Apr. 2000), p. 3370.

[138] S. A. Owerre. "Topological honeycomb magnon Hall effect: A calculation of thermal Hall conductivity of magnetic spin excitations". In: *Journal of Applied Physics* 120.4 (2016), p. 043903. DOI: 10.1063/1.4959815. eprint: https://doi.org/10.1063/1.4959815. URL: https://doi.org/10.1063/1.4959815.

[139] J. Paglione et al. "Field-induced quantum critical point in $CeCoIn_5$". In: *Physical Review Letters* 91.24 (Dec. 2003), p. 246405. ISSN: 0031-9007.

[140] S. Paschen et al. "Hall effect evolution across a heavy fermion quantum critical point". In: *Nature* 432.7019 (Dec. 2004), pp. 881–885. ISSN: 0028-0836.

[141] Aavishkar A. Patel, Michael J. Lawler, and Eun-Ah Kim. "Coherent superconductivity with a large gap ratio from incoherent metals". In: *Phys. Rev. Lett.* 121 (18 Oct. 2018), p. 187001. DOI: 10.1103/PhysRevLett.121.187001. URL: https://link.aps.org/doi/10.1103/PhysRevLett.121.187001.

[142] Aavishkar A. Patel and Subir Sachdev. "DC resistivity at the onset of spin density wave order in two-dimensional metals". In: *Phys. Rev. B* 90 (16 Oct. 2014), p. 165146. DOI: 10.1103/PhysRevB.90.165146. URL: https://link.aps.org/doi/10.1103/PhysRevB.90.165146.

[143] Aavishkar A. Patel and Subir Sachdev. "Theory of a Planckian metal". In: *Phys. Rev. Lett.* 123 (6 Aug. 2019), p. 066601. DOI: 10.1103/PhysRevLett.123.066601. URL: https://link.aps.org/doi/10.1103/PhysRevLett.123.066601.

[144] Aavishkar A. Patel et al. "Magnetotransport in a model of a disordered strange metal". In: *Phys. Rev. X* 8 (2 May 2018), p. 021049. DOI: 10.1103/PhysRevX.8.021049. URL: https://link.aps.org/doi/10.1103/PhysRevX.8.021049.

[145] I. Paul, C. Pépin, and M. R. Norman. "Equivalence of single-particle and transport Lifetimes from hybridization fluctuations". In: *Phys. Rev. Lett.* 110 (6 Feb. 2013), p. 066402. DOI: 10.1103/PhysRevLett.110.066402. URL: https://link.aps.org/doi/10.1103/PhysRevLett.110.066402.

[146] Fabio L. Pedrocchi, Stefano Chesi, and Daniel Loss. "Physical solutions of the Kitaev honeycomb model". In: *Phys. Rev. B* 84 (16 Oct. 2011), p. 165414. DOI: 10.1103/PhysRevB.84.165414. URL: https://link.aps.org/doi/10.1103/PhysRevB.84.165414.

[147] C. Petrovic et al. "Heavy fermion superconductivity in $CeCoIn_5$ at 2.3 K". In: *J. Phys. Condens. Matter* 13 (2001), pp. 337–342.

[148] Angelo Pidatella, Alexandros Metavitsiadis, and Wolfram Brenig. "Heat transport in the anisotropic Kitaev spin liquid". In: *Phys. Rev. B* 99 (7 Feb. 2019), p. 075141. DOI: 10.1103/PhysRevB.99.075141. URL: https://link.aps.org/doi/10.1103/PhysRevB.99.075141.

[149] A. N. Ponomaryov et al. "Unconventional spin dynamics in the honeycomb-lattice material $\alpha-RuCl_3$: High-field electron spin resonance studies". In: *Phys. Rev. B* 96 (24 Dec. 2017), p. 241107. DOI: 10.1103/PhysRevB.96.241107. URL: https://link.aps.org/doi/10.1103/PhysRevB.96.241107.

[150] Cyril Proust and Louis Taillefer. "The remarkable underlying ground states of cuprate superconductors". In: *Annual Review of Condensed Matter Physics* 10.1 (2019), 409–429. DOI: 10.1146/annurev-conmatphys-031218-013210. eprint: https://doi.org/10.1146/annurev-conmatphys-031218-013210. URL: https://doi.org/10.1146/annurev-conmatphys-031218-013210.

[151] Arnaud Ralko and Jaime Merino. "Novel Chiral Quantum Spin Liquids in Kitaev Magnets". In: *Phys. Rev. Lett.* 124 (21 May 2020), p. 217203.

[152] Kejing Ran et al. "Evidence for magnetic fractional excitations in a Kitaev quantum-spin-liquid candidate α-RuCl3". In: *Chinese Physics Letters* 39.2 (2022), p. 027501.

[153] Kejing Ran et al. "Spin-Wave Excitations Evidencing the Kitaev Interaction in Single Crystalline $\alpha-RuCl_3$". In: *Phys. Rev. Lett.* 118 (10 Mar. 2017), p. 107203. DOI: 10.1103/PhysRevLett.118.107203. URL: https://link.aps.org/doi/10.1103/PhysRevLett.118.107203.

[154] Jeffrey G. Rau, Eric Kin-Ho Lee, and Hae-Young Kee. "Generic Spin Model for the Honeycomb Iridates beyond the Kitaev Limit". In: *Phys. Rev. Lett.* 112 (7 Feb. 2014), p. 077204. DOI: 10.1103/PhysRevLett.112.077204. URL: https://link.aps.org/doi/10.1103/PhysRevLett.112.077204.

[155] Nicholas Read and DM Newns. "On the solution of the Coqblin-Schreiffer Hamiltonian by the large-N expansion technique". In: *Journal of Physics C: Solid State Physics* 16.17 (1983), p. 3273. URL: https://iopscience.iop.org/article/10.1088/0022-3719/16/17/014.

[156] S. N. Saadatmand and I. P. McCulloch. "Detection and characterization of symmetry-broken long-range orders in the spin-$\frac{1}{2}$ triangular Heisenberg model". In: *Phys. Rev. B* 96 (7 Aug. 2017), p. 075117. DOI: 10.1103/PhysRevB.96.075117. URL: https://link.aps.org/doi/10.1103/PhysRevB.96.075117.

[157] Subir Sachdev. "Bekenstein-Hawking Entropy and Strange Metals". In: *Phys. Rev. X* 5 (4 Nov. 2015), p. 041025. DOI: 10.1103/PhysRevX.5.041025. URL: https://link.aps.org/doi/10.1103/PhysRevX.5.041025.

[158] Subir Sachdev. "Holographic Metals and the Fractionalized Fermi Liquid". In: *Phys. Rev. Lett.* 105 (15 Oct. 2010), p. 151602. DOI: 10.1103/PhysRevLett.105.151602. URL: https://link.aps.org/doi/10.1103/PhysRevLett.105.151602.

[159] Subir Sachdev. *Quantum phase transitions*. Cambridge University Press, 2011.

[160] Subir Sachdev, Max A Metlitski, and Matthias Punk. "Antiferromagnetism in metals: from the cuprate superconductors to the heavy fermion materials". In: *Journal of Physics: Condensed Matter* 24.29 (2012), p. 294205.

[161] Subir Sachdev and Jinwu Ye. "Gapless spin-fluid ground state in a random quantum Heisenberg magnet". In: *Phys. Rev. Lett.* 70 (21 May 1993), pp. 3339–3342. DOI: 10.1103/PhysRevLett.70.3339. URL: https://link.aps.org/doi/10.1103/PhysRevLett.70.3339.

[162] Rhine Samajdar et al. "Quantum phases of Rydberg atoms on a kagome lattice". In: *Proceedings of the National Academy of Sciences* 118.4 (2021), e2015785118.

[163] Anjana M Samarakoon et al. "Extraction of the interaction parameters for *alpha*− RuCl _3 from neutron data using machine learning". In: *arXiv:2202.10715* (2022).

[164] Luke J. Sandilands et al. "Scattering Continuum and Possible Fractionalized Excitations in $\alpha-RuCl_3$". In: *Phys. Rev. Lett.* 114 (14 Apr. 2015), p. 147201. DOI: 10.1103/PhysRevLett.114.147201. URL: https://link.aps.org/doi/10.1103/PhysRevLett.114.147201.

[165] Ryoya Sano, Yasuyuki Kato, and Yukitoshi Motome. "Kitaev-Heisenberg Hamiltonian for high-spin d^7 Mott insulators". In: *Phys. Rev. B* 97 (1 Jan. 2018), p. 014408. DOI: 10.1103/PhysRevB.97.014408. URL: https://link.aps.org/doi/10.1103/PhysRevB.97.014408.

[166] Tarapada Sarkar et al. "Correlation between scale-invariant normal-state resistivity and superconductivity in an electron-doped cuprate". In: *Science Advances* 5.5 (2019), eaav6753.

[167] Toshihiro Sato and Fakher F. Assaad. "Quantum Monte Carlo simulation of generalized Kitaev models". In: *Phys. Rev. B* 104 (8 Aug. 2021), p. L081106. DOI: 10.1103/PhysRevB.104.L081106. URL: https://link.aps.org/doi/10.1103/PhysRevB.104.L081106.

[168] Lucile Savary and Leon Balents. "Quantum spin liquids: a review". In: *Reports on Progress in Physics* 80.1 (2016), p. 016502.

[169] Robert Schaffer, Subhro Bhattacharjee, and Yong Baek Kim. "Quantum phase transition in Heisenberg-Kitaev model". In: *Phys. Rev. B* 86 (22 Dec. 2012), p. 224417. DOI: 10.1103/PhysRevB.86.224417. URL: https://link.aps.org/doi/10.1103/PhysRevB.86.224417.

[170] A. Schröder et al. "Onset of antiferromagnetism in heavy-fermion metals". In: *Nature* 407.6802 (Sept. 2000), pp. 351–355.

[171] HJ Schulz. "Fermi liquids and non–Fermi liquids". In: *arXiv cond-mat/9503150* (1995).

[172] J. A. Sears et al. "Magnetic order in $\alpha-RuCl_3$: A honeycomb-lattice quantum magnet with strong spin-orbit coupling". In: *Phys. Rev. B* 91 (14 Apr. 2015), p. 144420. DOI: 10.1103/PhysRevB.91.144420. URL: https://link.aps.org/doi/10.1103/PhysRevB.91.144420.

[173] Urban F. P. Seifert, Tobias Meng, and Matthias Vojta. "Fractionalized Fermi liquids and exotic superconductivity in the Kitaev-Kondo lattice". In: *Phys. Rev. B* 97 (8 Feb. 2018), p. 085118. DOI: 10.1103/PhysRevB.97.085118. URL: https://link.aps.org/doi/10.1103/PhysRevB.97.085118.

[174] Giulia Semeghini et al. "Probing topological spin liquids on a programmable quantum simulator". In: *Science* 374.6572 (2021), pp. 1242–1247.

[175] T Senthil, Matthias Vojta, and Subir Sachdev. "Weak magnetism and non-Fermi liquids near heavy-fermion critical points". In: *Physical Review B* 69.3 (2004), p. 035111. URL: https://journals.aps.org/prb/abstract/10.1103/PhysRevB.69.035111.

[176] T. Senthil, S. Sachdev, and M. Vojta. "Fractionalized Fermi liquids". In: *Phys. Rev. Lett.* 90.21 (May 2003), p. 216403. ISSN: 00319007. DOI: 10.1103/physrevlett.90.216403.

[177] R. Settai et al. "Quasi-two-dimensional Fermi surfaces and the de Haas-van Alphen oscillation in both the normal and superconducting mixed states of $CeCoIn_5$". In: *J. Phys. Condens. Matter* 13 (2001), pp. 627–634.

[178] Qimiao Si and Frank Steglich. "Heavy fermions and quantum phase transitions". In: *Science* 329.5996 (2010), pp. 1161–1166. URL: https://science.sciencemag.org/content/329/5996/1161.

[179] V. A. Sidorov et al. "Superconductivity and quantum criticality in $CeCoIn_5$". In: *Phys. Rev. Lett.* 89.15 (Sept. 2002), p. 157004. ISSN: 0031-9007.

[180] Yogesh Singh and P. Gegenwart. "Antiferromagnetic Mott insulating state in single crystals of the honeycomb lattice material Na_2IrO_3". In: *Phys. Rev. B* 82 (6 Aug. 2010), p. 064412. DOI: 10.1103/PhysRevB.82.064412. URL: https://link.aps.org/doi/10.1103/PhysRevB.82.064412.

[181] Yogesh Singh et al. "Relevance of the Heisenberg-Kitaev Model for the Honeycomb Lattice Iridates A_2IrO_3". In: *Phys. Rev. Lett.* 108 (12 Mar. 2012), p. 127203. DOI: 10.1103/PhysRevLett.108.127203. URL: https://link.aps.org/doi/10.1103/PhysRevLett.108.127203.

[182] Kevin Slagle et al. "Theory of a quantum spin liquid in the hydrogen-intercalated honeycomb iridate $H_3LiIr_2O_6$". In: *Phys. Rev. B* 97 (11 Mar. 2018), p. 115159. DOI: 10.1103/PhysRevB.97.115159. URL: https://link.aps.org/doi/10.1103/PhysRevB.97.115159.

[183] Xue-Yang Song, Yi-Zhuang You, and Leon Balents. "Low-Energy Spin Dynamics of the Honeycomb Spin Liquid Beyond the Kitaev Limit". In: *Phys. Rev. Lett.* 117 (3 July 2016), p. 037209. DOI: 10.1103/PhysRevLett.117.037209. URL: https://link.aps.org/doi/10.1103/PhysRevLett.117.037209.

[184] Mary Beth Stearns. "Why is Iron Magnetic?" In: *Physics Today* 31.4 (1978), p. 34.

[185] G. R. Stewart. "Non-Fermi-liquid behavior in d- and f-electron metals". In: *Rev. Mod. Phys.* 73 (4 Oct. 2001), pp. 797–855. DOI: 10.1103/RevModPhys.73.797. URL: https://link.aps.org/doi/10.1103/RevModPhys.73.797.

[186] C. Stock et al. "Spin resonance in the d-wave superconductor $CeCoIn_5$". In: *Physical Review Letters* 100.8 (Feb. 2008), p. 087001.

[187] Shota Suetsugu et al. "Evidence for a Phase Transition in the Quantum Spin Liquid State of a Kitaev Candidate α-RuCl3". In: *Journal of the Physical Society of Japan* 91.12 (2022), p. 124703.

[188] K. Sugii et al. "Thermal Hall Effect in a Phonon-Glass $Ba_3CuSb_2O_9$". In: *Phys. Rev. Lett.* 118 (14 Apr. 2017), p. 145902. DOI: 10.1103/PhysRevLett.118.145902. URL: https://link.aps.org/doi/10.1103/PhysRevLett.118.145902.

[189] Aaron Szasz et al. "Chiral Spin Liquid Phase of the Triangular Lattice Hubbard Model: A Density Matrix Renormalization Group Study". In: *Phys. Rev. X* 10 (2 May 2020), p. 021042. DOI: 10.1103/PhysRevX.10.021042. URL: https://link.aps.org/doi/10.1103/PhysRevX.10.021042.

[190] Hirokazu Taguchi et al. "Role of Majorana fermions in spin transport of anisotropic Kitaev model". In: *Phys. Rev. B* 104 (12 Sept. 2021), p. 125139. DOI: 10.1103/PhysRevB.104.125139. URL: https://link.aps.org/doi/10.1103/PhysRevB.104.125139.

[191] Louis Taillefer. "Scattering and Pairing in cuprate Superconductors". In: *Annual Review of Condensed Matter Physics* 1.1 (2010), pp. 51–70. DOI: 10.1146/annurev-conmatphys-070909-104117.

[192] Hidenori Takagi et al. "Concept and realization of Kitaev quantum spin liquids". In: *Nature Reviews Physics* 1.4 (2019), pp. 264–280.

[193] Yasuhiro Tanaka and Kenji Yonemitsu. "Growth dynamics of photoinduced domains in two-dimensional charge-ordered conductors depending on stabilization mechanisms". In: *Journal of the Physical Society of Japan* 79.2 (2010), p. 024712.

[194] Mathieu Taupin and Silke Paschen. "Are Heavy Fermion Strange Metals Planckian?" In: *Crystals* 12.2 (2022), p. 251.

[195] Akira Terai and Yoshiyuki Ono. "Solitons and their dynamics in one-dimensional SDW systems". In: *Progress of Theoretical Physics Supplement* 113 (1993), pp. 177–190.

[196] K. S. Tikhonov, M. V. Feigel'man, and A. Yu. Kitaev. "Power-Law Spin Correlations in a Perturbed Spin Model on a Honeycomb Lattice". In: *Phys. Rev. Lett.* 106 (6 Feb. 2011), p. 067203. DOI: 10.1103/PhysRevLett.106.067203. URL: https://link.aps.org/doi/10.1103/PhysRevLett.106.067203.

[197] Y. Tokiwa, E. D. Bauer, and P. Gegenwart. "Zero-Field Quantum Critical Point in $CeCoIn_5$". In: *Physical Review Letters* 111.10 (Sept. 2013), p. 107003.

[198] Simon Trebst. "Kitaev materials". In: *arXiv preprint arXiv:1701.07056* (2017).

[199] Masafumi Udagawa. "Theoretical scheme for finite-temperature dynamics of Kitaev's spin liquids". In: *Journal of Physics: Condensed Matter* 33.25 (2021), p. 254001.

[200] C. M. Varma. "Theory of the pseudogap state of the cuprates". In: *Physical Review B* 73.15 (Apr. 2006), p. 155113. ISSN: 1098-0121.

[201] C. M. Varma et al. "Phenomenology of the normal state of Cu-O high-temperature superconductors". In: *Phys. Rev. Lett.* 63 (18 Oct. 1989), pp. 1996–1999. DOI: 10.1103/PhysRevLett.63.1996. URL: https://link.aps.org/doi/10.1103/PhysRevLett.63.1996.

[202] Wei Wang et al. "Theoretical investigation of magnetic dynamics in $\alpha - RuCl_3$". In: *Phys. Rev. B* 96 (11 Sept. 2017), p. 115103. DOI: 10.1103/PhysRevB.96.115103. URL: https://link.aps.org/doi/10.1103/PhysRevB.96.115103.

[203] Zhe Wang et al. "Magnetic Excitations and Continuum of a Possibly Field-Induced Quantum Spin Liquid in $\alpha-RuCl_3$". In: *Phys. Rev. Lett.* 119 (22 Nov. 2017), p. 227202. DOI: 10.1103/PhysRevLett.119.227202. URL: https://link.aps.org/doi/10.1103/PhysRevLett.119.227202.

[204] Steven R. White. "Density matrix formulation for quantum renormalization groups". In: *Phys. Rev. Lett.* 69 (19 Nov. 1992), pp. 2863–2866. DOI: 10.1103/PhysRevLett.69.2863. URL: https://link.aps.org/doi/10.1103/PhysRevLett.69.2863.

[205] Alexander Wietek and Andreas M. Läuchli. "Chiral spin liquid and quantum criticality in extended $S = \frac{1}{2}$ Heisenberg models on the triangular lattice". In: *Phys. Rev. B* 95 (3 Jan. 2017), p. 035141. DOI: 10.1103/PhysRevB.95.035141. URL: https://link.aps.org/doi/10.1103/PhysRevB.95.035141.

[206] Alexander Wietek, Antoine Sterdyniak, and Andreas M. Läuchli. "Nature of chiral spin liquids on the kagome lattice". In: *Phys. Rev. B* 92 (12 Sept. 2015), p. 125122. DOI: 10.1103/PhysRevB.92.125122. URL: https://link.aps.org/doi/10.1103/PhysRevB.92.125122.

[207] S. C. Williams et al. "Incommensurate counterrotating magnetic order stabilized by Kitaev interactions in the layered honeycomb $\alpha-Li_2IrO_3$". In: *Phys. Rev. B* 93 (19 May 2016), p. 195158. DOI: 10.1103/PhysRevB.93.195158. URL: https://link.aps.org/doi/10.1103/PhysRevB.93.195158.

[208] Stephen M Winter et al. "Breakdown of magnons in a strongly spin-orbital coupled magnet". In: *Nature Communications* 8.1 (2017), p. 1152.

[209] Stephen M Winter et al. "Models and materials for generalized Kitaev magnetism". In: *Journal of Physics: Condensed Matter* 29.49 (2017), p. 493002.

[210] Stephen M. Winter et al. "Challenges in design of Kitaev materials: Magnetic interactions from competing energy scales". In: *Phys. Rev. B* 93 (21 June 2016), p. 214431. DOI: 10.1103/PhysRevB.93.214431. URL: https://link.aps.org/doi/10.1103/PhysRevB.93.214431.

[211] Stephen M. Winter et al. "Probing $\alpha - RuCl_3$ Beyond Magnetic Order: Effects of Temperature and Magnetic Field". In: *Phys. Rev. Lett.* 120 (7 Feb. 2018), p. 077203. DOI: 10.1103/PhysRevLett.120.077203. URL: https://link.aps.org/doi/10.1103/PhysRevLett.120.077203.

[212] Liang Wu et al. "Field evolution of magnons in α-RuCl _3 by high-resolution polarized terahertz spectroscopy". In: *arXiv preprint arXiv:1806.00855* (2018).

[213] Ravi Yadav et al. "Kitaev exchange and field-induced quantum spin-liquid states in honeycomb α-RuCl 3". In: *Scientific reports* 6 (2016), p. 37925.

[214] Youhei Yamaji et al. "Clues and criteria for designing a Kitaev spin liquid revealed by thermal and spin excitations of the honeycomb iridate Na_2IrO_3". In: *Phys. Rev. B* 93 (17 May 2016), p. 174425. DOI: 10.1103/PhysRevB.93.174425. URL: https://link.aps.org/doi/10.1103/PhysRevB.93.174425.

[215] M Yamashita et al. "Sample dependence of half-integer quantized thermal Hall effect in the Kitaev spin-liquid candidate α- RuCl 3". In: *Physical Review B* 102.22 (2020), p. 220404.

[216] Wei-Wei Yang et al. "Doping a Mott insulator in an Ising-Kondo lattice: Strange metal and Mott criticality". In: *Phys. Rev. B* 104 (16 Oct. 2021), p. 165146. DOI: 10.1103/PhysRevB.104.165146. URL: https://link.aps.org/doi/10.1103/PhysRevB.104.165146.

[217] Feng Ye et al. "Direct evidence of a zigzag spin-chain structure in the honeycomb lattice: A neutron and x-ray diffraction investigation of single-crystal Na_2IrO_3". In: *Phys. Rev. B* 85 (18 May 2012), p. 180403. DOI: 10.1103/PhysRevB.85.180403. URL: https://link.aps.org/doi/10.1103/PhysRevB.85.180403.

[218] T Yokoi et al. "Half-integer quantized anomalous thermal Hall effect in the Kitaev material candidate α-RuCl3". In: *Science* 373.6554 (2021), pp. 568–572.

[219] Junki Yoshitake et al. "Majorana-magnon crossover by a magnetic field in the Kitaev model: Continuous-time quantum Monte Carlo study". In: *Phys. Rev. B* 101 (10 Mar. 2020), p. 100408. DOI: 10.1103/PhysRevB.101.100408. URL: https://link.aps.org/doi/10.1103/PhysRevB.101.100408.

[220] Li-Chuan Zhang et al. "Interplay of Dzyaloshinskii-Moriya and Kitaev interactions for magnonic properties of Heisenberg-Kitaev honeycomb ferromagnets". In: *Phys. Rev. B* 103 (13 Apr. 2021), p. 134414. DOI: 10.1103/PhysRevB.103.134414. URL: https://link.aps.org/doi/10.1103/PhysRevB.103.134414.

[221] Ya-Hui Zhang and Subir Sachdev. "From the pseudogap metal to the Fermi liquid using ancilla qubits". In: *Phys. Rev. Research* 2 (2 May 2020), p. 023172. DOI: 10.1103/PhysRevResearch.2.023172. URL: https://link.aps.org/doi/10.1103/PhysRevResearch.2.023172.

[222] Su-Ming Zhang and Zheng-Xin Liu. "Phase diagram for hole-doped Kitaev systems on the honeycomb lattice". In: *Phys. Rev. B* 104 (11 Sept. 2021), p. 115108. DOI: 10.1103/PhysRevB.104.115108. URL: https://link.aps.org/doi/10.1103/PhysRevB.104.115108.

[223] Shang-Shun Zhang et al. "Variational study of the Kitaev-Heisenberg-Gamma model". In: *Phys. Rev. B* 104 (1 July 2021), p. 014411. DOI: 10.1103/PhysRevB.104.014411. URL: https://link.aps.org/doi/10.1103/PhysRevB.104.014411.

[224] B. B. Zhou et al. "Visualizing nodal heavy fermion superconductivity in $CeCoIn_5$". In: *Nat. Phys.* 9.8 (Aug. 2013), pp. 474–479. ISSN: 1745-2473. DOI: 10.1038/nphys2672. URL: http://www.nature.com/articles/nphys2672.

[225] Zheng Zhu et al. "Robust non-Abelian spin liquid and a possible intermediate phase in the antiferromagnetic Kitaev model with magnetic field". In: *Phys. Rev. B* 97 (24 June 2018), p. 241110. DOI: 10.1103/PhysRevB.97.241110. URL: https://link.aps.org/doi/10.1103/PhysRevB.97.241110.

[226] Zhenyue Zhu and Steven R. White. "Spin liquid phase of the $S = \frac{1}{2}$ $J_1 - J_2$ Heisenberg model on the triangular lattice". In: *Phys. Rev. B* 92 (4 July 2015), 041105(R). DOI: 10.1103/PhysRevB.92.041105. URL: https://link.aps.org/doi/10.1103/PhysRevB.92.041105.